A STUDY OF PHOTOCHEMICAL AEROSOL FORMATION AND THE COAGULATIVE MASS TRANSPORT IN NATURAL AND LABORATORY AEROSOL - GAS MIXTURES

A STUDY OF PHOTOCHEMICAL AEROSOL FORMATION AND THE COAGULATIVE MASS TRANSPORT IN NATURAL AND LABORATORY AEROSOL-GAS MIXTURES

by

Richard Adolph Zalabsky

A Dissertation Submitted to the Faculty of the

DEPARTMENT OF ATMOSPHERIC SCIENCES

In Partial Fulfillment of the Requirements
For the Degree of

DOCTOR OF PHILOSOPHY

In the Graduate College

THE UNIVERSITY OF ARIZONA

1 9 7 8

THE UNIVERSITY OF ARIZONA

GRADUATE COLLEGE

I hereby recommend that this dissertation prepared under my direction by Richard Adolph Zalabsky

entitled A Study of Photochemical Aerosol Formation and the Coagulative Mass Transport in Natural and Laboratory Aerosol-Gas Mixtures

be accepted as fulfilling the dissertation requirement for the degree of Doctor of Philosophy

S. Twomey — Jan 31 1978

Dissertation Director — Date

As members of the Final Examination Committee, we certify that we have read this dissertation and agree that it may be presented for final defense.

S. Twomey	1-31-78
D. O. Staley	1-31-78
E. P. Kinder	1-31-78
T. Theodore Bowen	2-1-78

Final approval and acceptance of this dissertation is contingent on the candidate's adequate performance and defense thereof at the final oral examination.

STATEMENT BY AUTHOR

This dissertation has been submitted in partial fulfillment of requirements for an advanced degree at The University of Arizona and is deposited in the University Library to be made available to borrowers under rules of the Library.

Brief quotations from this dissertation are allowable without special permission, provided that accurate acknowledgment of source is made. Requests for permission for extended quotation from or reproduction of this manuscript in whole or in part may be granted by the head of the major department or the Dean of the Graduate College when in his judgment the proposed use of the material is in the interests of scholarship. In all other instances, however, permission must be obtained from the author.

SIGNED: Richard Adolph Zaldbsby

To Mr. and Mrs. Adolph Zalabsky

for their unceasing help and encouragement.

ACKNOWLEDGMENTS

I would like to express my gratitude to my dissertation committee, Dr. Sean Twomey, Dr. Dean Staley, Dr. E. Philip Krider and Dr. Ted Bowen. My special thanks go to Dr. Twomey for originally stimulating my interest in the mechanisms of atmospheric Aitken nucleus formation and for his continued interest and encouragement and to Dr. E. Philip Krider for his ever present help and support.

This research was supported by a grant from the Atmospheric Sciences Section of the Office of Naval Research, Contract N00014-67-A0209-0015.

TABLE OF CONTENTS

		Page
	LIST OF ILLUSTRATIONS	viii
	LIST OF TABLES	xiii
	ABSTRACT	xiv
1.	INTRODUCTION	1
2.	MULTIFILTER TECHNIQUE FOR EXAMINATION OF THE SIZE DISTRIBUTION OF THE NATURAL AEROSOL	7
	Principles of the Technique for the Determination of Aerosol Size Distributions	8
	Basic Problem	8
	The Inversion Procedure	10
	The Resolving Power of the Inversion Procedure	11
	Experimental Arrangement	16
	Experimental Procedure	16
	Treatment of Storage Losses	19
	Results	20
	Typical Data Set	20
	Tucson Samples	20
	Australian Samples	25
	Comparison of Tucson and Australian Samples	25
	Photochemical Aerosols	27
	Comparison with the Whitby Aerosol Analyzer	30
	Summary and Conclusions	30
3.	THE AEROSOL MASS TRANSPORT	37
	Derivation of the Basic Equations	38
	Derivation of the Mass Transport Equation	38
	Integral Equation for a Constant Mass Transport	42
	Coagulation Coefficients	43
	The Mass Transport for Several Hypothetical Cases	43
	Constant Coagulation Coefficient	43
	Realistic Coagulation Coefficient	44
	The Mass Transport for Measured Aerosol Size Distributions	47

TABLE OF CONTENTS--Continued

	Page
Arizona Samples	47
Australian Samples	52
Photochemical Aerosol	55
Summary and Conclusions	55
Comparison of Estimated Global Transport to Total Gaseous Emissions	55
Location of Sources and Sinks in Dry, Urban Air	58
Location of Sources and Sinks in Polar-Maritime Air	58
Calculation of the Mass Transport for $r \leq .01\ \mu$	59
Mass Transports in Tucson Air Samples	59
4. PHOTOCHEMICAL EXPERIMENTS	60
Experimental Apparatus and Procedure	62
Experimental Arrangement	62
Experimental Procedure	62
The Photoreactors	64
Sources of Radiation	67
Discussion of Contaminants	72
Photochemical Production of Nuclei	82
Tucson Environmental Air	82
Nucleus Formation in Remote Air Samples in the Short UV	113
Miscellaneous Experiments	116
Aerosol Formation in the Dark	116
Ion-Induced Aerosol Formation	117
Evaporation of Photochemical Nuclei	119
Summary and Conclusions	119
Solar-Induced Nucleus Formation	119
Comparison With the Results of Other Workers	123
Nucleus Formation With the HPXeHg Sources	124
Nucleus Formation With the LPHg-(UF) UV Source	124
Miscellaneous Experiments	126
APPENDIX A: COAGULATION COEFFICIENTS $K(r_1, r_2)$	128
APPENDIX B: SURVIVAL TIMES	130
Survival Times in the Presence of the Existing Atmospheric Aerosol	131
Newly Formed Aerosol Particles of Radius x	131
Survival Times for Molecules	131

TABLE OF CONTENTS--Continued

Page

Survival Times in the Presence of Photoreactor Walls 132
Static Diffusion Model 132
Mixed Interior Diffusion Through a Boundary Layer . . . 133

APPENDIX C: ESTIMATING THE SPECTRAL IRRADIANCE OF THE 1850 Å LINE 139

APPENDIX D: H_2SO_4 AEROSOL FORMATION IN SO_2-AIR-H_2O MIXTURES AT 1850 Å 142

LIST OF REFERENCES 148

LIST OF ILLUSTRATIONS

Figure		Page
1.	A summary of the various possible mechanisms for the formation of Aitken nuclei in the atmosphere	3
2.	Block diagram of the interrelationships between the various topics to be presented	6
3.	A characteristic set of Nuclepore filter transmission kernels, $K_i(r)$	9
4.	The test function $S_a(x-\xi)$ used to analyze the resolving power of the inversion algorithm	13
5.	The retrieved "delta functions" for various values of ξ	15
6.	Diagram of the Nuclepore filter arrangement	17
7.	A typical set of filter data and volumetric flow rates used in a set of measurements	21
8.	A typical set of Tucson size distributions with particle concentrations on the order of 1-2 x 10^4 cm^{-3}	22
9.	Tucson size distributions with particle concentrations on the order of 3-4 x 10^4 cm^{-3}	23
10.	Several dusty day size distributions	24
11.	A set of Australian size distributions	26
12.	Behavior of a photochemical H_2SO_4 aerosol stored in the mylar bag.	28
13.	Photochemical H_2SO_4 aerosol size distributions	29
14.	Size distributions of a photochemical aerosol taken with the Nuclepore filters and with the Whitby Aerosol Analyzer	31

LIST OF ILLUSTRATIONS--Continued

Figure		Page
15.	Size distributions of the ambient aerosol taken with the Nuclepore filters and the Whitby Aerosol Analyzer . . .	32
16.	Average survival times of newly formed particles in the presence of the existing aerosol	34
17.	Average survival times of nucleogen molecules in the presence of the existing aerosol	35
18.	Mass transport for the ideal case $\frac{dN}{d\ell nr} = c_0 r^{-3}$ and $K(r_1,r_2)$ a constant	45
19.	Mass transport for the hypothetical case $\frac{dN}{d\ell nr} = c_0 r^{-3/2}$ and realistic $K(r_1,r_2)$	46
20.	A set of Tucson size distributions corresponding to the mass transports in Figure 21	48
21.	A set of Tucson mass transports	49
22.	Sensitivity of the mass transport in the $r \leq .1\mu$ region to the aerosol size distribution in the $r \geq .1\mu$ region	50
23.	The coagulative residence time as a function of particle radius	51
24.	A set of Australian size distributions corresponding to the mass transports shown in Figure 25.	53
25.	The Australian mass transports	54
26.	Size distribution of a photochemical H_2SO_4 aerosol corresponding to the mass transport shown in Figure 27	56
27.	Mass transport for the photochemical H_2SO_4 aerosol	57
28.	Experimental arrangement for the photochemical experiments	63
29.	Solar induced nucleus formation in atmospheric air enriched in SO_2	66

LIST OF ILLUSTRATIONS--Continued

Figure		Page
30.	Transmission curves for the 24 ℓ reactor	69
31.	Relative spectrum of the HPXeHg-(UF) UV source	70
32.	Relative spectrum of the HPXeHg-(0-53) UV source	71
33.	Relative spectrum of the LPHg-(UF) UV source	73
34.	Relative spectrum of the LPHg-(0-53) UV source	74
35.	Relative spectrum of the LPHg-(0-54) UV source	75
36.	Results of experiment to determine whether or not aerosol formation was due to atmospheric trace gases	79
37.	Spontaneous (dark phase) aerosol formation in the mylar bag	81
38.	Solar photooxidation of ambient air with added SO_2	83
39.	Solar photooxidation of atmospheric air without added SO_2 at 70% RH	84
40.	Rate of nucleus formation with and without the 1850 Å line present in the photoreactor	87
41.	Photochemical nucleus formation with the various LPHg radiation sources	88
42.	Nucleus formation at various relative humidities with the LPHg-(UF) UV source (1850 Å)	90
43.	Nucleus formation in atmospheric air enriched in SO_2 using 1850 Å UV radiation	91
44.	Role of SO_2 in accounting for nucleus formation	92
45.	Condensational growth of the nuclei produced in atmospheric air samples with 1850 Å UV radiation	95
46.	Relationship between the total number of nuclei, the number transmitted through the number 4 Nuclepore filter and the number of CCN	96

LIST OF ILLUSTRATIONS--Continued

Figure		Page
47.	Nuclei formed during the irradiation of unfiltered atmospheric air	98
48.	Formation of nuclei during storage using the quartz reactor and 1850 Å UV radiation	100
49.	Size distributions of the nuclei corresponding to curves a and e in Figure 48	101
50.	Effect on nucleus formation of passing the irradiated gas samples through a Nuclepore filter before storing in the mylar bag	103
51.	Nuclei formed during storage with a 1 minute filling time	104
52.	Size distributions of the nuclei corresponding to the curves in Figure 51	105
53.	Effect of storing irradiated SO_2-Air-H_2O mixtures in atmospheric and in scrubbed bottled air	107
54.	Effect of storing irradiated atmospheric air in filtered atmospheric and scrubbed bottled air	108
55.	Effect of storing irradiated atmospheric air in unfiltered atmospheric air	110
56.	Effect of storing irradiated atmospheric air in air containing previously formed photochemical nuclei	112
57.	The remote air sampler	114
58.	Comparison of photochemical nucleus formation between Tucson and rural air samples	115
59.	Aerosol formation in the dark	118
60.	The apparent evaporation of photochemical nuclei	120
B.1.	Characteristic decay curves for the 24 ℓ reactor used to estimate ξ	135

LIST OF ILLUSTRATIONS--Continued

Figure		Page
B.2.	Calculated and measured decay curves for different size particles	136
B.3.	Comparison of the average survival times of newly formed aerosol in the photoreactor with that in the presence of the existing aerosol	138
C.1.	[O_3] produced in continuous flow using the various LPHg sources of UV	140
D.1.	Experimental arrangement for studying the photooxidation of SO_2-Air-H_2O mixtures at 1850 Å	143
D.2.	Nuclei formed when SO_2-Air-H_2O mixtures were irradiated with the LPHg-(UF) UV source (1850 Å)	144
D.3.	Nuclei formed when SO_2-Air-H_2O mixtures were irradiated with and without the 1850 Å UV.	147

LIST OF TABLES

Table | Page

1. Summary of the Various Sources Used and the Wavelengths Present in the Photoreactor 76

2. Summary of Study of the Effects of Various Materials in Causing Spurious Nucleus Formation 78

ABSTRACT

Photochemical Aitken nucleus formation in filtered atmospheric air has been examined using both solar irradiation and ultraviolet radiation from artificial sources. In contrast to previous work, extreme care has been taken to insure that nucleus formation is due to trace gases in the air and not to system contaminants and the photochemical experiments have been analyzed in light of measurements of the ambient aerosol size distribution and the associated coagulative mass transport.

Photochemically induced nucleus formation has been observed only when 1850 Å UV radiation (from low pressure Hg sources) is present. Once sufficient precautions have been taken to clean the photoreactor walls, solar radiation does not produce nuclei in filtered atmospheric air even after irradiation for 2-3 hours. The diffusive survival time of a newly formed nucleogen molecule, estimated using measured aerosol size distributions, is only some 5-10 minutes. Based on these time scales it is concluded that the most likely fate of photochemical nucleogen is attachment to the existing aerosol rather than new particle formation. The small amount of aerosol in the $r \leq .005$ μ region of the measured size distributions and the inability of solar induced nucleus formation to account for the aerosol removed by coagulative mass transport both indicate that the photochemical mechanisms which have

been observed are of minor importance for producing new Aitken nuclei in Tucson air.

Spontaneous (in the dark) aerosol formation has not been observed using filtered atmospheric air. Aerosol formation in the dark has been observed only when the air samples have been enriched in both SO_2 and O_3.

Attempts to produce nuclei in filtered atmospheric air with radioactive sources of ions have consistently failed.

CHAPTER 1

INTRODUCTION

The origin of Aitken nuclei in the atmosphere remains to a large extent unknown. Of particular interest in this context is the formation of nuclei in the atmosphere via conversion of existing trace gases into aerosol, i.e., gas-to-particle conversion mechanisms. Although a number of such mechanisms are known to produce aerosol in the laboratory, the extent to which various mechanisms are important in the atmosphere is as yet poorly understood. For example, it has long been known, both from laboratory studies of the photooxidation of SO_2 and from chemical analyses of aerosol samples, that nucleation of H_2SO_4-H_2O is an important source of aerosol. It is not known, however, under what conditions in the atmosphere new aerosol particles are formed via nucleation in the H_2SO_4-H_2O system. Since there invariably is preexisting aerosol present, it is not clear whether or not (in a given atmospheric environment) sufficient concentrations of H_2SO_4 (or hydrated H_2SO_4) nucleogen are obtained to allow homogeneous nucleation to take place or whether condensation on existing aerosol surfaces is, in fact, the dominant mechanism. Doyle (1961) concludes, based solely on a theoretical calculation of the rate of homogeneous nucleation in the H_2SO_4-H_2O system, that acid nuclei will be produced abundantly in

an urban environment with [SO_2] on the order of 10 ppb. Hoppel (1975), on the other hand, concludes, based on an approximate heterogeneous nucleation calculation, that the formation of new H_2SO_4 aerosol is a rare event in either rural or urban air, due to the dominance of the existing aerosol surface. Cox (1973), based on an experimental study of the photooxidation of SO_2, concludes that new nucleus formation is a likely event in urban environments ([SO_2] = .1 ppm), while highly unlikely in rural environments. Went (1960) has advocated the importance of natural organic trace gases (terpenes) as being an important source of atmospheric nuclei. Though natural organics certainly are photo-oxidized into aerosol near their source regions, it does not follow that they are present in sufficient concentrations to homogeneously nucleate in the bulk of the atmosphere. Unfortunately, to the author's knowledge, no laboratory experiments have been done with natural organics at realistic concentrations to determine nucleation rates, the influence of RH and other trace constituents, etc. The same criticism applies to H_2SO_4-H_2O nucleation, as detailed confirmation of nucleation rates remains to be obtained.

Mohnen (1971), Martell (1977), Bricard, Billard and Madelaine (1969) and others have proposed that ion-induced gas-to-particle conversion may be an important source of Aitken nuclei. These arguments are based on mechanisms which have yet to be tested in the laboratory or even carefully examined using atmospheric air samples.

A brief summary of the various possible mechanisms involved in aerosol formation and growth is presented in Figure 1. The following

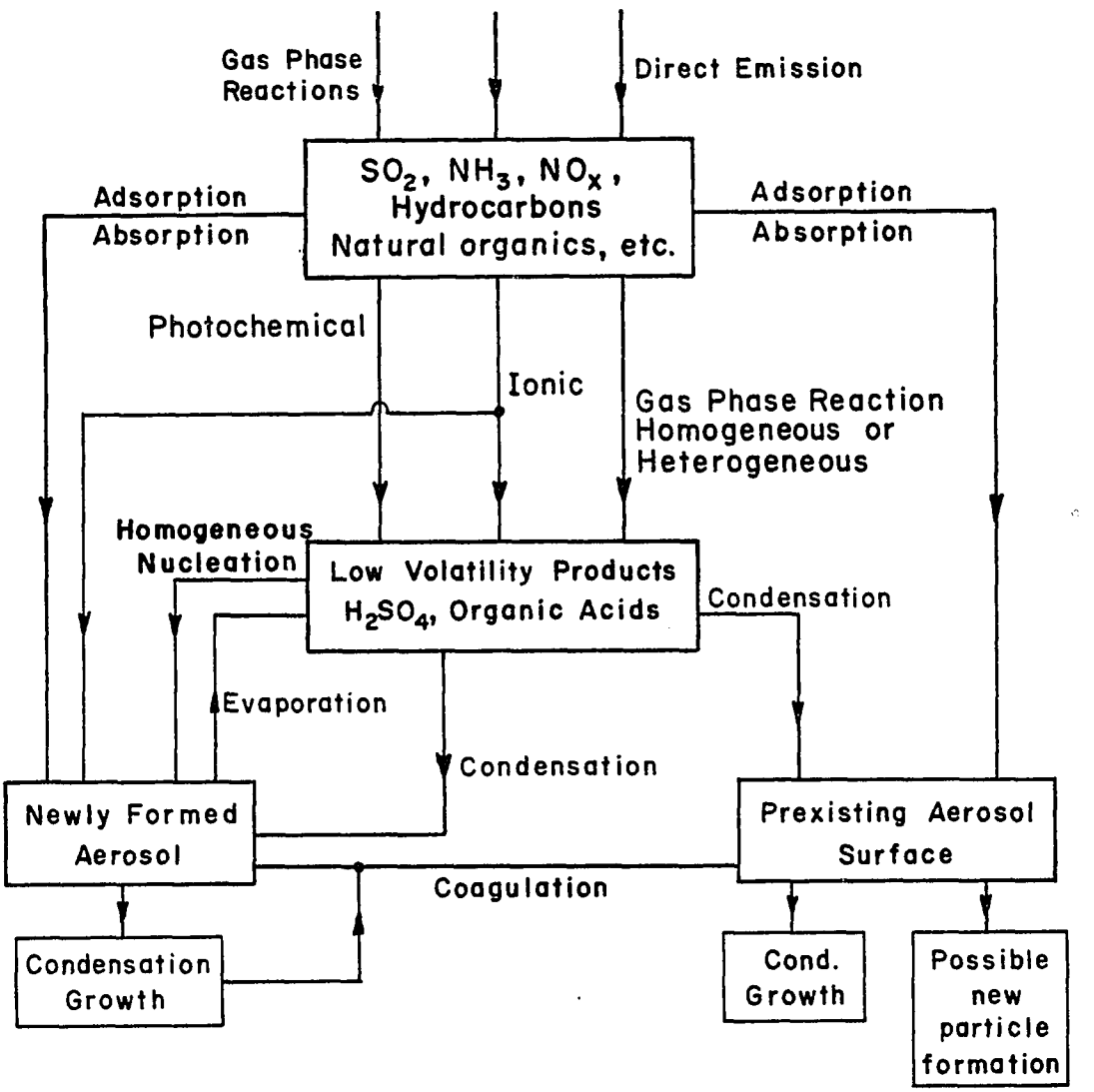

Figure 1. A summary of the various possible mechanisms for the formation of Aitken nuclei in the atmosphere.

study deals with the rate at which new Aitken nuclei are photochemically produced at wavelengths ranging from those present in solar radiation to the short UV (1850 Å). The photochemical measurements are combined with measurements of the existing aerosol size distribution, in order to assess the importance of photochemical mechanisms for the formation of new nuclei in atmospheric air. The presented material is divided into three chapters, as follows:

Chapter 2. A multifilter technique for the measurement of aerosol size distributions in the $r \leq 0.1$ μ region is the topic of this chapter. Several theoretical and experimental considerations are discussed and a number of aerosol size distributions are presented.

Chapter 3. The coagulative mass transport in both ideal and measured size distributions is examined.

Chapter 4. Photochemical Aitken nucleus formation is discussed. The rates of photochemical formation and properties of the nuclei produced are examined using both solar and UV radiation from artificial sources. The photochemical results are analyzed in conjunction with the measured size distributions and resulting coagulative mass transports, as follows:

a. The size distributions are used to estimate the average diffusive survival time of a newly formed nucleogen molecule in the presence of the existing aerosol. This basic, important time scale is then compared with the measured time scale for the onset of new particle formation (homogeneous nucleation) by photochemical mechanisms.

b. The mass transports obtained from the measured size distributions are used to calculate the rate of coagulative mass

transport out of the gas-to-particle conversion size domain. To the extent that the aerosol size distributions represent a steady-state situation, this aerosol mass must on average be replaced. The extent to which photochemical mechanisms can account for this mass is then assessed by comparing the rate of transport with the rate of photochemically induced nucleus formation. Figure 2 presents these relationships in schematic form.

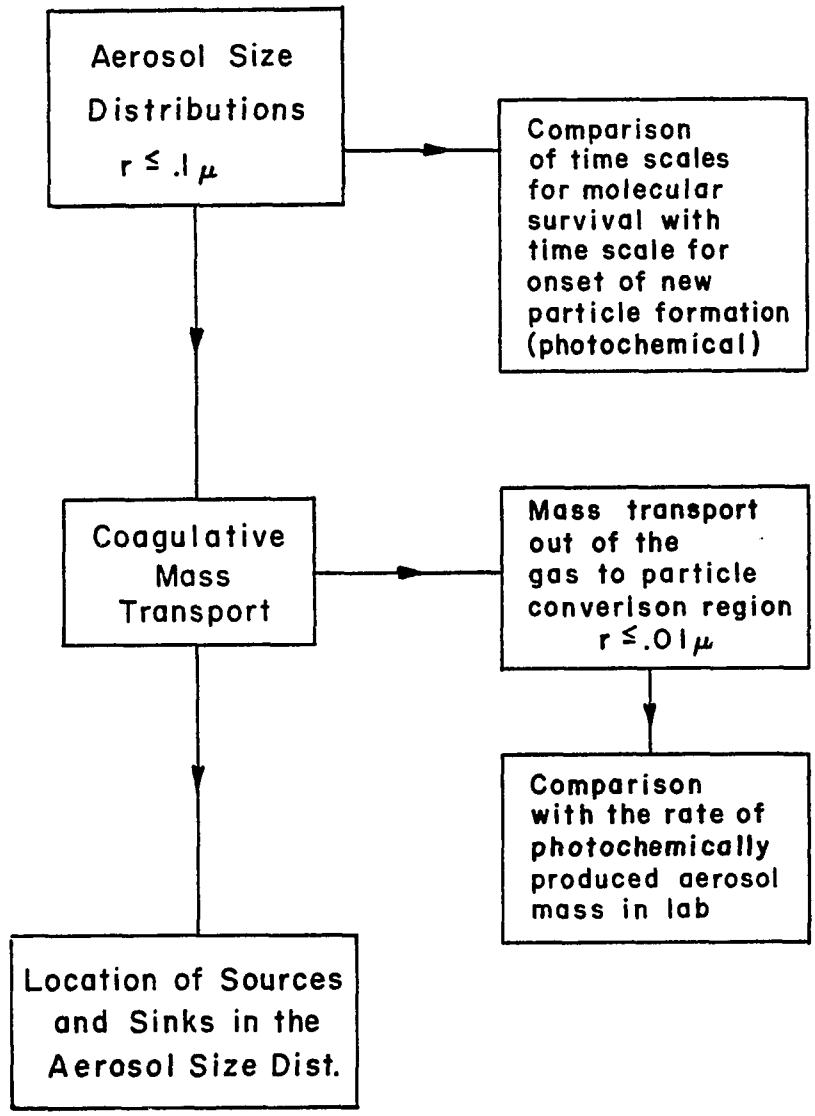

Figure 2. Block diagram of the interrelationships between the various topics to be presented.

CHAPTER 2

MULTIFILTER TECHNIQUE FOR EXAMINATION OF THE SIZE DISTRIBUTION OF THE NATURAL AEROSOL

In recent years, greater attention has been given to the question of what typically is the size distribution of natural aerosols, and a great demand has arisen for useful methods for determining this. Direct sampling and observation of the particles individually, whether by optical or electron microscopy, is a difficult and time-consuming process. In the case of the smaller particles which can be observed only by electron microscopy, the question of possible evaporation of collected particles before and during observations by electron microscopes is one which as yet is not fully resolved. Uncertainty about the size distribution becomes even more obvious when one moves into the submicron region, and an inspection of the rather sparse literature suggests that even the position of the maximum of the size distribution, i.e., the modal radius, is uncertain. It has been estimated to be as high as 0.1 microns by Junge and Jaenicke (1969), while Whitby, Husar and Liu (1972) have published size distribution data which indicate a modal radius closer to 0.001 microns. These results differ in radius by two orders of magnitude or in mass by six orders of magnitude, and even though the samples were obtained in different geographic regions, one certainly cannot conclude that there is general agreement concerning

the gross features and the general shape of the size distribution of the natural atmospheric aerosol.

Recently Twomey (1976) has developed and successfully used a multifilter technique to obtain size distributions of the natural aerosol in S.E. Australia. The present chapter will briefly review the techniques present size distributions of both natural and photochemical aerosols using the technique, examine the resolving power of the inversion algorithm and present the results of a comparison experiment between the filter technique and an electrical mobility sizing technique. The natural aerosol size distributions are discussed in light of their relationship to the material presented in later chapters.

Principles of the Technique for the Determination of Aerosol Size Distributions

Basic Problem

Corresponding to each Nuclepore filter-flow rate combination is a particular transmission kernel $K_i(x)$. A characteristic set of particle transmission kernels is shown in Fig. 3. For details concerning the calculation of the kernels and a discussion of the various particle removal mechanisms the reader is referred to Twomey (1976) and Twomey and Zalabsky (1978). By passing air samples through the filters and measuring the transmitted particle concentrations one obtains a number of values of the integral

$$g_i = \int_{x_L}^{x_U} K_i(x)\, f(x)\, dx, \qquad (1)$$

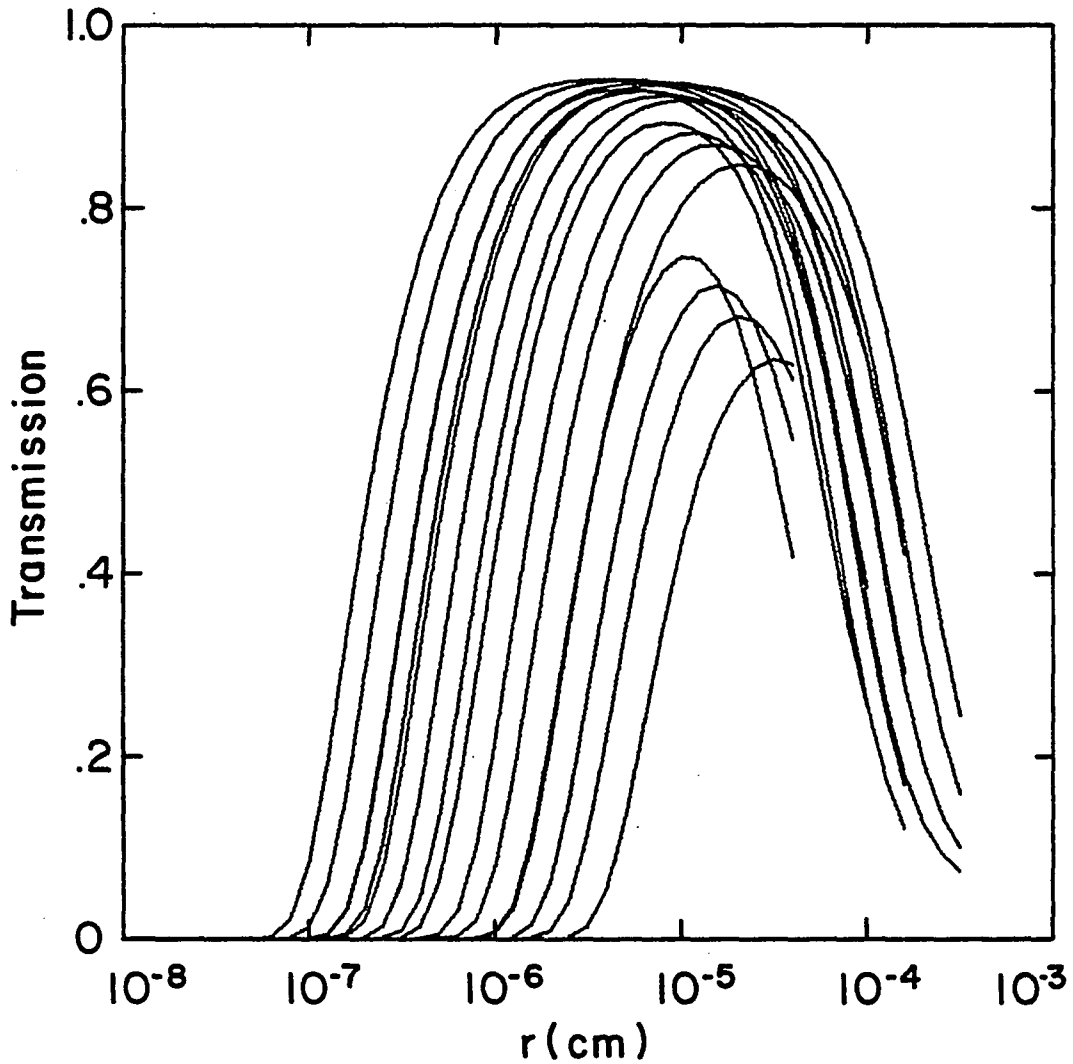

Figure 3. A characteristic set of Nuclepore filter transmission kernels, $K_i(r)$.

where the subscript i refers to a particular flow rate-filter combination, f(x) is the unknown aerosol size distribution, and the g_i are the measured particle concentrations. The basic problem is to infer f(x) given a sufficient number of measurements, that is, a suitable number of the components of $\tilde{g}$.

The Inversion Procedure

A non-linear algorithm suitable for inverting equation (1) for the unknown f(x) has been examined in detail by Twomey (1975) who has demonstrated its insensitivity to the form of the first guess and carried out a number of numerical experiments to verify its usefulness in inferring natural size distributions. Briefly, the iterative procedure is as follows: one commences with a first guess and iterates through the set of measured g_i [and the corresponding $K_i(x)$] according to the formula

$$f_{n+1}(x) = [1 + (r_n - 1)\, K_i(x)]\, f_n(x).$$

where

$$r_n = \frac{g_i}{\int_{x_L}^{x_U} K_i(x)\, f(x)\, dx}.$$

The iterative procedure is continued until the calculated g_i^n agree with the measured g_i to within the experimental error of the measurements, or $|\tilde{g}-\tilde{g}^n|$ is diminishing too slowly to make further iterations effectual.

The Resolving Power of the Inversion Procedure

In order to assess the reality of various structural features in the measured aerosol size distributions, it is necessary to obtain an objective estimate of the resolving power of the inversion procedure. By inversion procedure is meant here the resolving power of the $K_i(x)$ themselves, as well as the particular type of mathematical inversion being used, i.e., linear methods, algorithms, etc. In the case of the nonlinear algorithm used here, the iterative procedure to some extent filters the high-frequency components of the unknown f(x). This can be seen as follows: following Twomey (1975) for a sequence of small changes

$$f(x) \sim [1 + \beta_1 K_1(x)][1 + \beta_2 K_2(x)][1 + \beta_3 K_3(x)] \cdots$$

$$\sim 1 + \beta_1 K_1(x) + \beta_2 K_2(x) + \beta_3 K_3(x) + \cdots O(\beta^2).$$

That is, to first order, f(x) is being expanded as a linear combination of the kernel functions. Since the $K_i(x)$ themselves are "smooth" functions, the higher frequency components of f(x) will not be represented in the expansion. From another point of view, the high-frequency components of f(x) are outside of the function space spanned by the $K_i(x)$. Note, however, that as the iteration proceeds, the products of the kernels, $K_i(x)K_j(x)$, come into play and admit to some extent the higher frequency components of f(x).

An objective test of the inversion procedure's resolving power may be made using a delta function (or a suitable numerical

representation thereof) as the unknown function f(x). For f(x) = $\delta(x - \xi)$, we have simply

$$g_i = \int_0^\infty K_i(x)\ \delta(x - \xi)\ dx = K_i(\xi).$$

A "perfect" inversion for f(x) with $g_i = K_i(\xi)$ should therefore retrieve a delta function at $x = \xi$. In practice, a numerical representation of the "best" $\delta(x - \xi)$ which could be retrieved exactly is needed. Since no features finer than the numerical grid spacing can be resolved, the grid spacing Δx will determine the best $\delta(x - \xi)$ which could be retrieved exactly is needed. Since no features finer than the numerical grid spacing can be resolved, the grid spacing Δx will determine the best $\delta(x - \xi)$ which can be retrieved. Consider then a triangular spike function defined as:

$$S_a(x - \xi) = \begin{cases} \frac{1}{a^2}\ (x - \xi + a) & x < \xi \\ -\frac{1}{a^2}\ (x - \xi - a) & x > \xi \\ 0 & |x - \xi| \geq a\ . \end{cases}$$

$S_a(x - \xi)$, which has a width of 2a and a height of 1/a, is shown in Figure 4. For $a = \Delta x$, the grid spacing, $S_a(x - \xi)$ is an appropriate representation of $\delta(x - \xi)$, in the sense that $S_a(x - \xi) \to \delta(x - \xi)$ $\lim a \to 0$. For this spike function

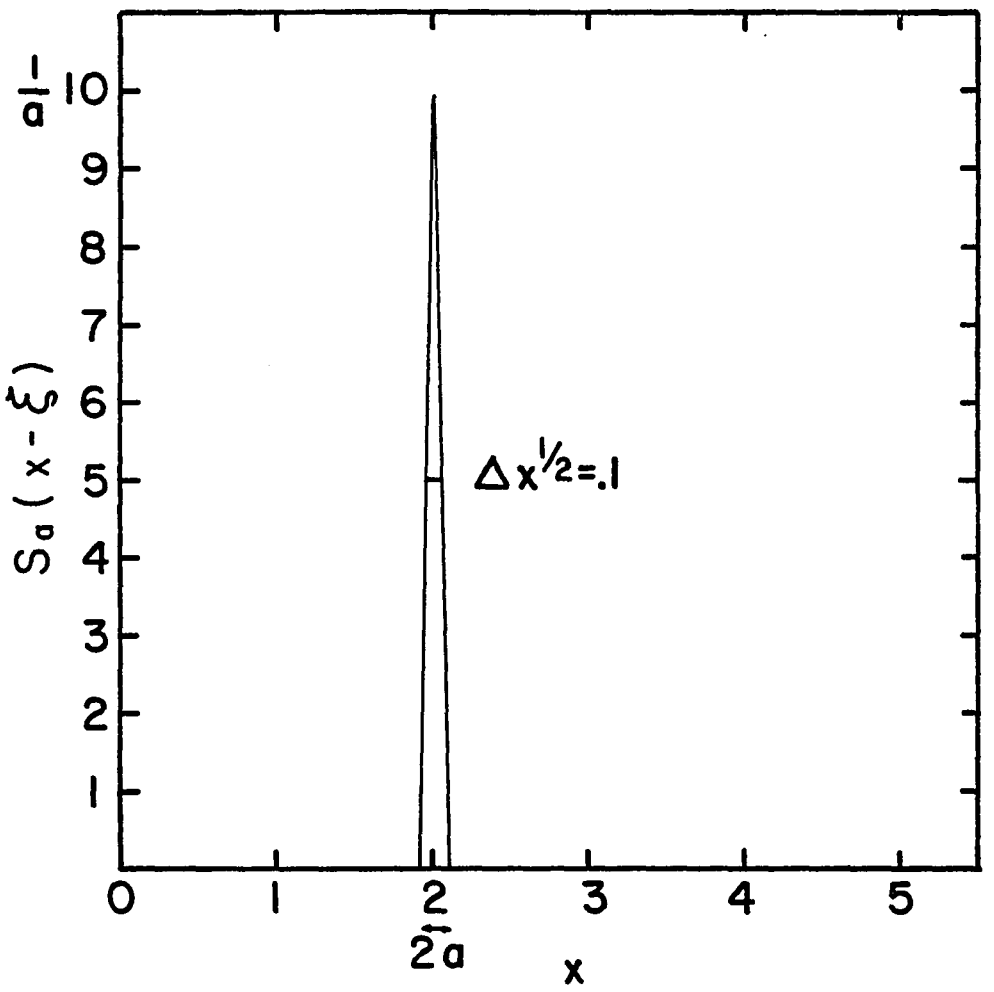

Figure 4. The test function $S_a(x-\xi)$ used to analyze the resolving power of the inversion algorithm.

$$g_i = \int_0^\infty S_a(x - \xi)\, K_i(x)\, dx = K_i(\xi)$$

for finite a as well.

In the following sections, x will represent log r (r is the aerosol particle radius) and f(x) will represent dN/(d log r). For the purposes of the present discussion, x will be defined as $x = \log r/10^{-8}$, so that for $10^{-8} \leq r \leq 10^{-3}$ cm we have $0 \leq x \leq 5$. With 50 equally spaced intervals $\Delta x = .1$, $S_a(x - \xi)$ has the appearance shown in Figure 4. The functions $S_a(x - \xi)$ are inherently high-frequency entities. In a spectral sense, the ratio $R \sim (2\Delta x)/5$ determines the high-frequency components necessary to reproduce the function $S_a(x - \xi)$. Upon inversion, some of the higher frequency components will be removed and the $S_a(x - \xi)$ functions degraded. The results of inverting $g_i = K_i(\xi)$ for various $S_a(x - \xi)$ are shown in Figure 5. The resolution is best at $\xi = 2$ ($r = 10^{-6}$ cm) with a half width of .19, i.e., about $2\Delta x$. [The half width of $S_a(x - \xi)$ being Δx.] For $\xi = 3$ ($r = 10^{-5}$ cm), $S_a(x - \xi)$ is poorly retrieved with a half width of .55, about $5\Delta x$. Hence from both the point of view of the theoretical knowledge of the $K_i(x)$ and the resolving power of the inversion procedure, the size distributions obtained are most reliable in the range from 10^{-7} to 10^{-5} cm, the highest resolution of structural features being obtained in the range from 10^{-7} to 10^{-6} cm, where a structural feature of about .2 decade is resolvable.

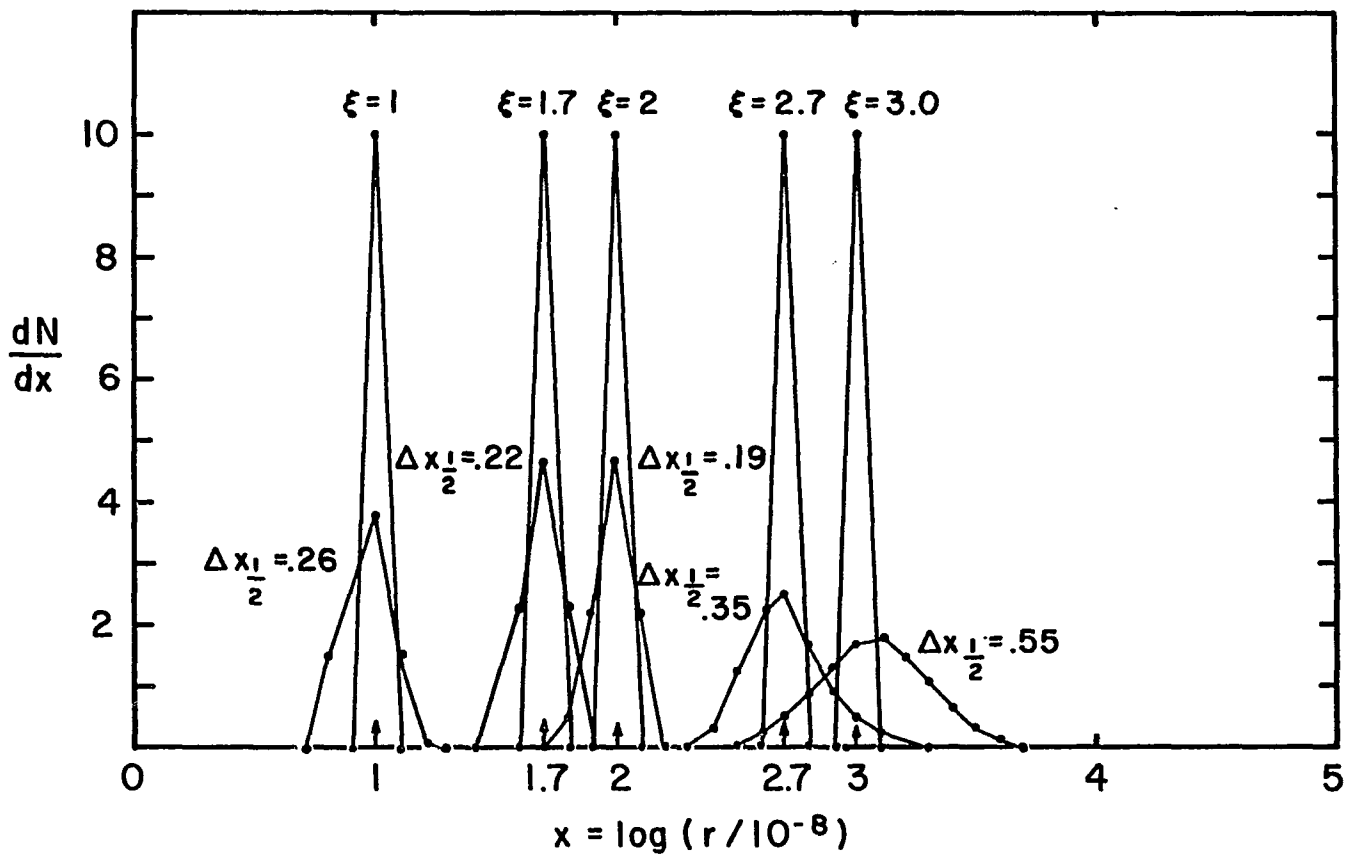

Figure 5. The retrieved "delta functions" for various values of ξ.

The curves are labeled according to their various half-widths. The test functions $S_a(x-\xi)$ are also shown for comparison.

Experimental Arrangement

Experimental Procedure

The schematic diagram Figure 6 shows the equipment used for the size distribution measurements. The essential components are the storage bag (1), the filter holder (2), and the Pollak counter (3). Because of the variability of particle concentration in natural samples, it is evidently not practical to draw outside air directly into a counter via the filter holders in an experiment of this sort. For this reason, a large 200-liter aluminized Mylar bag was used as a storage reservoir for sample air. The filling of this bag from the outside was carried out as quickly as possible through a large diameter stainless steel intake tube. The air from the storage reservoir was then introduced into the Pollak counter via one or another of the filters contained in the filter holder. Frequent samples were also taken through a "blank" filter holder which contained no Nuclepore filters and was used as a zero reference. In a typical experiment, some 5 or 6 zero measurements would be taken at different times during the progress of the experiment, while each of the other four Nuclepore filters contained in the remaining four filter holders was used in transmission at flow rates of 1, 2, 4 and 8 liters per minute. The result of such a sequence of measurements consists of a number of direct (unfiltered) counts at various times plus the filtered measurements which serve in combination as inputs to the inversion procedure. For every measurement, it was necessary to flush the Pollak counter with a liter or more of sample air. The time taken to do this at the lower flow rates plus the necessary operating and

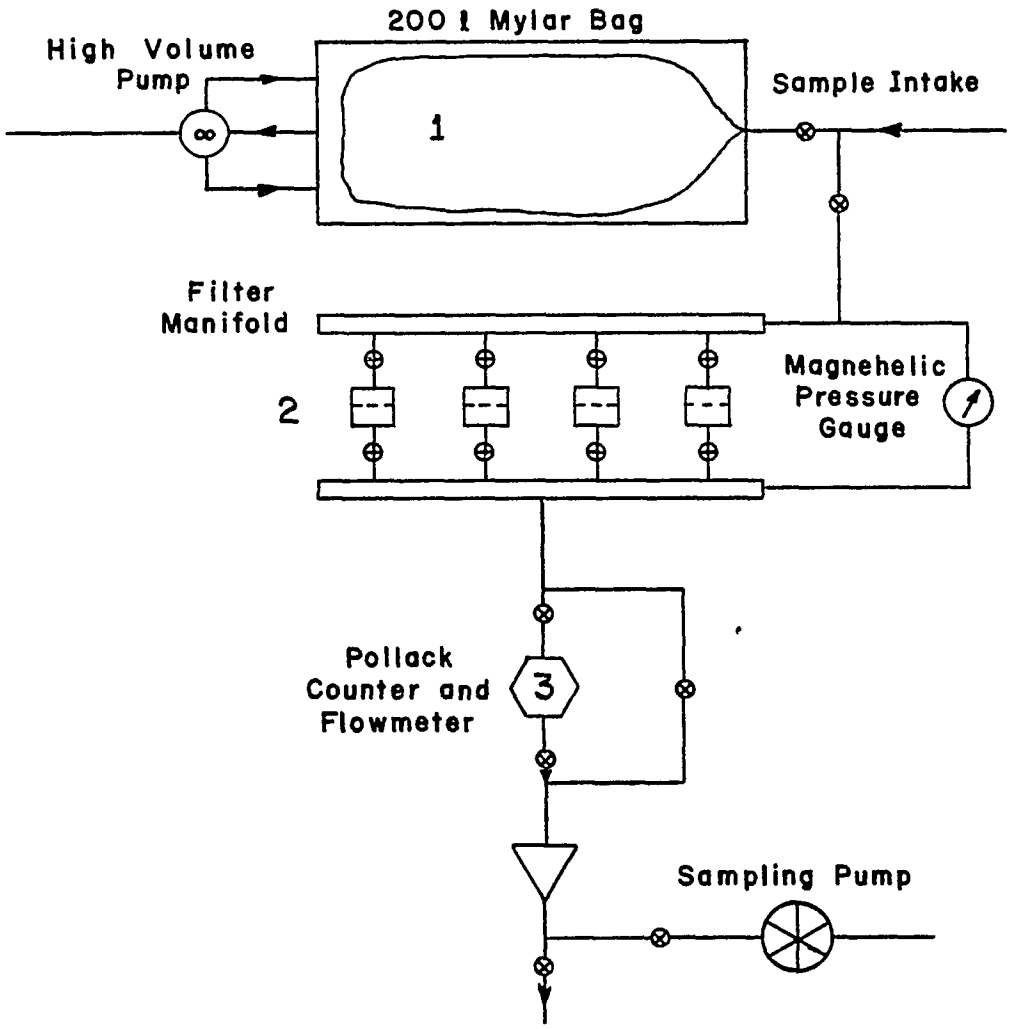

Figure 6. Diagram of the Nuclepore filter arrangement.

Samples are stored in the mylar bag and then blown or pulled through the filters at different flow rates.

waiting time involved in operation of the Pollak counter caused roughly one minute to be consumed by each such measurement. In order to make five or so zero measurements, plus measurements at four flow rates through each of four Nuclepore filters, a total time of at least 20 minutes was involved. That is clearly undesirable, but there was no way in which it could be avoided. An attempt was made to minimize the effect of particle loss during storage by always carrying out first those measurements which involved filters which transmitted the smaller particles in appreciable proportions. In other words, the filter which transmitted the smallest particles was used first, and the last filter used was that for which the transmission cutoff occurred at the largest size. Flow rate was monitored by measuring the differential pressure drop across a length of precision tubing used as load and applying the Pouissille formula to determine the flow rate. These measurements were cross-calibrated against flow meters of good quality. The Nuclepore filters were clamped between O-rings in individual filter holders which were arranged in parallel in combination with valves by means of which any one of the filter holders could be selected. Stainless steel inlet and exit manifolds were placed immediately before and immediately following the filter holders to insure (so far as possible) that the flow paths through each filter holder and filter combination were identical. The filters themselves were changed frequently, and the pressure drop across the filters was also monitored, as this is a sensitive indication of any appreciable clogging of the filter pores. The lines through which the air flowed were stainless steel tubes, and

some care was taken to insure that the length of runs through the tubing was kept as short as possible. The length of tubing from the storage bag to the Pollak counter via the filters was approximately 100 centimeters. The Pollak counter was operated in the manner recommended by Metnieks and Pollack (1959), with the exception of the waiting period. For that Pollak specified one minute, but a series of experiments in which the same air was observed using different waiting periods suggested that the waiting period could safely be reduced to 10 seconds without causing any change in the reading obtained from the instrument. The shorter waiting period was used throughout the measurements which are to be described. In a typical experimental run, the range of concentrations which were recorded through the various filters covered approximately two decades. For example, with an initial particle concentration of 20,000 cm^{-3}, the particle concentrations measured emerging from the finer Nuclepore filters at the lower flow rates might be one or two hundred cm^{-3}.

Treatment of Storage Losses

The loss of aerosol to the walls of the storage bag is a problem which had to be accounted for in order to obtain an acceptable degree of agreement between the calculated and measured g_i. The storage losses have been corrected for [see Twomey (1976) and Twomey and Zalabsky (1978)] by including in the kernels a time dependent decay term as follows:

$$g_i = \int_{x_L}^{x_U} K_i(x)\, e^{-\eta D(x) t_i}\, f(x)\, dx.$$

Here D(x) is the particle diffusion coefficient and η is an empirically determined decay parameter. In practice η is determined by carrying out the inversion for various values of η and choosing the value which gives the best agreement between the calculated and measured g_i. The insensitivity to the value of η of the f(x) obtained on inversion has been clearly demonstrated by Twomey (1975).

Results

Typical Data Set

For purposes of illustration, a typical data set, along with the volumetric flow rates and filter data, is shown in Figure 7.

Tucson Samples

Size distributions obtained under fair-weather conditions in a somewhat polluted urban environment (samples taken on the campus of The University of Arizona in Tucson) are shown for various total particle concentrations in Figures 8 and 9. Several distributions taken when the air was filled with dust raised by strong winds are shown in Figure 10. The total number of Aitken nuclei did not significantly increase under these conditions; in fact, the number of small nuclei tends to be lower. The modal radius is essentially unaffected, but these distributions do tend to fall off appreciably more rapidly between .01 and .1 μ than is usually the case. On the dusty days, the total nucleus counts averaged some 18,000 cm^{-3} vs. and average of some 29,500 cm^{-3} under fair-weather conditions. The somewhat lower total counts could be explained by diffusive loss to the large wind-raised

Measurement No.		Q(cm^3s^{-1})	Time (min)	N(cm^{-3})
1	Filter 1	171.6	1.0	9866
2		85.81	6.0	7849
3		42.90	11.0	6074
4		24.20	17.0	4527
5	Filter 2	171.6	2.0	9044
6		85.81	7.0	6793
7		42.90	12.0	4763
8		24.20	19.0	3209
9	Filter 3	171.6	3.0	6291
10		85.81	8.0	4176
11		42.90	13.0	2571
12		24.20	21.0	1592
13	Filter 4	171.6	4.0	983
14		85.81	9.0	622
15		42.90	14.0	235
16		24.20	23.0	118
Unfiltered				
1		-----	0.0	11877
2		-----	5.0	10268
3		-----	10.0	9228
4		-----	15.0	8571
5		-----	25.0	6247

	Filter Data			
	1	2	3	4
Pore diameter (μ)	.95	2.7	7.0	4.5
Pore density (cm^{-2})	$2x10^7$	$1.8x10^6$	$1.0x10^5$	$3.7x10^5$
Thickness (μ)	11.	10.	7.5	8.0

Meas. No.	VFR* ($cm^{+3}s^{-1}$)	Meas. No.	VFR* ($cm^{+3}s^{-1}$)	Meas. No.	VFR* ($cm^{+3}s^{-1}$)	Meas. No.	VFR* ($cm^{+3}s^{-1}$)
1	171.6	5	171.6	9	171.6	13	171.6
2	85.8	6	85.8	10	85.8	14	85.8
3	42.9	7	42.9	11	42.9	15	42.9
4	24.2	8	24.2	12	24.2	16	24.2

*VFR = Volumetric Flow Rate

Figure 7. A typical set of filter data and volumetric flow rates used in a set of measurements.

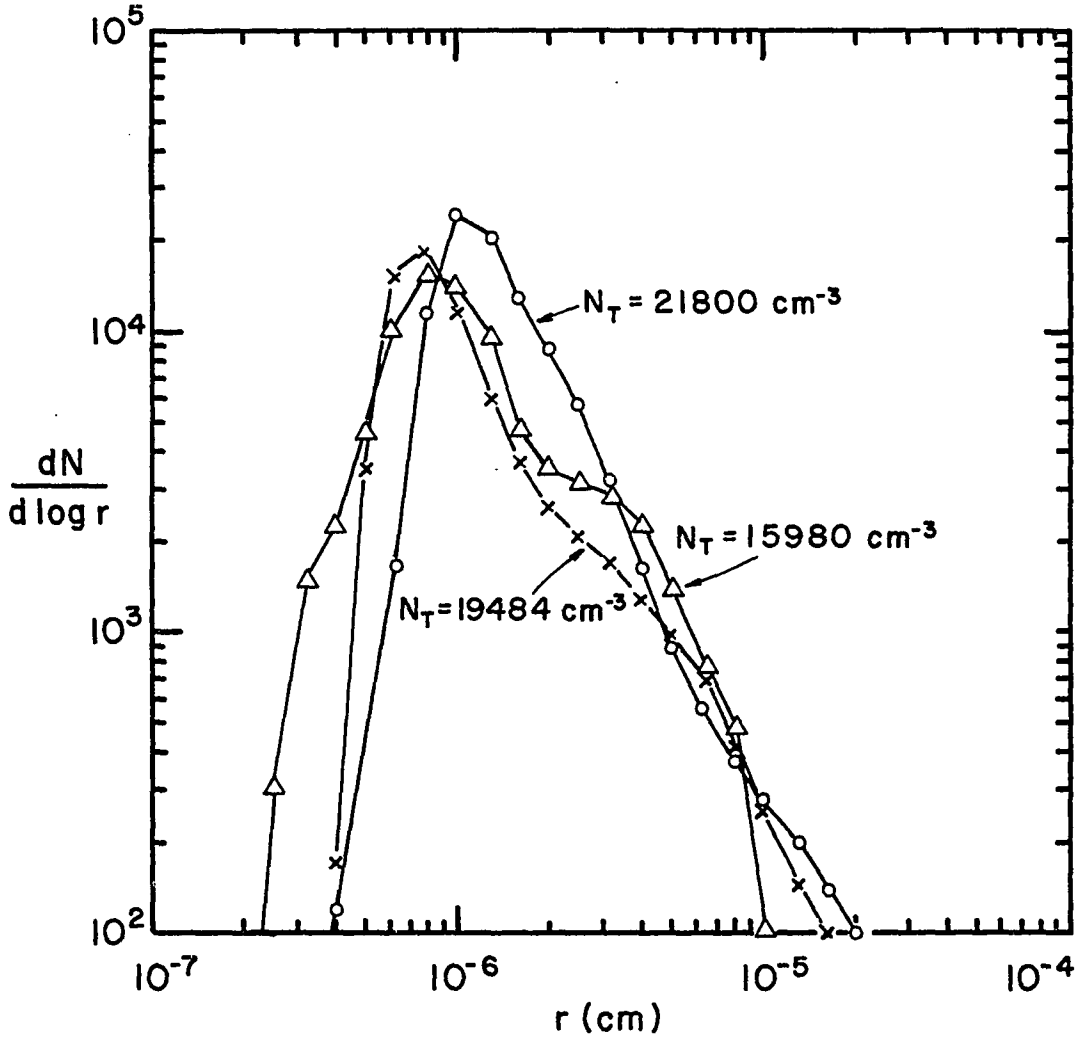

Figure 8. A typical set of Tucson size distributions with particle concentrations on the order of 1-2 x 10^4 cm^{-3}.

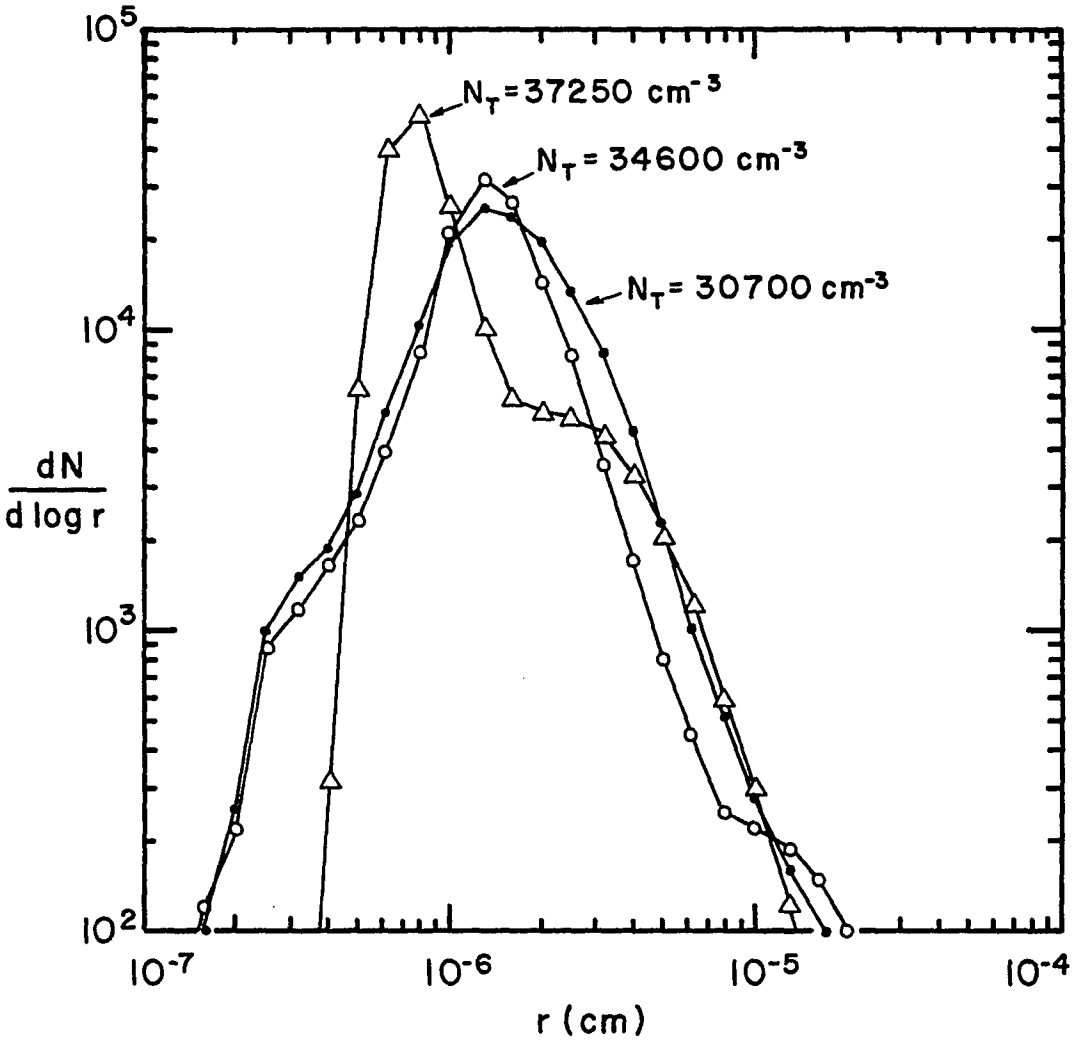

Figure 9. Tucson size distributions with particle concentrations on the order of 3-4 x 10^4 cm^{-3}.

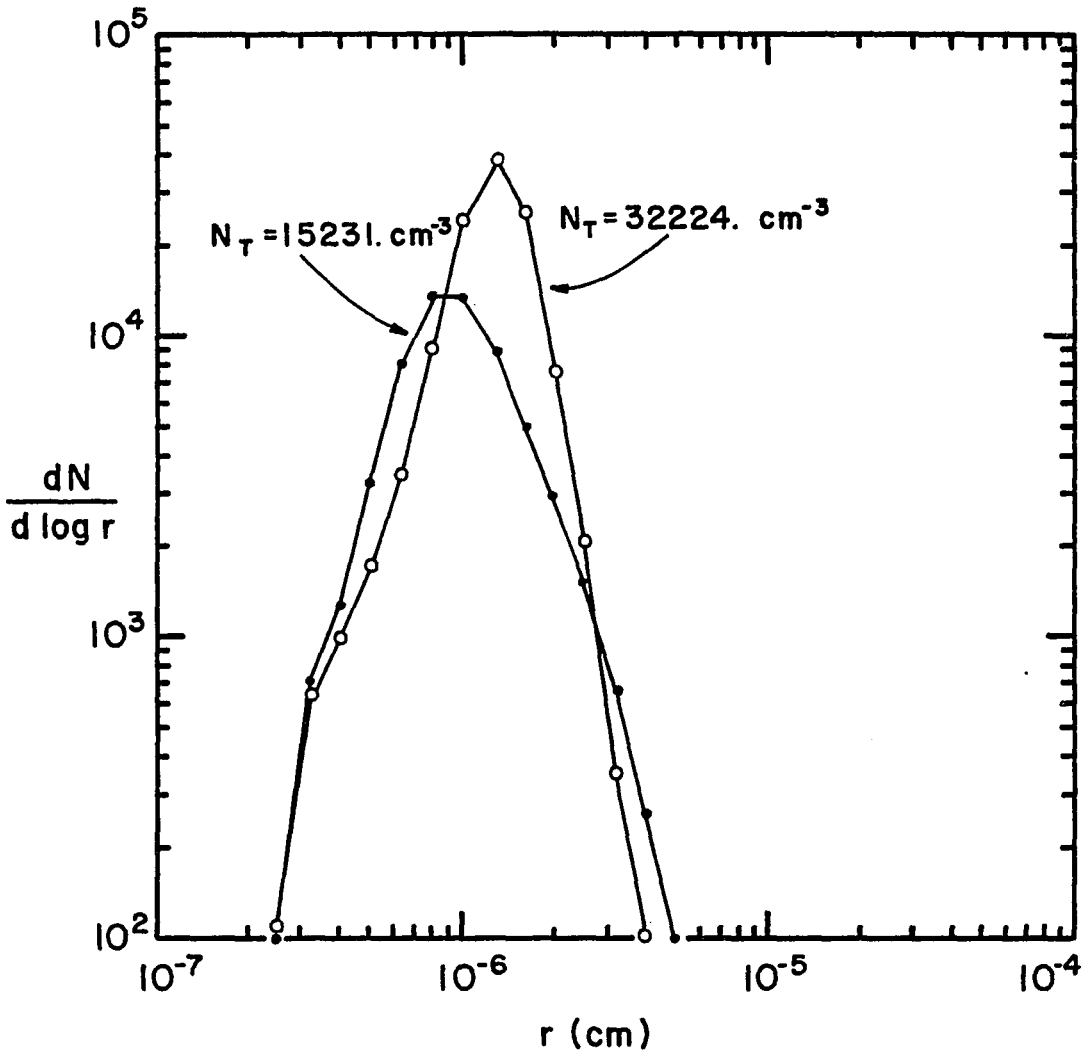

Figure 10. Several dusty day size distributions.

aerosol; however, it could also have been influenced by the air mass associated with the strong surface winds. (These dusty days were usually associated with strong polar outbreaks.)

Australian Samples

Size distributions obtained in clean, modified polar maritime air are shown in Figure 11. These measurements were made at a rural site in Southeastern Australia by Twomey (1976).

Comparison of Tucson and Australian Samples

Size distributions measured at these two quite different locations show marked similarities. In the Australian samples, the modal radii vary from 5×10^{-7} to 1.5×10^{-6} cm, with a Junge distribution prevailing down to about .02 μ. Again, however, these distributions turn over and fall rapidly for $r < .01$ μ. Few particles with radii less then 5×10^{-7} cm were present in either location (certainly much less than that predicted by a Junge distribution).

The primary result to be emphasized is, in fact, the apparent absence of any appreciable amount of aerosol material below 5×10^{-7} cm. radius. This raises some questions as to the reliability of this result, since such very small aerosol is readily lost by diffusion upon storage and sampling and in the Pollak counter during the waiting period, as to the ability of the Pollak counter to detect such small aerosol with efficiency, etc. The work of Nolan and O'Toole (1959) and of Peddar (1971) suggests that the Pollak counter can detect particles down to about .001 μ, so that too high an instrumental detection threshold

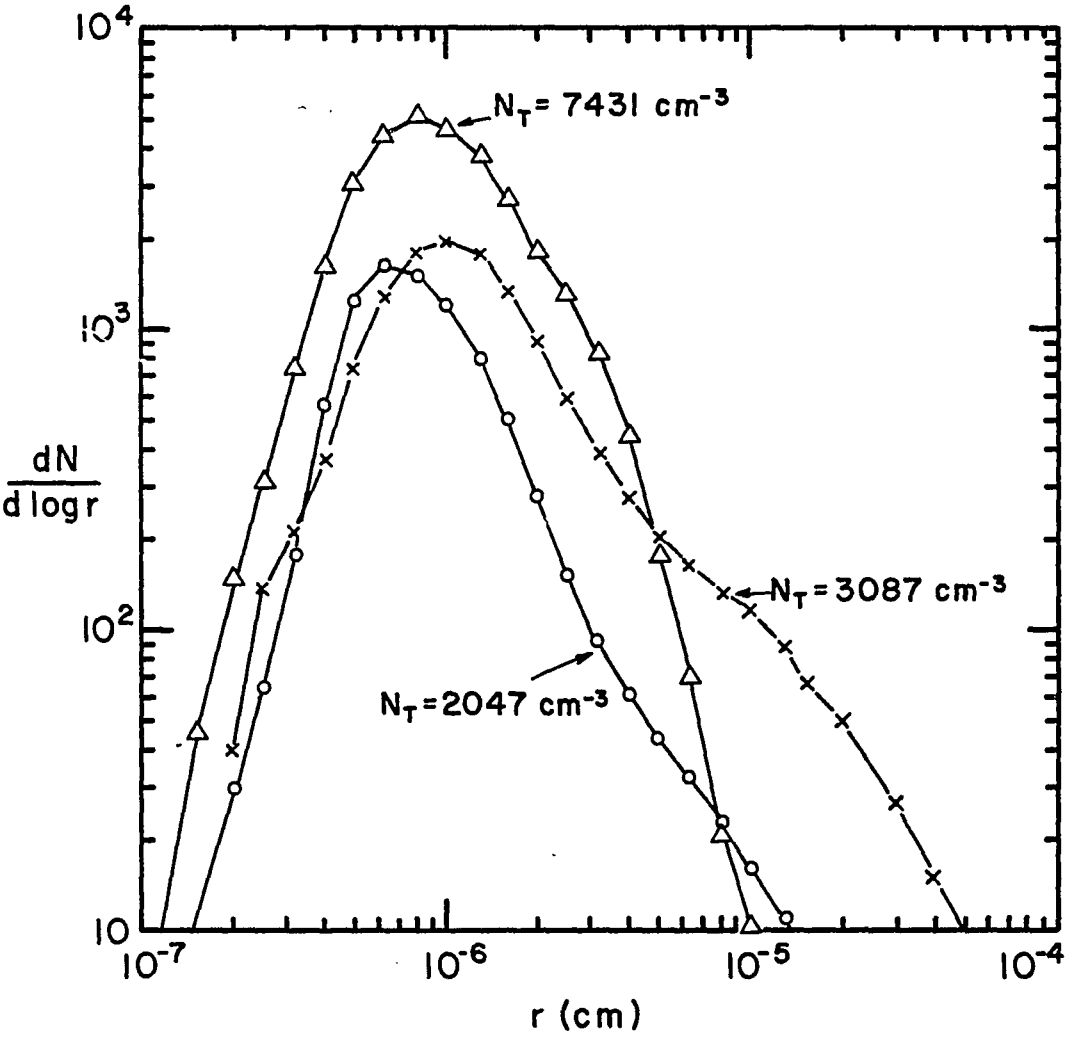

Figure 11. A set of Australian size distributions.

would not appear to be a problem. For appreciable loss within the counter in the 10-second waiting period, the particle diffusion coefficient would have to be on the order of .1 cm^2 s^{-1}, which is much larger than that for particles even with radii as small as .001 μ.

Photochemical Aerosols

In order to directly assess whether or not such small aerosol could be sized with the present experimental arrangement and inversion procedure, a photochemical H_2SO_4 aerosol was generated and sized. The H_2SO_4 aerosol was generated by photooxidizing SO_2 with 1850 Å UV radiation in a quartz photoreactor. The number and size of the generated nuclei were controlled by varying both the relative humidity and the reactor residence time. The aerosol-gas mixtures were stored in the 200-liter mylar bag and then sized using the filter technique. Shown in Figures 12 and 13 is the behavior of the particle number during storage and the resulting size distributions after 10 minutes of storage. The photochemical aerosol so produced is highly monodisperse with a modal radius of .004 μ cm and with little aerosol larger than .006 μ. By reducing the reactor residence times, size distributions with modal radii as small as .003 μ cm could be obtained. The filter sizing technique appears to be capable of sizing small aerosol quite well, as these results indicate. In addition, these distributions indicate that the previously discussed theoretical resolutions are obtainable with measured data. The theoretical half width at 5 x 10^{-7} cm is .2 decade, while the half widths of these highly monodisperse distributions are also about .2 decade.

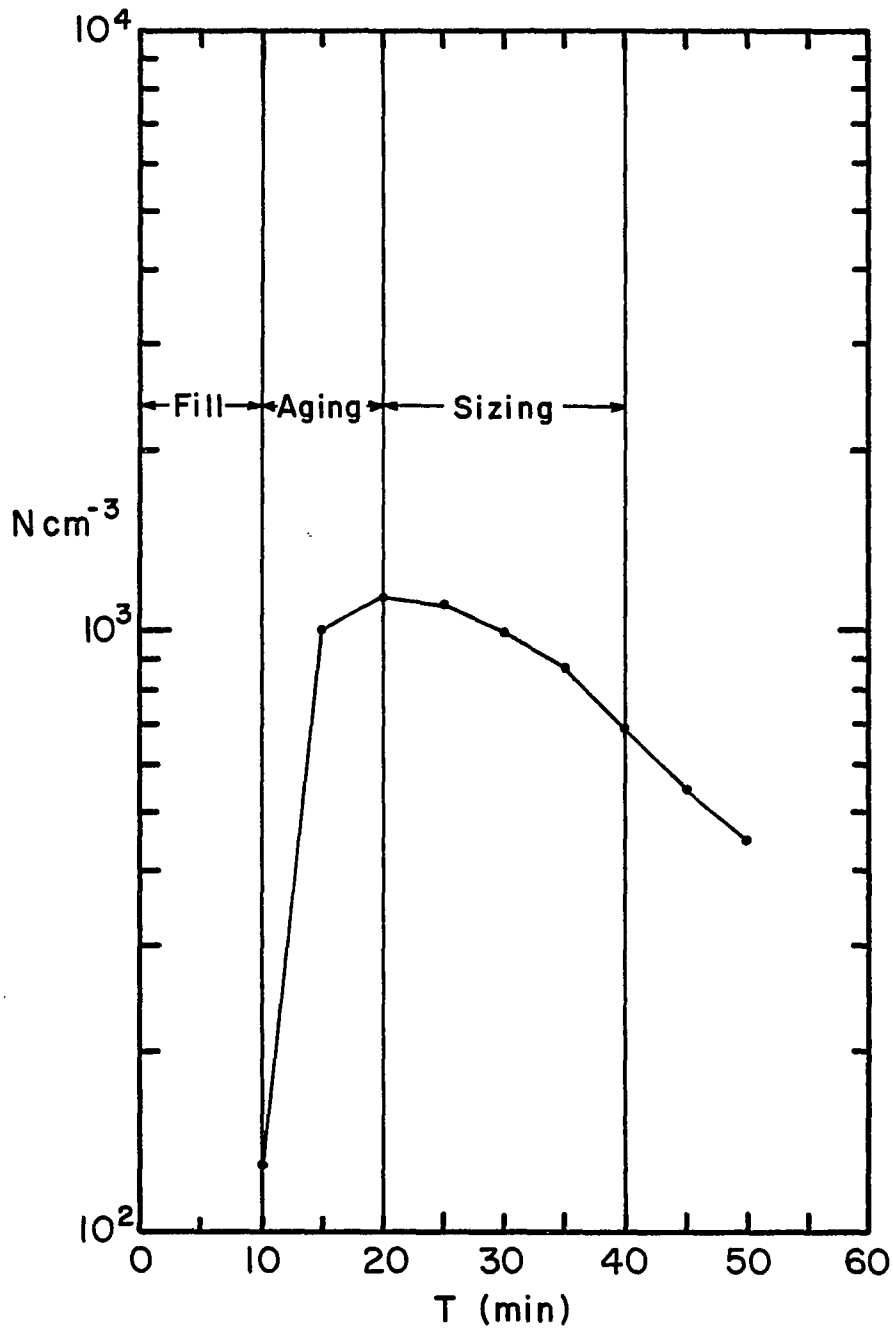

Figure 12. Behavior of a photochemical H_2SO_4 aerosol stored in the mylar bag.

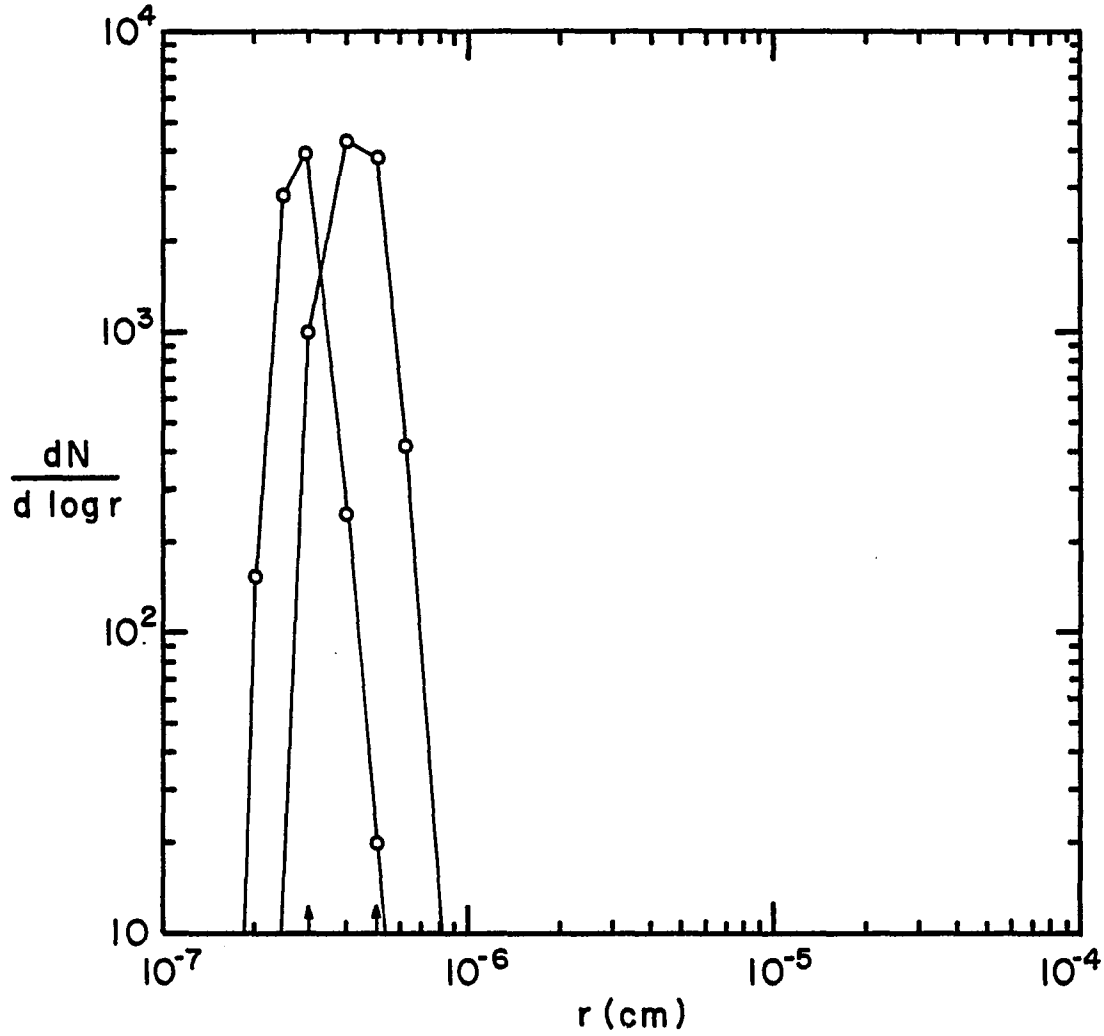

Figure 13. Photochemical H_2SO_4 aerosol size distributions.

Comparison with the Whitby Aerosol Analyzer

The filter technique was compared directly with a Whitby (Thermal System Inc.) Electrical Mobility Analyzer. Outside air samples were stored in a 200-liter aluminized mylar bag. The Whitby analyzer was used to obtain size distributions before and after sizing with the filter technique. A photochemically generated aerosol was also sized. The two techniques were compared over the .0065 to .067 μ region. The results are shown in Figures 14 and 15. The two techniques are in good agreement from .007 to .04 μ. The secondary peak consistently observed by the Whitby at larger sizes ($r \sim 5 \times 10^{-6}$ cm) is the major difference between the two distributions. The occurrence of this peak in the photochemical aerosol seems highly unlikely, however, so that one suspects that the secondary peak may be an artifact. The lowest two channels of the Whitby proved unreliable, so that it was not possible to directly compare the distributions for radii less than .0065 μ.

Summary and Conclusions

1. The multiple filter sizing technique is a useful tool for determining aerosol size distributions in the .001 to .1 μ region. Features of the size distributions with half widths greater than or equal to about .2 decade are resolvable with the filter characteristics (kernels) and inversion procedure currently in use. The filter and electrical mobility analyzer (Whitby) are in reasonable agreement over the .007 - .04 μ region. The discrepancies between .04 - .067 μ have yet to be resolved.

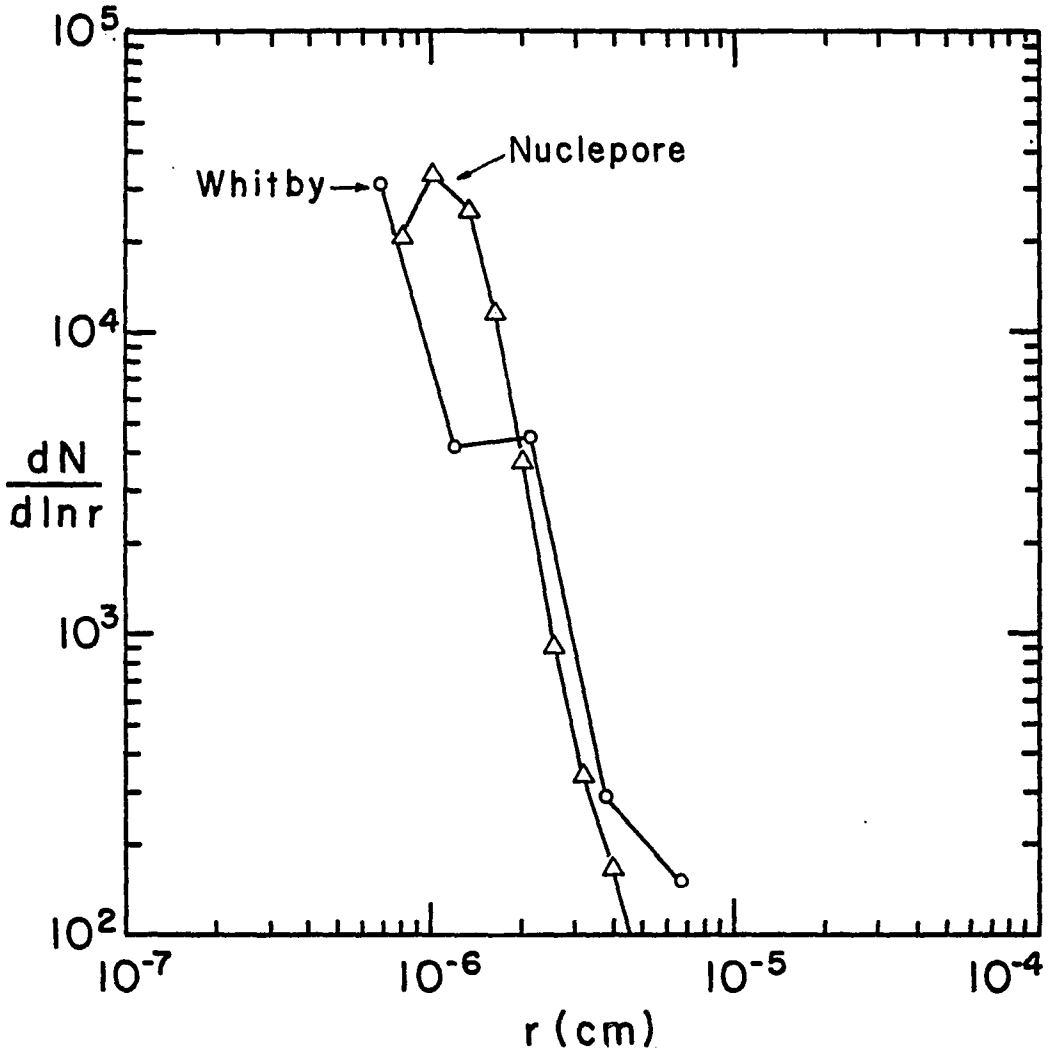

Figure 14. Size distributions of a photochemical aerosol taken with the Nuclepore filters and with the Whitby Aerosol Analyzer.

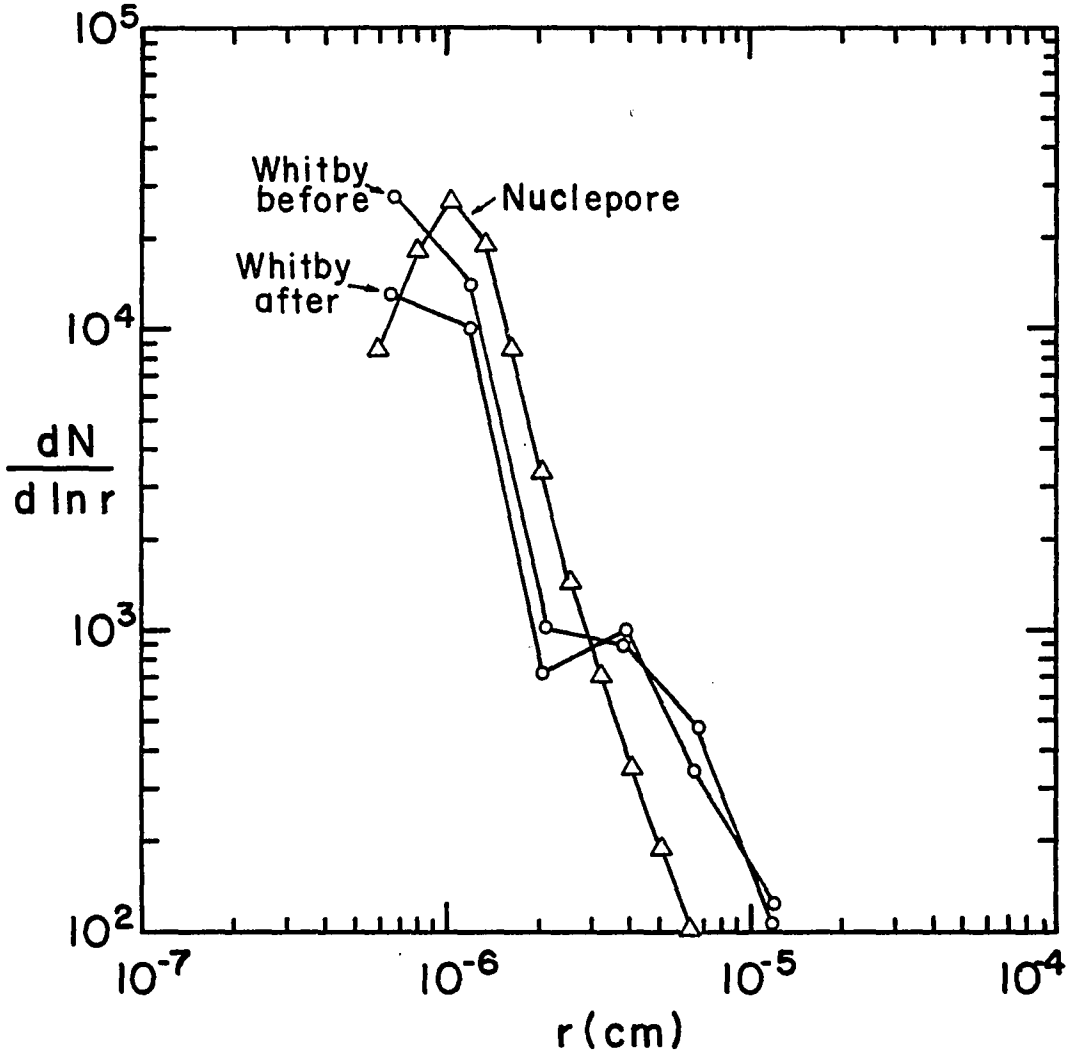

Figure 15. Size distributions of the ambient aerosol taken with the Nuclepore filters and the Whitby Aerosol Analyzer.

2. Size distributions measured in clean rural air in Southeast Australia and in more polluted air in Tucson, Arizona, show marked similarities. Both have modal radii ranging between .006 and .015 μ. In both cases, the distributions turn over and fall rapidly with diminishing size for particle radii less than .01 μ. For both sampling locations, a Junge distribution is reasonably valid down to .02 - .03 μ but does not hold at all for smaller sizes.

3. The .001 - .005 μ region does not appear to contain any appreciable amount of aerosol material in atmospheric air in either location. The presence or absence of such aerosol in the atmosphere is a matter of fundamental interest, since one would expect that newly formed aerosol (e.g., aerosol arising via gas-to-particle conversion) would be initially in this size range. Subsequent condensational growth and coagulation with existing aerosol will remove the newly formed aerosol. The rate of condensational growth cannot be evaluated without detailed knowledge of the physiochemical properties of the aerosol-gas mixture; one can, however, easily estimate the average lifetime of the newly formed (very small) aerosol due to coagulative removal mechanisms alone. To a good approximation, $\langle t_s \rangle_x \simeq Ka_x^{-1}$, where $Ka_x = \int_0^\infty n_a(y)\, K(x,y)\, dy$ and $n_a(y)$ is the existing aerosol size distribution. (See Appendix A for details.) Figure 16 presents $\langle t_s \rangle_x$ for various particle sizes (x) for a typical Australian and Tucson size distribution. Figure 17 shows the average survival times for newly formed nucleogen molecules as a function of the accommodation coefficient. For perfect accommodation ($\alpha = 1$), a nucleogen molecule

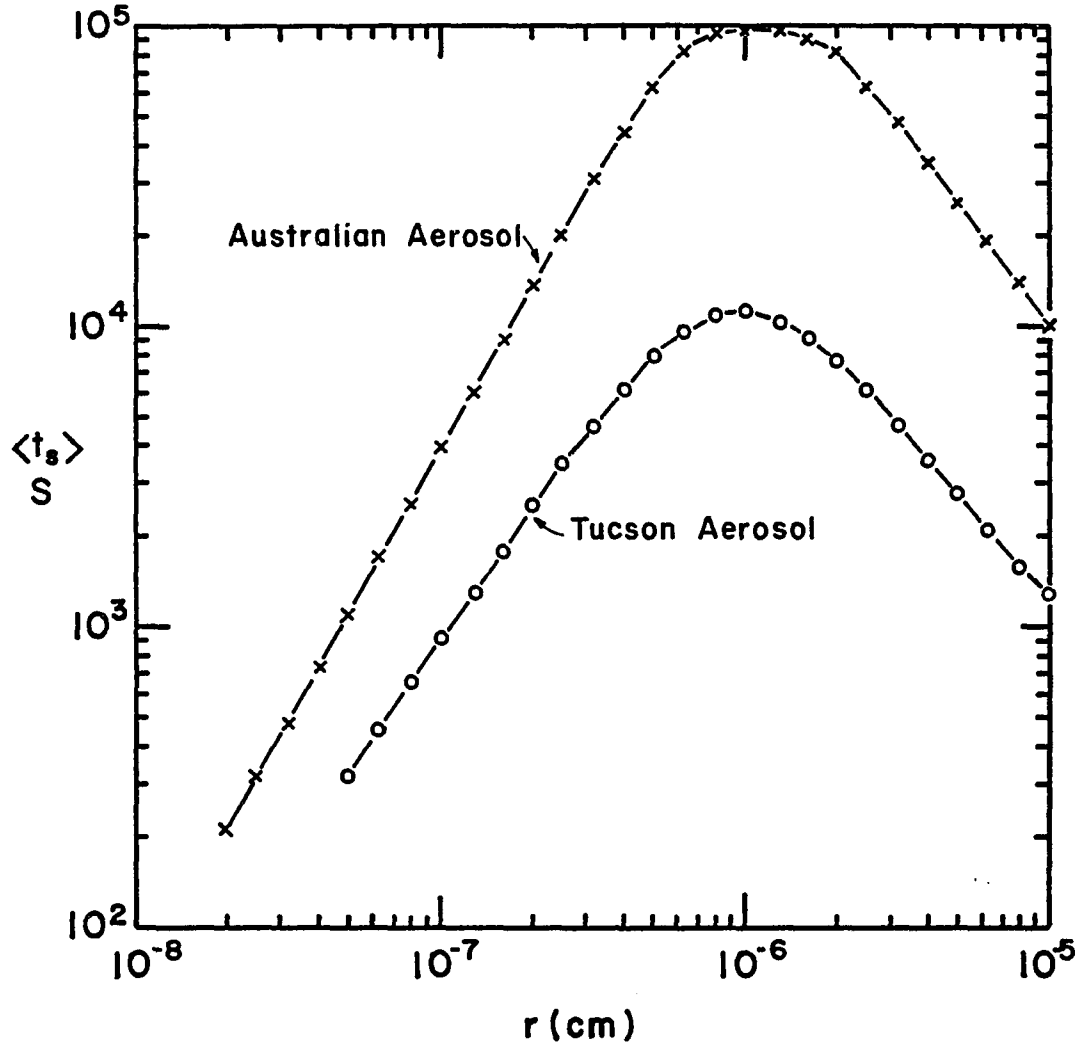

Figure 16. Average survival times of newly formed particles in the presence of the existing aerosol.

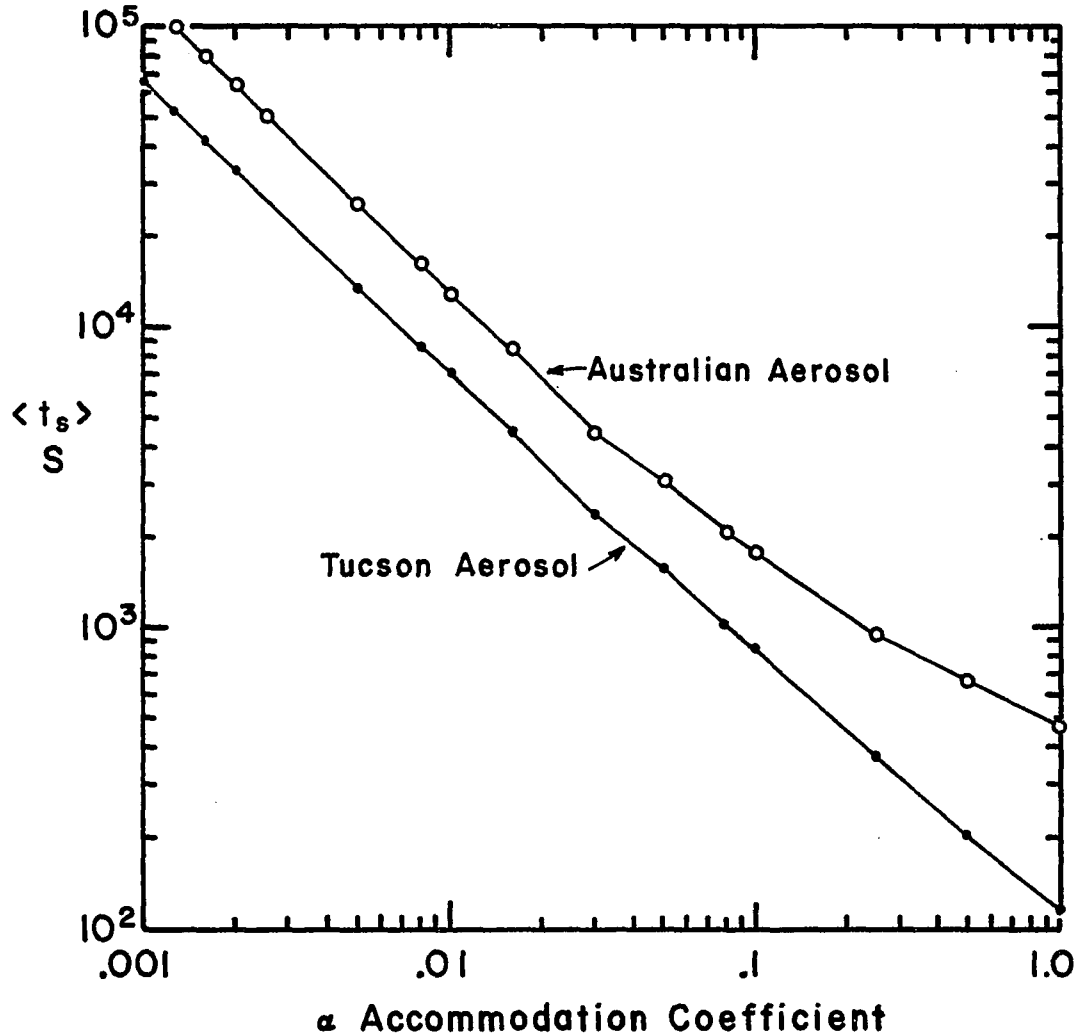

Figure 17. Average survival times of nucleogen molecules in the presence of the existing aerosol.

survives on average only several minutes in the presence of the aerosol already present in the Tucson environment. This result will be of particular importance with regard to the photochemical nucleus formation to be discussed in Chapter 4.

4. The measurement of a large number of size distributions in the Tucson environment (specifically, two distributions per day were taken 12 hours apart for a period of two months) indicates that these distributions are markedly persistent in time, with no appreciable changes in shape being observable on time scales at least on the order of days. This fact will be of importance in conjunction with the discussions of the mass transport and photochemical nucleus formation presented in the following chapters.

CHAPTER 3

THE AEROSOL MASS TRANSPORT

Coagulation is constantly transporting aerosol mass from smaller to larger size domains within the aerosol size distribution. In cloud-free regions of the atmosphere, i.e., in the absence of wet removal processes, the coagulative mass transport is the primary mechanism for removal of aerosol particles less than about .1 μ in radius. Particles less than .1 μ in radius probably arise primarily from gas-to-particle conversion within the atmosphere itself and from surface emissions, e.g., combustion, automobiles, etc. Apart from surface sources, many of which are anthropogenic in nature, gas-to-particle conversion is expected to constitute the major source for small particles. With gas-to-particle conversion functioning as the major source and coagulative mass transport the major small particle sink, it is not unreasonable to expect that something approaching a steady-state situation may be reached. Real aerosol size distributions cannot represent a steady-state situation over the entire size domain, but it is, nevertheless, of interest to inquire as to whether or not subranges exist within which the coagulative mass transport is constant or approximately so. By assuming that a particular size distribution represents an approximately steady-state situation, the mass transport, in conjunction with its divergence and convergence, allows for easy

identification of those size domains where sources and sinks, respectively, are operative, except in the unlikely event that particles of a given size are being produced and removed at balancing rates.

Derivation of the Basic Equations

Derivation of the Mass Transport Equation

By definition the mass transported from smaller to larger sizes across a reference value x of volume x is given at time t per unit time per unit volume by

$$\varepsilon(x,t) = - \rho_p \frac{\partial}{\partial t} \int_0^x u\, n(u,t)\, du,$$

ρ_p being the particle mass density and $n(u,t)$ the size distribution in volume space. If the transport divergence $\frac{\partial \varepsilon(x,t)}{\partial x} = 0$, then

$$- \rho_p \frac{\partial}{\partial t} \frac{\partial}{\partial x} \int_0^x u\, n(u,t)\, du = - \rho_p\, x \frac{\partial}{\partial t} n(x,t) = 0$$

i.e., $n(x,t)$ is constant for all x and the size distribution represents a steady state. In the subsequent discussion the transport is evaluated at a particular time, t_o, and $\varepsilon(x,t_o) \to \varepsilon(x)$ $n(u,t_o^-) \to n(u)$ $\frac{\partial}{\partial t} \to \frac{d}{dt}$ so that the working defintion is:

$$\varepsilon(x) = - \rho_p \frac{d}{dt} \int_0^x u\, n(u)\, du$$

which is to be understood as applying to a particular time t_o. The explicit integral expression for the mass transport is most directly obtained by a consideration of the u,v plane in volume space:

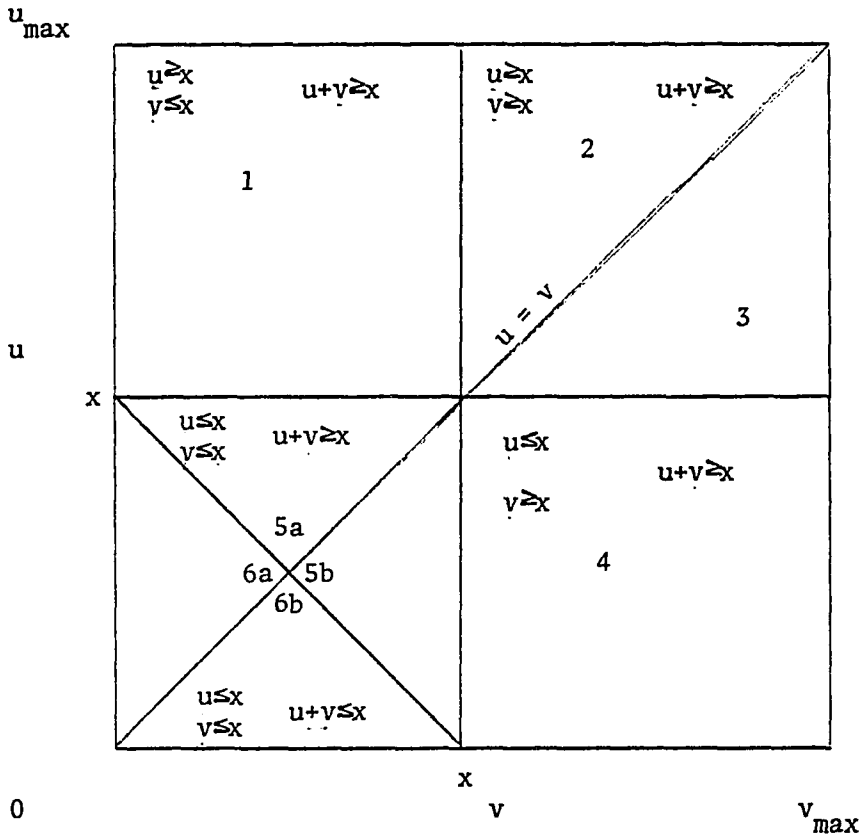

Each point in this plane represents a pair of particle volumes. By inspection, one can see that only in regions 1, 4 and 5 will coagulation result in aerosol mass being transported across x. In regions 1 and 4, a mass (volume) v,u respectively is transported, while in region 5a, mass u+v is transported. One may then write for the total time rate of change of the total mass of all particles with volume less than x:

$$\varepsilon(x) = \frac{\rho}{2}\int_0^x n(v)v\int_x^\infty n(u)\ K(u,v)^{1}\ du\ dv + \frac{\rho}{2}\int_0^x n(u)u\int_x^\infty n(v)\ K(u,v)^{4}\ dv\ du$$

$$+ \frac{\rho}{2}\int_0^x n(u)\int_{x-u}^x (u+v)\ n(v)\ K(u,v)^{5}\ dv\ du,$$

the factors of 1/2 being necessary because of the definition of coagulation coefficient being used here (see subsequent discussion). Since the first two integrals are identical and since the third integral is symmetric with respect to the u=v line, we may write:

$$\varepsilon(x) = \rho_p\int_0^x n(v)v\int_x^\infty n(u)\ K(u,v)\ du\ dv$$

$$+ \rho_p\int_{x/2}^x n(u)\int_{x-u}^u (u+v)\ n(v)\ K(u,v)\ dv\ du. \quad (1)$$

This equation can also be written in other coordinate representations; e.g., for volume (u), radius (r), and ℓn r space it is:

$$\varepsilon_v(x) = \rho_p\int_0^x n(v)v\int_x^\infty n(u)\ K(u,v)\ du\ dv$$

$$+ \rho_p\int_{x/2}^x n(u)\int_{x-u}^u (u+v)\ n(v)\ K(u,v)\ dv\ du$$

u

$$\varepsilon_r(r_m) = \frac{4\pi\rho_p}{3}\left[\int_0^{r_m} n(r) r^3 \int_{r_m}^{\infty} n(r')\, K(r,r')\, dr'\, dr + \int_{r_m/2^{1/3}}^{r_m} n(r) \int_{(r_m^3 - r^3)^{1/3}}^{r} (r^3 + r'^3)\, n(r')\, K(r,r')\, dr'\, dr\right]$$

r

$$\varepsilon(y_0) = \frac{4\pi\rho_p}{3}\left[\int_{-\infty}^{y_0} n(y)\, e^{3y} \int_{y_0}^{\infty} n(y')\, K(y,y')\, dy'\, dy + \int_{y_0 - [(\ln 2)/3]}^{y_0} n(y') \int_{[\ln(e^{3y_0} - e^{3y})]/3}^{y} (e^{3y} + e^{3y'})\, n(y')\, K(y,y')\, dy' dy\right]$$

$\ln r \qquad y = \ln r$

The terms of the mass transport equation have a straightforward physical interpretation. The first term represents the aerosol mass transported when a particle of volume v ($v \leq x$) coagulates with a particle of volume u ($u > x$) such that a volume v is transported across x. In the second term, both particles are individually smaller than x and their sum is greater than x, thereby transporting a volume u+v. Only in these two ways can aerosol mass be transported across x by coagulation.

In the present case, the numerical integrations were carried out in ℓn r space. The double integral was treated as an iterated integral using a trapezoid quadrature with 500 equally spaced intervals (Δ ℓn r = .023) from r = 10^{-8} to 10^{-3} cm, the range in radius of the aerosol size distributions.

Integral Equation for a Constant Mass Transport

The integral equation which must be satisfied by an aerosol size distribution which provides a constant mass transport is easily derived by setting the derivative of Eq. (1) equal to zero, that is:

$$\frac{1}{\rho_p}\frac{d\varepsilon(x)}{dx} = -\, n(x)\int_0^x n(u)u\,K(x,u)\,du + n(x)x\int_x^\infty n(u)\,K(x,u)\,du$$

$$-\, x\int_{x/2}^x n(u)\,n(x-u)\,K(u,x-u)\,du + n(x)\int_0^x (x+u)\,n(u)\,K(u,x)\,du$$

$$\frac{d\varepsilon(x)}{dx} = 0 \Rightarrow \text{for all } x$$

$$n(x)\int_0^\infty n(u)\,K(x,u)\,du = \int_{x/2}^x n(u)\,n(x-u)\,K(u,x-u)\,du \qquad (2)$$

The behavior of realistic coagulation coefficients makes it difficult to obtain an analytical solution to this equation; special cases of interest will, however, be discussed below.

Coagulation Coefficients

The $K(r_1,r_2)$ used here were essentially twice those given by Fuchs (1964). (See Appendix A.) The applicability of these coagulation coefficients in the difficult transition region between Stokes and free molecular conditions has been experimentally confirmed by Kerker (1972).

The Mass Transport for Several Hypothetical Cases

Constant Coagulation Coefficient

For a constant coagulation coefficient Friedlander (1960) deduced by dimensional analysis that a size distribution of the form $dn/(d\ \ell n\ r) = c_0 r^{-3/2}$, gave rise to a steady state in which mass transport was constant with size. For this special case, Eq. (2) may be integrated directly, yielding:

$$\frac{2}{\sqrt{x}}\frac{1}{\sqrt{x-u}}\Bigg|_{\lim u \to +x} = \frac{2}{\sqrt{x}}\frac{1}{\sqrt{u}}\Bigg|_{\lim u \to +0}$$

for

$$K(u,v) = K_c \qquad \frac{dn}{d\ \ell n\ r} = c_0 r^{-3/2} \qquad n(u) = \alpha u^{-3/2}$$

The equation is identically satisfied, but strictly so only in a limiting sense.

In order to examine end effects and to evaluate the constant itself, Eq. (1) was analytically integrated over the range $V_1 \leq x \leq V_2$, yielding

$$\varepsilon(x) = \frac{4\pi\rho_p K_c C_0^{\,2}}{27}\left[4\left(\frac{V_1}{V_2}\right)^{1/2} - 4\left(\frac{x}{V_2}\right)^{1/2} - 2\left(\frac{V_1}{x}\right) + 2\left(\frac{x}{V_1}\right)^{1/2}\right.$$

$$\left. - 2\left(\frac{x - V_1}{V_1}\right)^{1/2} - 4\sin^{-1}\left(\frac{V_1}{x}\right)^{1/2} + 2\pi\right] . \quad (3)$$

In the limit $V_1 \to 0$, $V_2 \to \infty$, $\varepsilon(x) = (8\pi^2\rho_p K_c C_0^{\,2})/27$, thereby explicitly evaluating the value of the constant. Equation (3) is plotted in Figure 18 in log r space for the range $10^{-8} \leq r \leq 10^{-3}$ cm. Also shown in this figure are the contributions corresponding to the two integrals in Eq. (1). For this special case, both terms make substantial contributions to $\varepsilon(x)$, and the two terms are individually constant. This special case also serves as a check on the accuracy of the numerical integration which reproduced the exact result to the third decimal place.

Realistic Coagulation Coefficient

The mass transport with realistic $K(r_1,r_2)$ for the Friedlander distribution law $dn/(d\ \ell n\ r) = c_0 r^{-3/2}$ is shown in Figure 19. With realistic coagulation coefficients, the mass transport now exhibits a constant value over only a narrow subrange, about 0.01 μ. Furthermore, the contribution of the second integral, $\varepsilon_2(x)$, is now considerably less than the first, i.e., transport arising via coagulation between two particles with volumes $u \leq x$, $v \leq x$, but such that $u + v > x$, is of lesser importance than for that of particles for which $u \leq x$, $v \geq x$. The same will be seen to be true for observed aerosol size distributions in the region $r \leq 0.01$ μ.

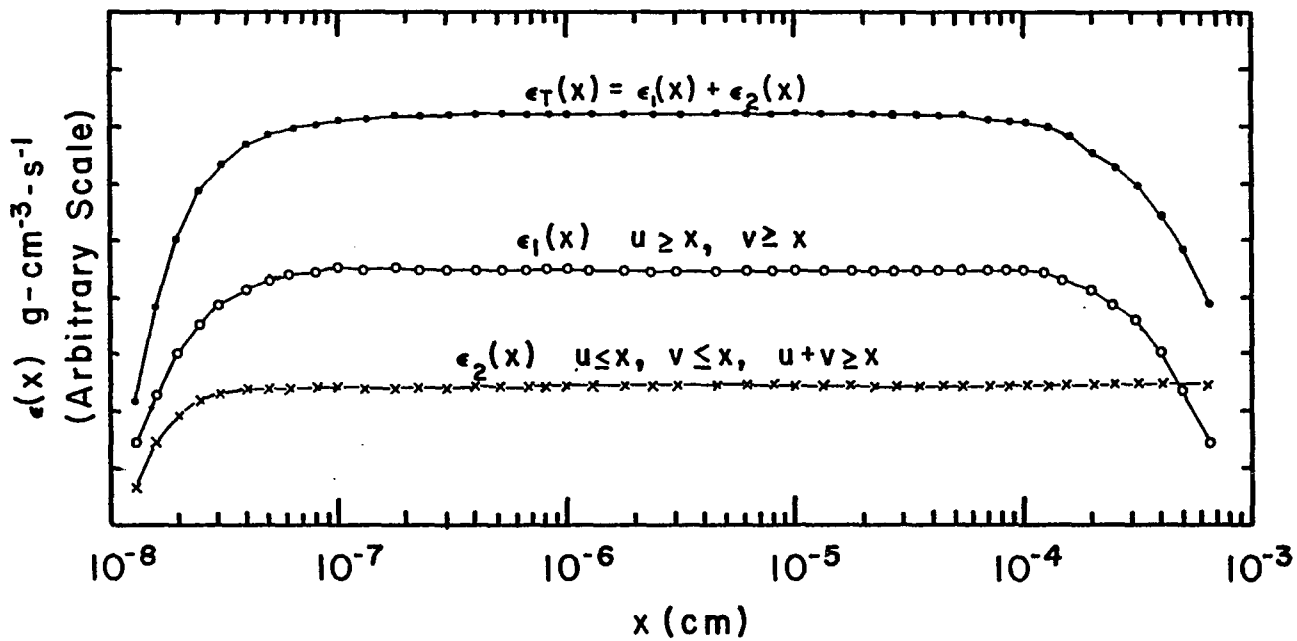

Figure 18. Mass transport for the ideal case $\frac{dN}{d\ell nr} = c_0 r^{-3}$ and $K(r_1, r_2)$ a constant.

The curve labeled $\varepsilon_1(x)$ corredponds to the first term of equation (1) and $\varepsilon_2(x)$ to the second term.

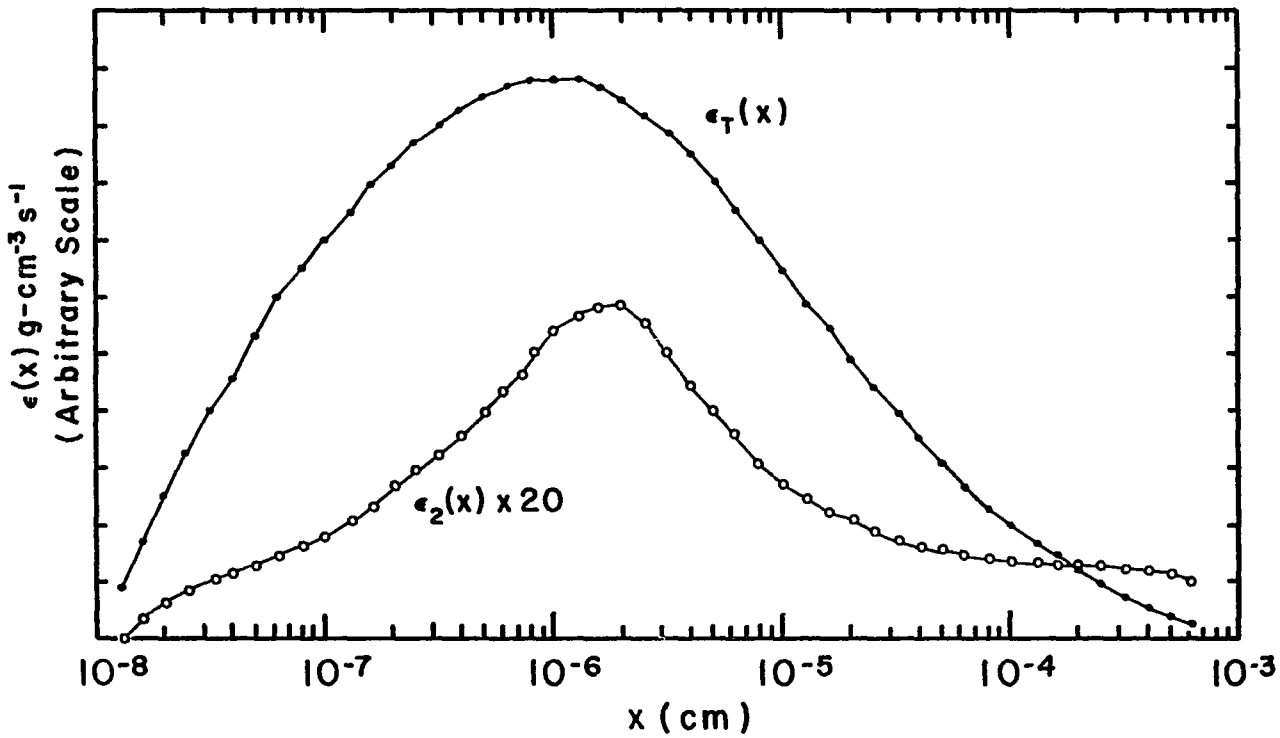

Figure 19. Mass transport for the hypothetical case $\frac{dN}{d\ell nr} = c_0 r^{-3/2}$ and realistic $K(r_1, r_2)$.

The curve labeled $\varepsilon_2(x)$ corresponds to the second term in equation (1).

The Mass Transport for Measured Aerosol Size Distributions

Arizona Samples

The authors have obtained a number of aerosol size distributions in dry, urban air in the desert Southwest (Zalabsky and Twomey 1974). Several size distributions characteristic of those measured on the campus of The University of Arizona in Tucson are shown in Figure 20. The associated mass transports are shown in Figure 21. The distributions are believed to be quite reliable up to 0.1 μ and reasonably so up to 1.0 μ (Twomey and Zalabsky 1978). For particles larger than 1.0 μ, the filter technique used here is no longer reliable so in order to assess the effect of particles greater than 1.0 μ in radius on the mass transport in the small size domain ($r \leq 0.1$ μ), a sensitivity test was done by assuming a Junge size distribution for $r \geq 1.0$ μ. A size distribution of the form $dn/(d \ln r) = N_0 r^{-3}$ was used to extend the measured distribution beyond 1.0 μ and the mass transport was recalculated. (See Figure 22.) For reasonable values of N_0, the transport was essentially unaffected up to 0.1 μ by the aerosol mass in the $r \geq 1.0$ μ region. The form of these size distrubtions is markedly persistent over time scales of at least days. To the extent that these distributions represent a steady state, maintenance of the size distributions demands a source in the $r \leqslant 0.01$ μ region and a sink at larger sizes for mass removal. The time scales (i.e., the coagulative residence times) for characteristic distributions are shown in Figure 23. The total mass in the $r \leqslant 0.01$ μ region would be transported out of that region

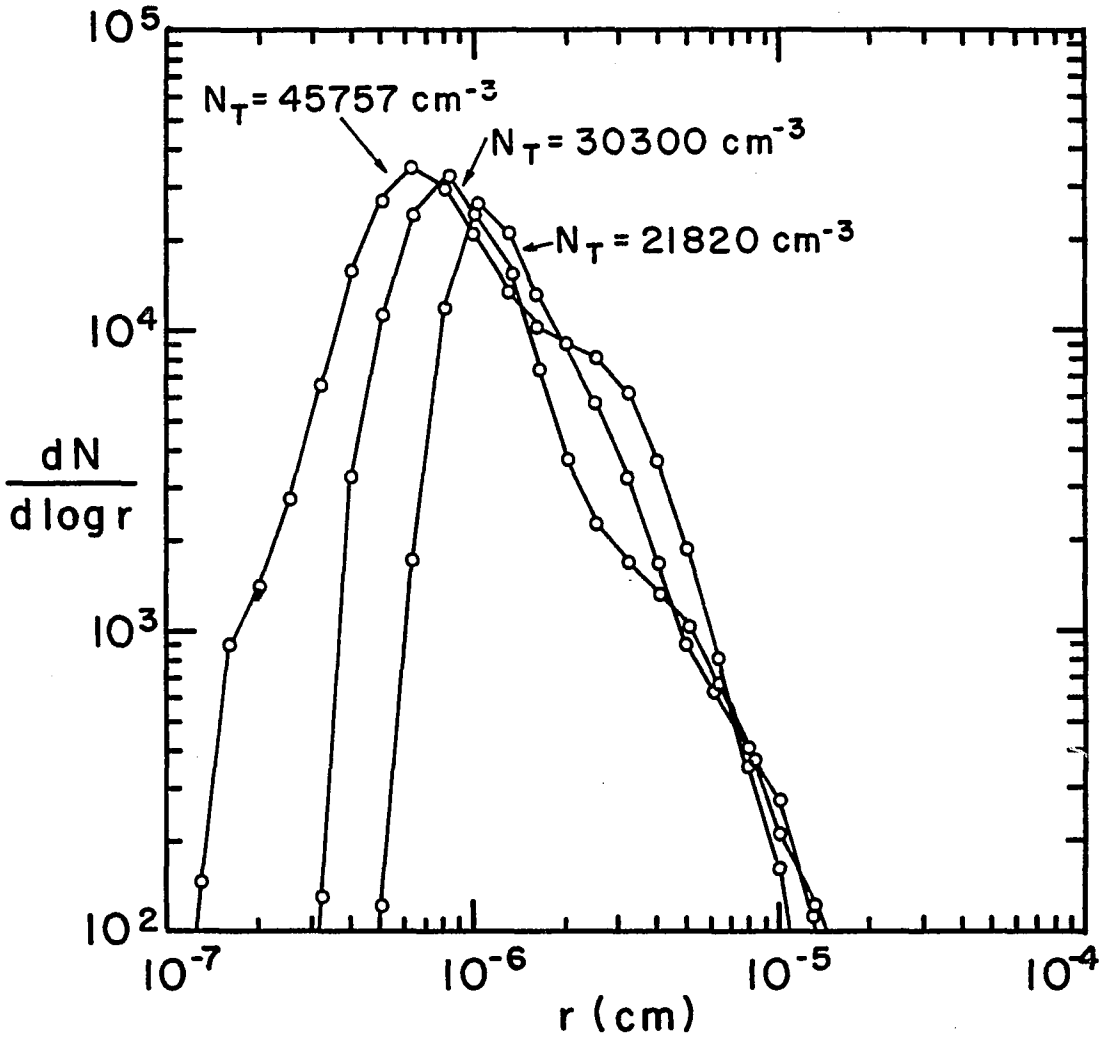

Figure 20. A set of Tucson size distributions corresponding to the mass transports in Figure 21.

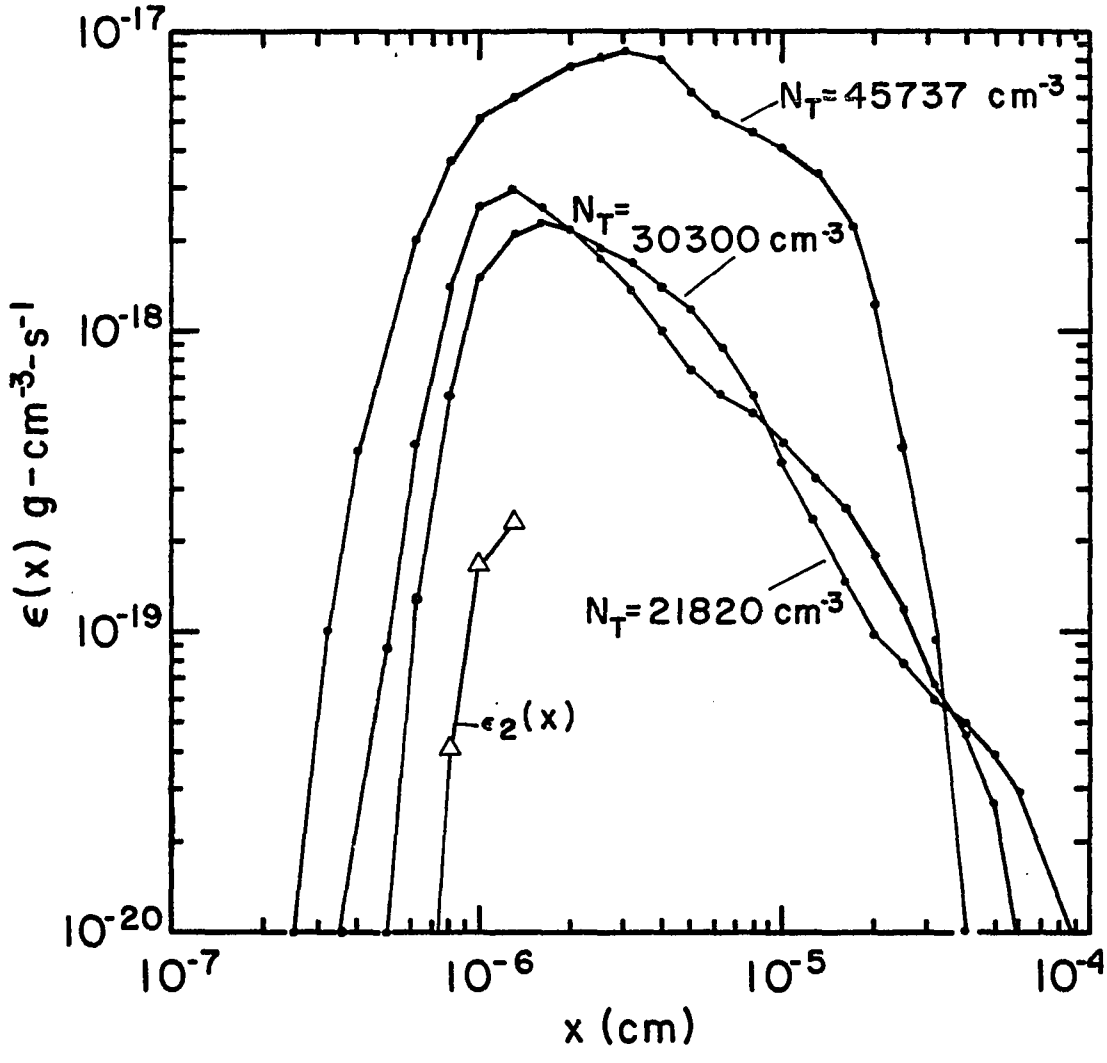

Figure 21. A set of Tucson mass transports.

The curve labeled $\varepsilon_2(x)$ corresponds to the N_T = 21820 cm^{-3} transport curve and illustrates the small contribution that $\varepsilon_2(x)$ makes to the total transport in the $r \leq .01\mu$ region.

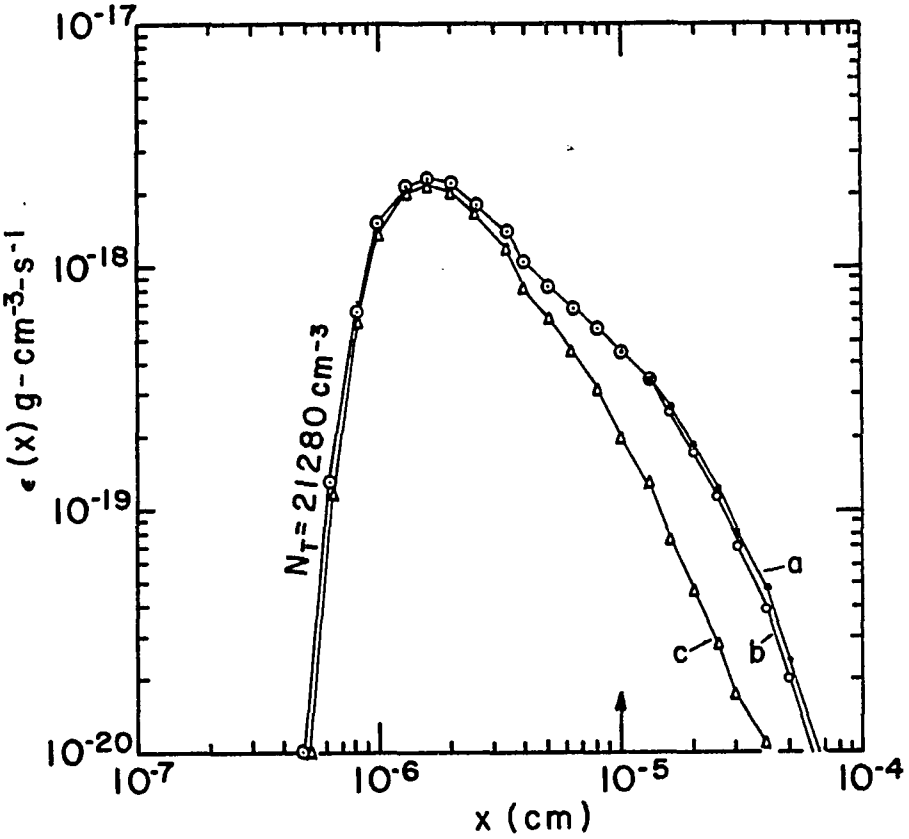

Figure 22. Sensitivity to the mass transport in the $r \leq .1\mu$ region to the aerosol size distribution in the $r \geq .1\mu$ region.

The curves are labeled as follows: a is the original transport, b was calculated using a realistic Junge distribution in the $r \geq 1\mu$ region, and c using a Junge distribution in the $r \leq .1\mu$ region.

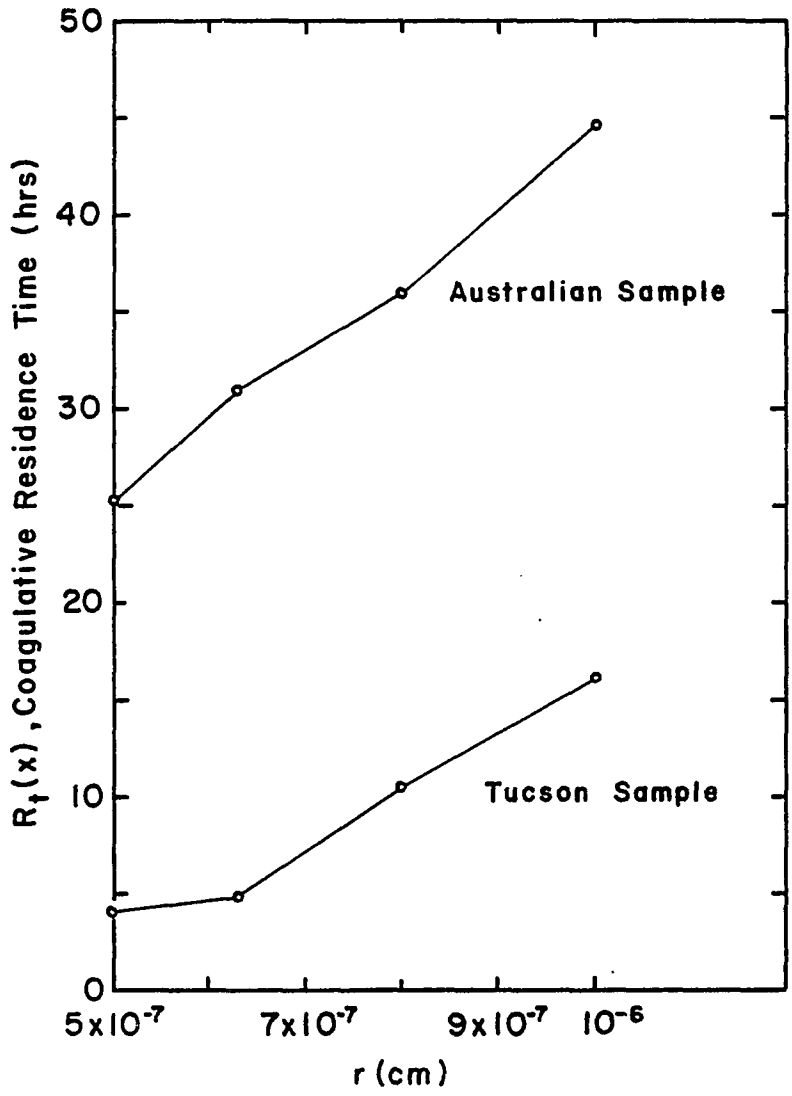

Figure 23. The coagulative residence time as a function of particle radius.

$R_t(x)$ is defined as

$$R_t(x) = \rho_p \int_0^x n(u)udu/\varepsilon(x).$$

in about 10-15 hr and the size distribution appreciably distorted by coagulation alone. Direct measurement of the distributions (in one case, 2 distributions a day were measured 12 hours apart for some two months) indicates that, apart from total number concentration (the total particle numbers varied from about 2×10^4 to 4.5×10^4 cm^{-3}), the size distributions are maintained on time scales of at least days. This, in turn, implies that new aerosol production in the $r \leq 0.01$ μ region must be operating on time scales of at most hours, in order that the size distributions be maintained. In these air samples, this aerosol may be replaced via gas-to-particle conversion within the atmosphere or by the surface sources present in the Tucson urban environment. Because these air samples are subject to local particle sources, they may not be entirely representative of dry, continental aerosol size distributions. Future plans are for a series of measurements in an area remote from urban influence (the mountains of the desert Southwest). They are of interest, however, for purposes of comparison with size distributions and mass transports in regions less susceptible to local particle sources, i.e., the Australian distributions to be presented shortly.

Australian Samples

Several size distributions measured in clean rural air in Southeastern Australia (Twomey 1976) are shown in Figure 24. These distributions do, on occasion, exhibit a region of constant mass transport. At the time of this study, only three distributions were available, but two of the three show an approximately constant transport

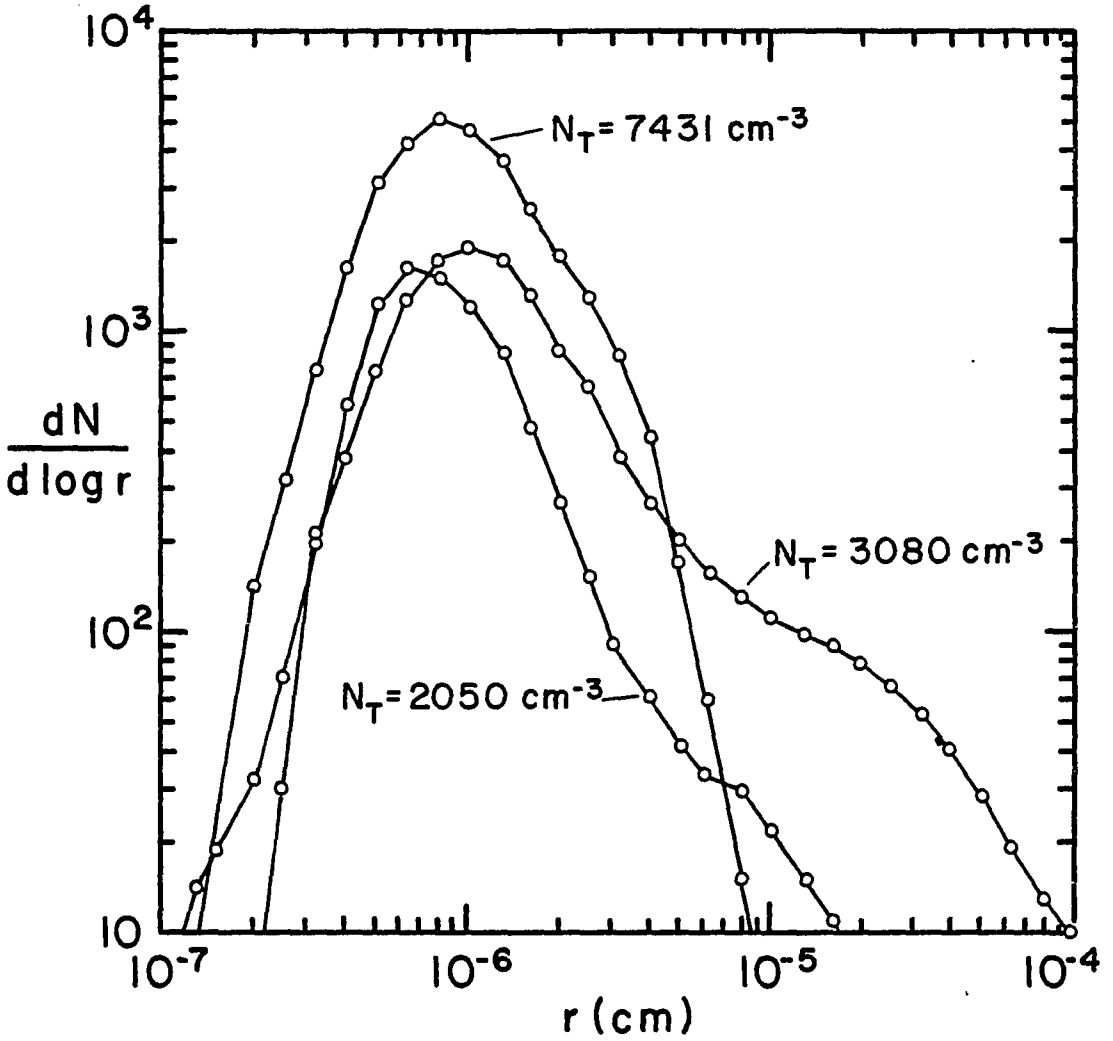

Figure 24. A set of Australian size distributions corresponding to the mass transports shown in Figure 25.

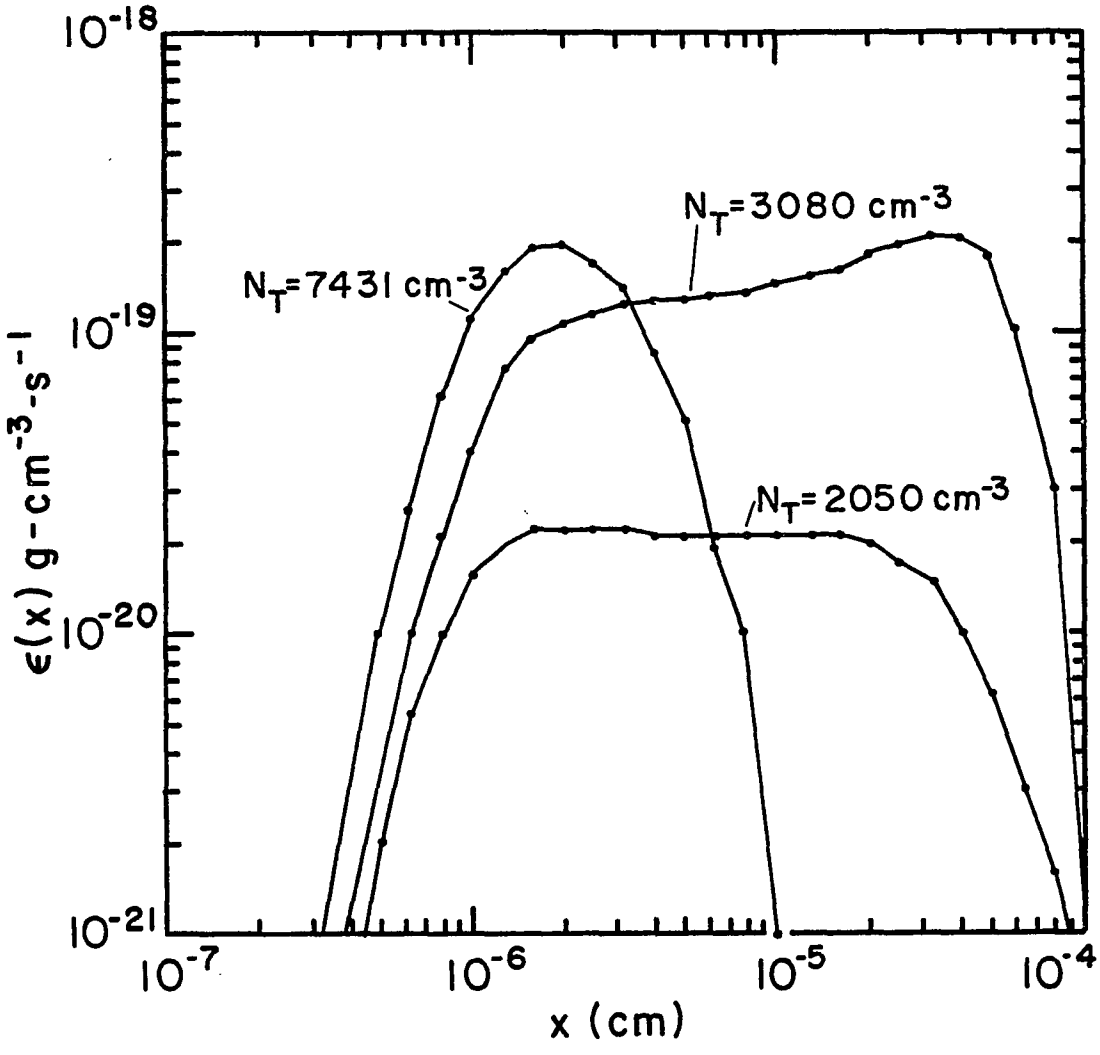

Figure 25. The Australian mass transports.

in the 0.02 - 0.1 μ region, suggesting that under certain conditions (these distributions were measured in modified polar maritime air) atmospheric aerosol size distributions may exhibit constant transport subranges.

Photochemical Aerosol

The mass transport in a freshly generated artificial aerosol (see Figure 26) is shown in Figure 27, for purposes of comparison with the natural aerosol.

Summary and Conclusions

Comparison of Estimated Global Transport to Total Gaseous Emissions

The mass transports calculated here may be used to estimate the rate at which aerosol mass is transported out of the gas-to-particle conversion region ($r \leq 0.01$ μ) on a global basis. Using the Australian distributions as reasonable for somewhat modified maritime air and the Tucson samples as representative of continental distributions with corresponding total number concentrations of 10^3 and 10^4 cm^{-3}, the mass transports are 5×10^{-21} and 5×10^{-19} g cm^{-3} s^{-1}, respectively. With an approximate aerosol scale height of some 2 km, a total global annual transport of some 4 megatons/yr results. This represents only a small fraction of the estimated total global gaseous emissions, which are on the order of hundreds of megatons per year (SMIC, 1971). From this point of view, gas-to-particle conversion followed by coagulation past 0.01 μ is a relatively minor sink for gaseous emissions. It should be

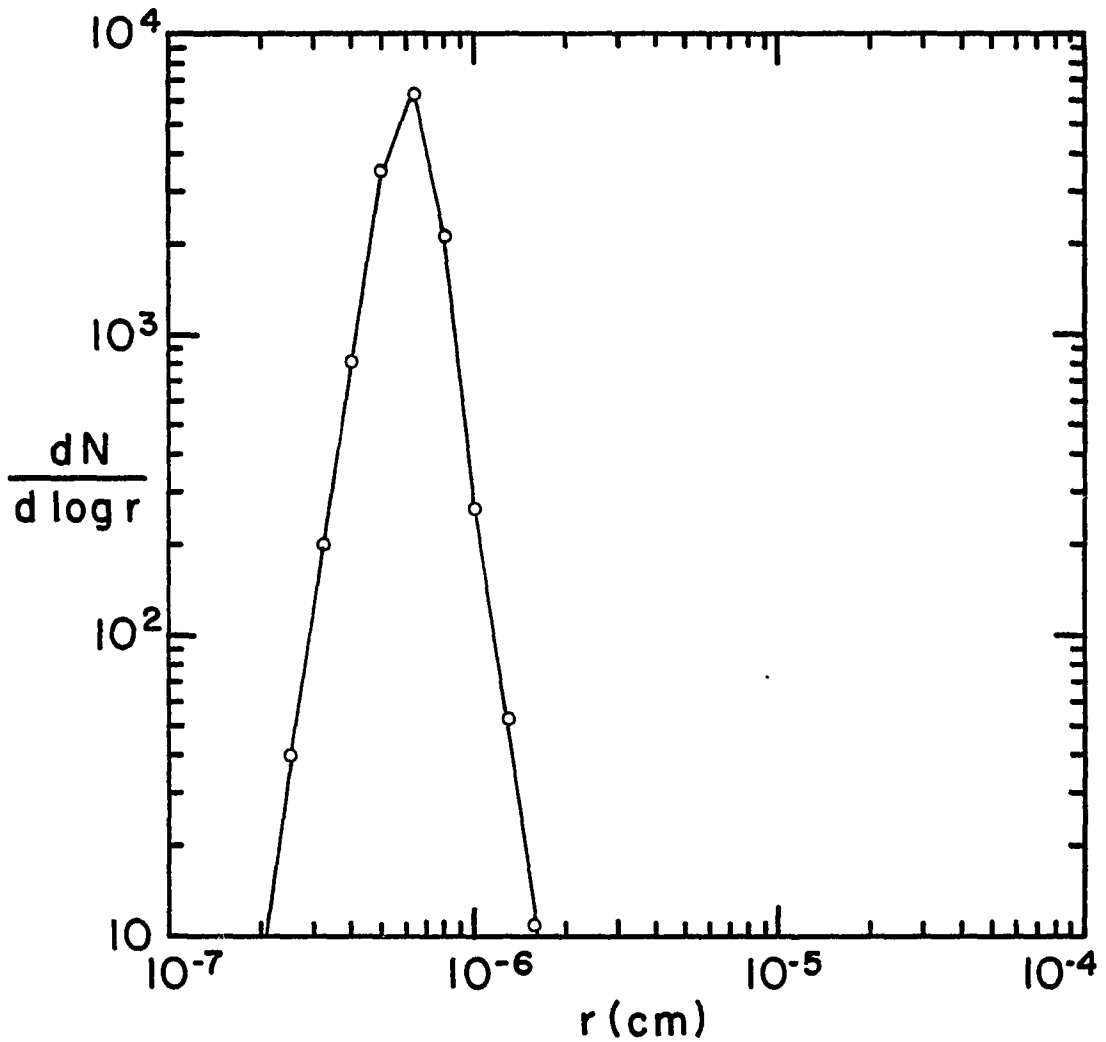

Figure 26. Size distribution of a photochemical H_2SO_4 aerosol corresponding to the mass transport shown in Figure 27.

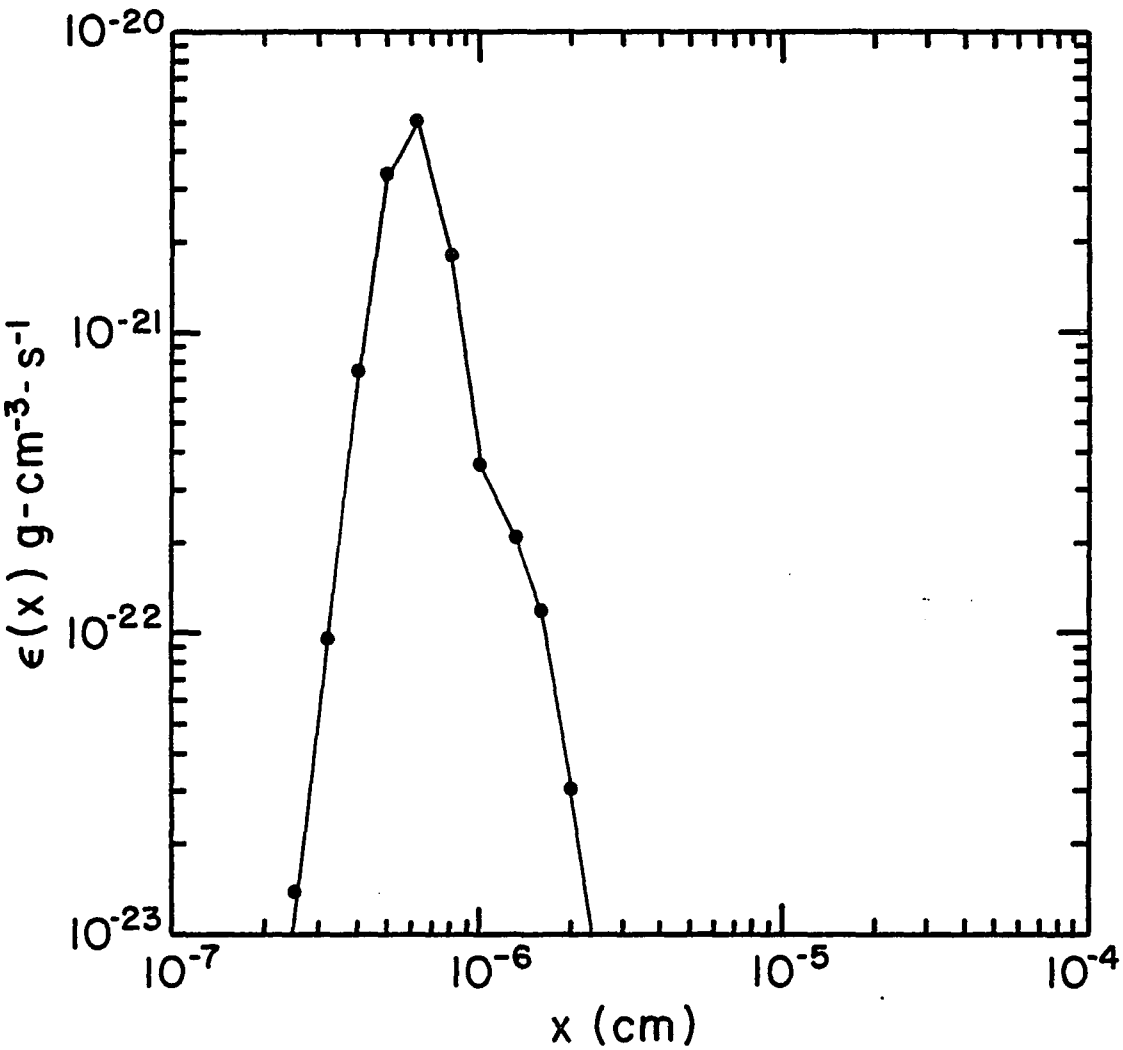

Figure 27. Mass transport for the photochemical H_2SO_4 aerosol.

borne in mind, however, that this transport is solely a coagulative one and that other mechanisms, e.g., condensational growth of small aerosol, also serve to transport aerosol mass. The rate of transfer via condensational growth mechanisms cannot be evaluated without detailed information concerning the physiochemical nature of the aerosol gas system. Evaporation of nuclei, some evidence for which will be presented in Chapter Four, also removes aerosol mass. The coagulative transport therefore represents a lower limit on the rate of mass removal.

Location of Sources and Sinks in Dry, Urban Air

Size distributions measured in dry, urban air do not show constant transport subranges. The transport consistently shows a peak in the 0.01 to 0.03 μ region, thus demanding[1] (if the size distribution is to be maintained) a small particle ($r \leq 0.01$ μ) source and a sink between 0.02 ~ 0.1 μ. The rate of transport is such that the total mass in the $r \leq 0.01$ μ region would be removed in some 15 hours.

Location of Sources and Sinks in Polar-Maritime Air

Distributions measured in cleaner, polar-maritime air in Southeastern Australia show (in two our of the three samples currently available) an approximately constant coagulative mass transport in the

---

[1]Since the urban samples are subject to local (surface) particle sources as well as mixing and advective effects the source and sink analysis must be considered as qualitative only. For these samples the emphasis is to be placed more on the magnitude of the transport rather than its dependence on radius (functional form).

0.02 - 0.1 μ region. For these samples, time scales on the order of several days are required to coagulatively remove the aerosol mass in the $r \leq 0.01$ μ region.

Calculation of the Mass Transport for $r \leq .01$ μ

For all of the measured size distributions discussed here, the coagulative mass transport out of the gas-to-particle conversion region ($r \leq 0.01$ μ) may be calculated to within a few percent using only the first term of Eq. (2), i.e.,

$$x \leq 0.01 \text{ μ} \qquad \varepsilon(x) \simeq \int_0^x n(v)v \int_x^\infty n(u)\ K(u,v)\ du\ dv.$$

Mass Transports in Tucson Air Samples

The mass transports in the Tucson air samples (with respect to the reference size 0.01 μ) ranged from 2×10^{-18} to 8×10^{-18} g cm^{-3} s^{-1}, the variations being primarily a reflection of the variation in total particle concentration. The average transport was some 3×10^{-18} g cm^{-3} s^{-1}. Since, as discussed in the previous chapter, the measured size distributions were maintained in time (apart from total number fluctuations), a source of small particles is demanded which could replace aerosol mass <u>at least</u> at the rate of 3×10^{-18} g cm^{-3} s^{-1}. This rate of removal will subsequently be compared with the rates of photochemically induced aerosol formation.

CHAPTER 4

PHOTOCHEMICAL EXPERIMENTS

The subject of the photochemical production of Aitken nuclei with solar and UV radiation has a rather long history. Recently Friend, Leifer and Trichon (1973) and Cox (1973) have examined the formation of H_2SO_4 aerosol formed during the photooxidation of laboratory gas mixtures. Verzar and Evans (1961) have reported the formation of nuclei in industrial N_2 using solar radiation. Most recently, reports of nucleus formation in filtered atmospheric air using solar radiation have been given by Bricard, Cabane, Madelaine and Vigla (1972) and by Vohra, Vasudevan and Nair (1970). The formation of nuclei using UV radiation has been reported by Atkinson (1955), and recently by Hoppel and Dinger (1973). The basic question here is whether or not such observations of nucleus formation have direct importance for nucleus formation in the atmosphere. It is essential to establish that nucleus formation is due to trace gases in the air and not to system contaminants and identify the wavelengths of UV radiation responsible for aerosol formation. It is often unclear as to what pains have been taken previously to insure that the results were not a consequence of system contaminants.

In the present study, the photochemical formation of nuclei was examined, using both solar radiation and wavelengths ranging from 1850 to 2900 Å in the UV. The question of contaminants will be discussed in detail. When working with atmospheric air, it is not possible to identify with certainty the trace gases responsible for aerosol formation. The role of SO_2 in nucleus formation is of particular interest,[1] however, and was investigated here. The aerosol size distributions measured concurrently with the photochemical measurements provided a number of useful pieces of information relating to the importance of solar photochemical mechanisms, namely:

1. The shape of the size distribution itself (particularly whether or not large amounts of small aerosol, $r \leq 0.005$ μ, are present) is suggestive as to whether or not large amounts of new small aerosol are being produced via gas-to-particle conversion.

2. The survival time of newly formed molecular nucleogen in the presence of the existing aerosol was estimated, using the measured size distributions. This survival time was then compared with the time necessary to achieve the homogeneous nucleation level in filtered air samples.

3. The coagulative mass transports previously presented were used to compare the rate at which aerosol mass is photochemically

---

[1]Because of the well known presence of H_2SO_4 and $(NH_4)_2SO_4$ in the atmospheric aerosol, attention has tended to focus on SO_2 as a precursor for aerosol formation.

produced with the rate at which aerosol is being transported out of the small particle size domain, i.e., out of the gas-to-particle conversion region.

Experimental Apparatus and Procedure

Experimental Arrangement

The experimental system is shown in schematic form in Figure 28. The main sampling lines are stainless steel tubing. The particle filter is made of stainless steel and uses glass wool as a filtering element. The manifolds upstream of the photoreactors are glass. Connections are made with Teflon tubing, with small pieces of Tygon serving as the glass-to-Teflon connectors. The main storage bag was a 200-liter aluminized mylar bag. The particle counter, a 1957 model Pollak condensation nucleus counter, was operated at 160 mm Hg overpressure. Air samples could be passed through 500 cm^3 of Linde 13X molecular sieve and 1000 cm^3 of freshly activated charcoal to remove moisture and traces of impurities. SO_2 was metered into the system via a permeation membrane immersed in an H_2O bath for temperature control. H_2O vapor was added by passing the air stream over several wash bottles. The RH was measured using a Model 800 EG&G thermoelectrically cooled dewpoint hygrometer. For the range of humidities of interest here ($10 \leq RH \leq 85\%$), the hygrometer was calibrated against a sling psychrometer.

Experimental Procedure

Static Irradiation. For these experiments, air samples (filtered or unfiltered) were pulled through the 24-liter photoreactor

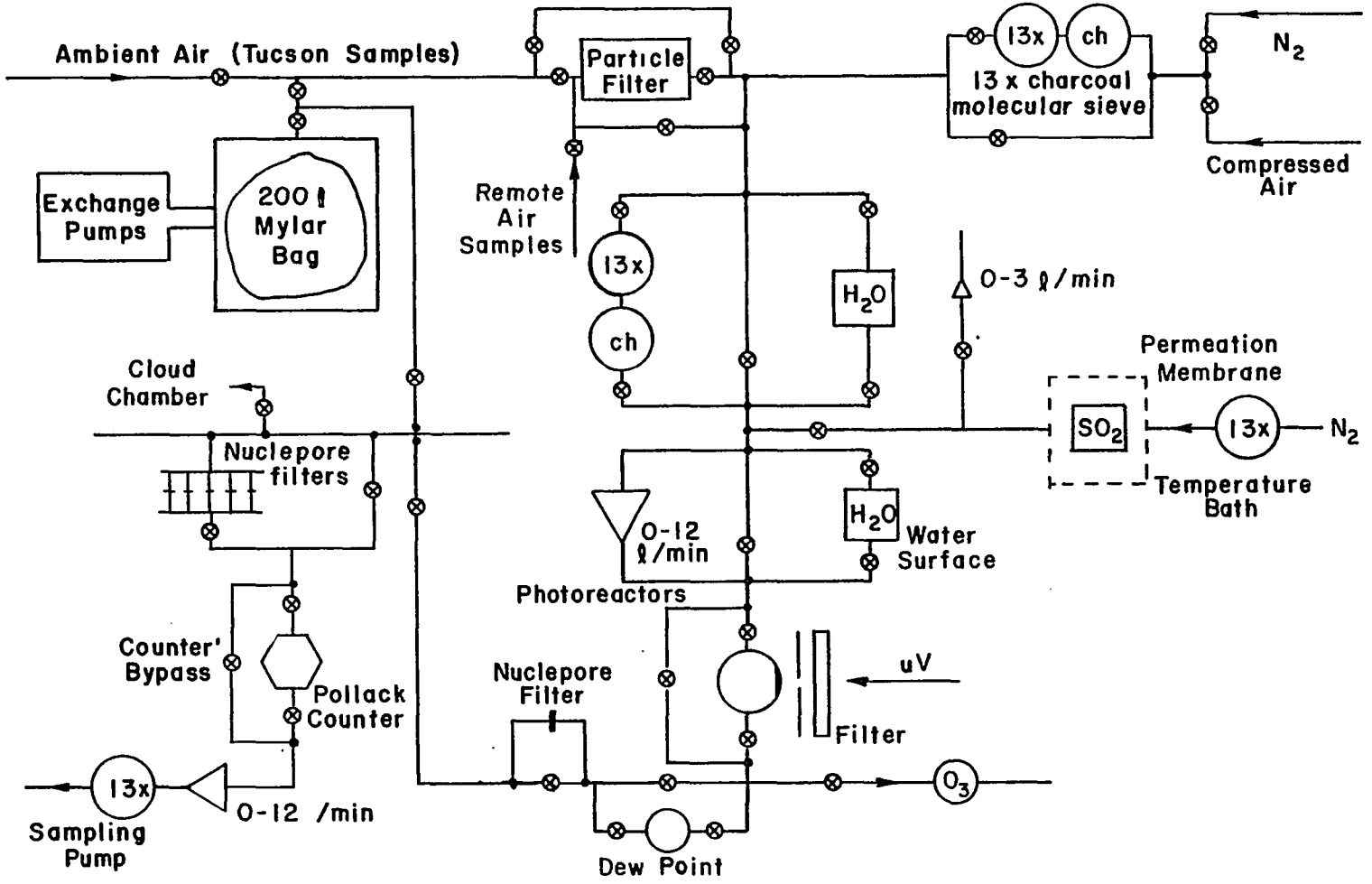

Figure 28. Experimental arrangement for the photochemical experiments.

for a time sufficient to insure complete flushing. The samples were then irradiated continuously and periodically sampled with the Pollak counter or CCN counter. The samples were passed through a set of Nuclepore filters to facilitate sizing of the photochemical aerosol.

Continuous Flow. In this case, air samples were drawn continuously through the flow reactors, and the particle concentrations were monitored.

Storage of Irradiated Air. These experiments were carried out by pulling the air samples through the photoreactors and into the 200-liter aluminum mylar bag. The all-quartz reactor (described in the following section) was used exclusively for these experiments. Subsequent aerosol formation and growth were then observed by sampling from the storage bag. The use of this configuration allowed the irradiated air to be injected into gas samples (or gas particle mixtures) already present in the bag.

The Photoreactors

200-liter Mylar Bag. A 200-liter aluminized mylar bag was used to store irradiated air samples, in order to observe the subsequent aerosol formation and growth mechanisms. The bag itself was never directly illuminated, either externally or internally.

24-liter Glass Reactor. A 24-liter Pyrex glass reactor was used to carry out experiments where the air samples were continuously irradiated and the reactor periodically sampled. The Pyrex walls were 4 mm thick and removed radiation with wavelengths less than 3000 Å. A 2.54-cm diameter Suprasil quartz window attached to the reactor with a

graded quartz-glass seal admitted radiation with less than 5% attenuation, well below the solar UV limit. Only this reactor was used to investigate aerosol formation with solar radiation.

The question of reactor size is an important one, since the reactor walls provide macroscopic surfaces not present in the atmosphere which invariably affect the rate of aerosol formation. In particular, both newly formed photochemical nucleogen and aerosol are lost by diffusion to the reactor walls. Also, the walls provide surface sites which may function catalytically to produce effects which would not take place in the free atmosphere. Though it is not possible to completely describe analytically the rates at which nucleogen or newly formed aerosol are lost to the reactor walls, two simplified models were used to estimate reasonable upper and lower bounds on the loss rate. These loss rates were calculated and compared with the loss rates due to the existing environmental aerosol. The calculations are presented in detail in Appendix B. Also presented in Appendix B are the measured rates of aerosol decay for particles of known size distribution.

A particularly important question is one of time scale, i.e., what is the slowest rate of aerosol formation which is observable in a given photoreactor. The result of photooxidizing environmental (Tucson) air enriched in SO_2 is shown in Figure 29. These experiments will be described in greater detail later. The curves shown are the average of three repetitions of the experiment. As can be seen, the reactor is of sufficient size to allow the onset of nucleus formation to take

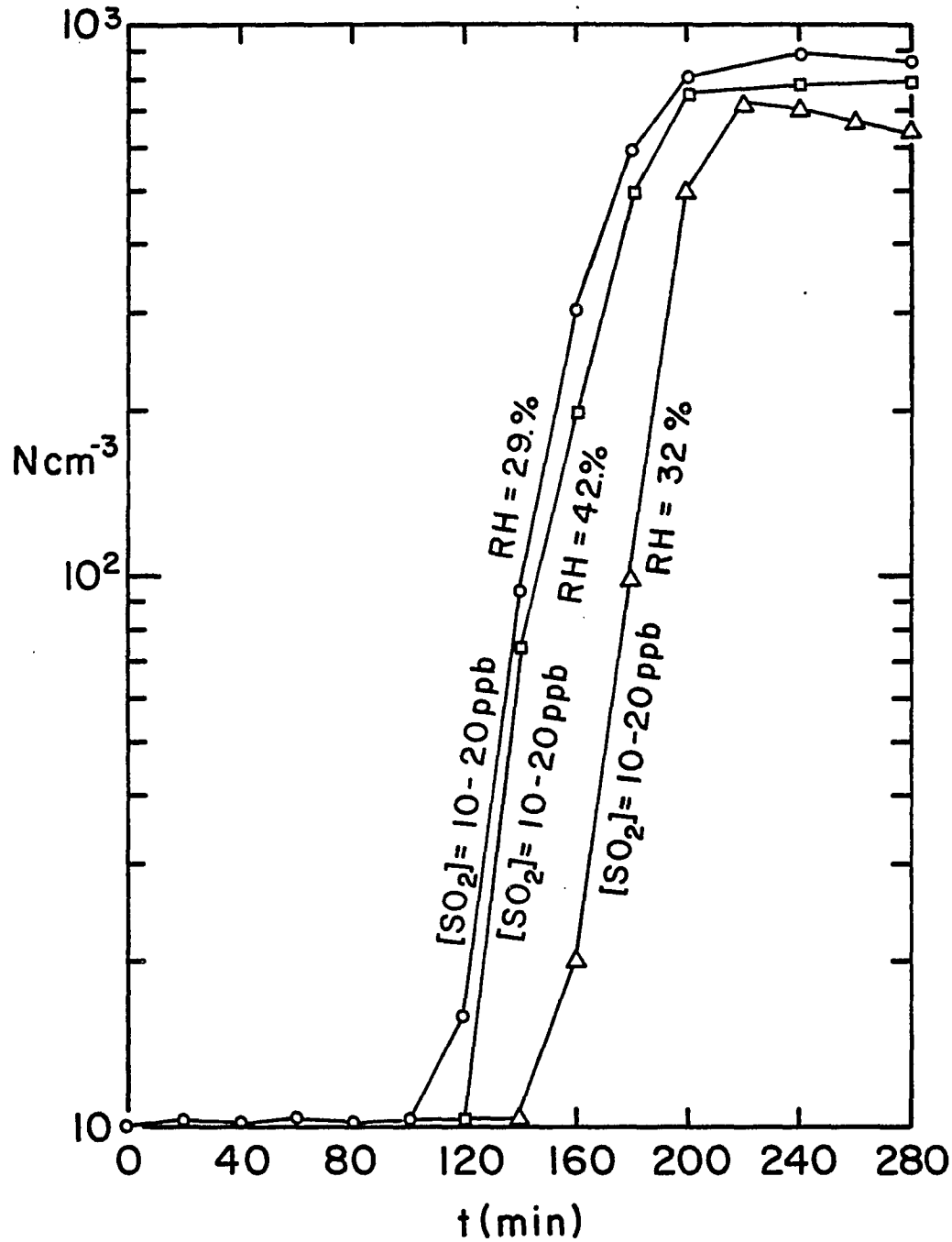

Figure 29. Solar induced nucleus formation in atmospheric air enriched in SO_2.

In this and subsequent figures, curves drawn with different symbols represent different runs of the experiment.

place on time scales of at least 2-3 hours. The H_2SO_4 aerosol which forms after 2-3 hours of solar irradiation has an approximate model size of 2-3 x 10^{-7} cm.

All-Quartz Flow Reactor. An all-quartz reactor was used for experiments utilizing the short UV (the 1850 Å line of the low-pressure Hg sources). The reactor itself is a fused quartz tube (40% transmission at 1850 Å), 31.75 cm long and 35 mm in diameter. The ends of the reactor were covered with aluminum foil to prevent irradiation of the connecting tubing and to provide a well-defined irradiated volume. The well-defined flow geometry of the reactor allows an accurate determination of the sample residence time to be made. This reactor was used to expose the air samples to the UV for a short time (residence time on the order of tens of seconds) with the radiated air sample then transferred to the 200-liter mylar bag for storage.

Sources of Radiation

Three different sources of radiation were used in the photochemical experiments. Solar radiation was used to provide radiation with wavelengths longer than approximately 3000 Å. For wavelengths less than 3000 Å, two Hg lamp sources were used. A number of glass transmission filters were used to remove various wavelengths from the Hg sources. Each source with the various filter combinations is discussed in detail below:

Solar Radiation. Experiments using solar radiation were carried out using the 24-liter Pyrex glass reactor with a Suprasil

quartz window. The glass itself (4 mm wall) removes radiation with wavelengths less than 3000 Å. The quartz window admits UV radiation (95% transmission) well below the solar UV limit (∿2900 Å), so that all solar UV entering the reactor through the window is attenuated only some 5%. The transmission curves for the reactor glass walls and the quartz window are shown in Figure 30.

High-pressure 200 w Xe-Hg Source. This source is an Oriel 200 w Xe-Hg lamp operated in an air-cooled housing. A quartz condensing lens was used to provide an intense, partially collimated beam. An optical stop was used to insure that only the reactor window was externally illuminated. The relative, unfiltered, spectrum of this source measured at the entrance window of the photoreactor (with a McPherson .3m monochromator) is shown in Figure 31, which shows substantial amounts of radiation in the 2100-2450 Å region to effectively photodissociate O_2. The intensity in this region was measured relative to the 1850 Å line of a low-pressure Hg source. (See Appendix C.) The intensity in the 2500-3000 Å region was not absolutely determined since, as will subsequently be discussed, this radiation is of insufficient intensity to result in aerosol formation. This source, unfiltered, will subsequently be designated as HPXeHg-(UF). Removal of wavelengths less than 2500 Å (see Figure 32) was accomplished with a glass transmission filter (Corning O-53). The filtered source will be designated as HPXeHg-(O-53). For purposes of subsequent comparison (with the low-pressure Hg sources), it is to be noted that this source contains no significant amounts of radiation less than 2000 Å and that the 2537 Å line is strongly suppressed.

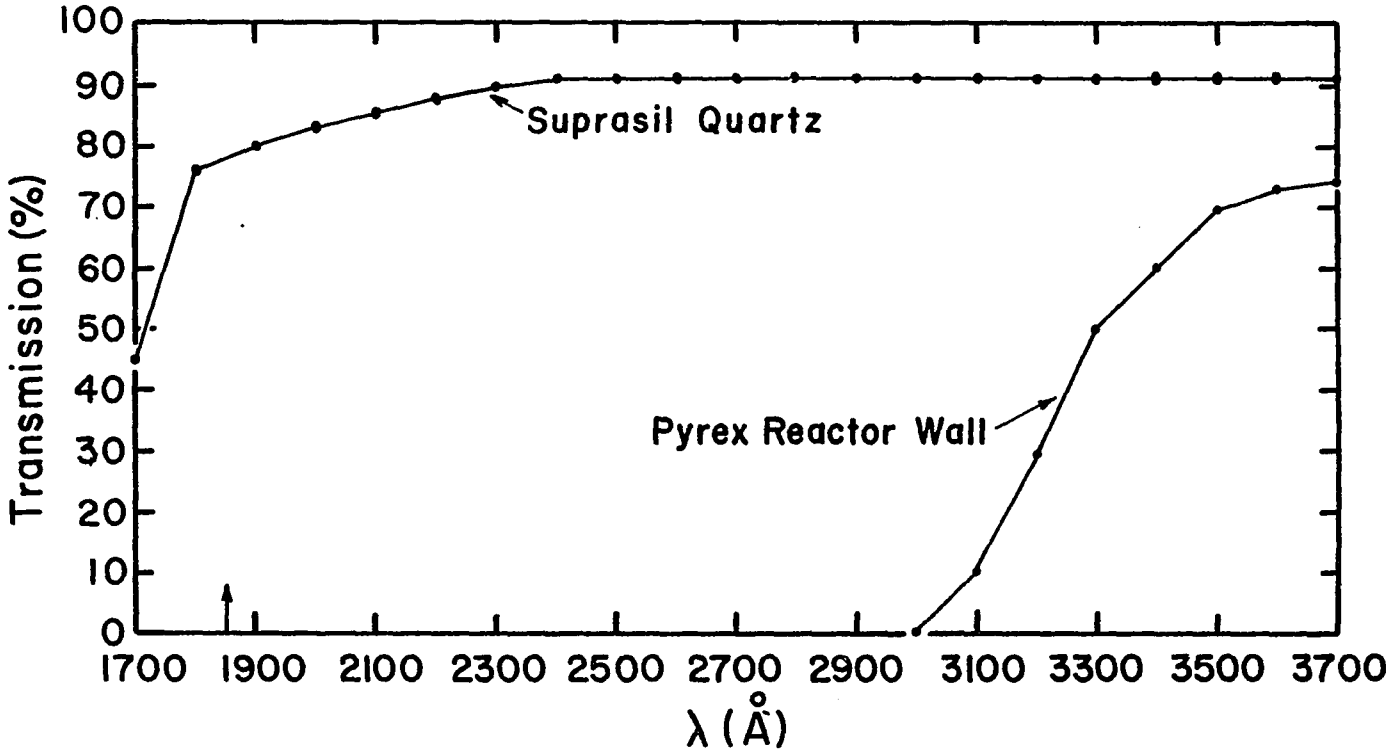

Figure 30. Transmission curves for the 24 ℓ reactor.

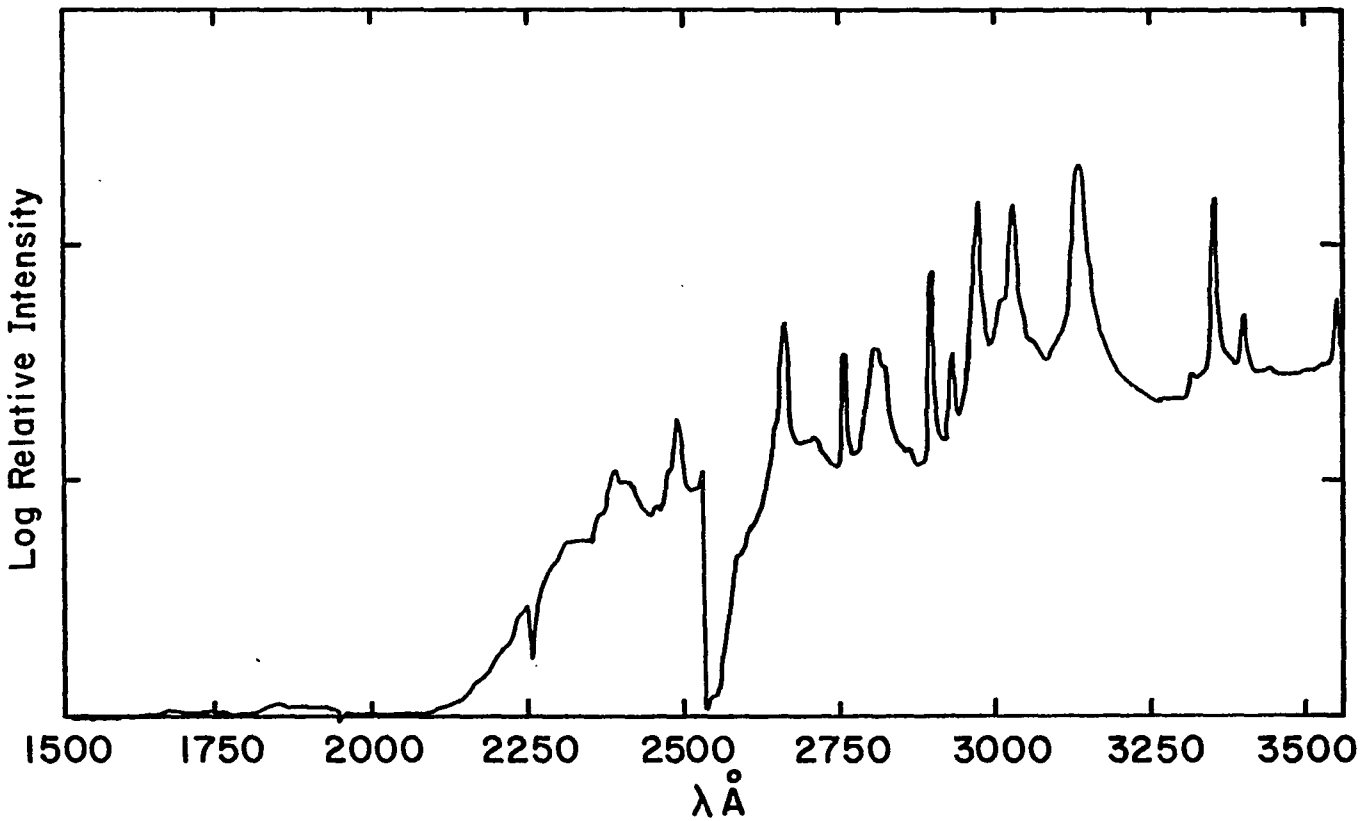

Figure 31. Relative spectrum of the HPXeHg-(UF) UV source.

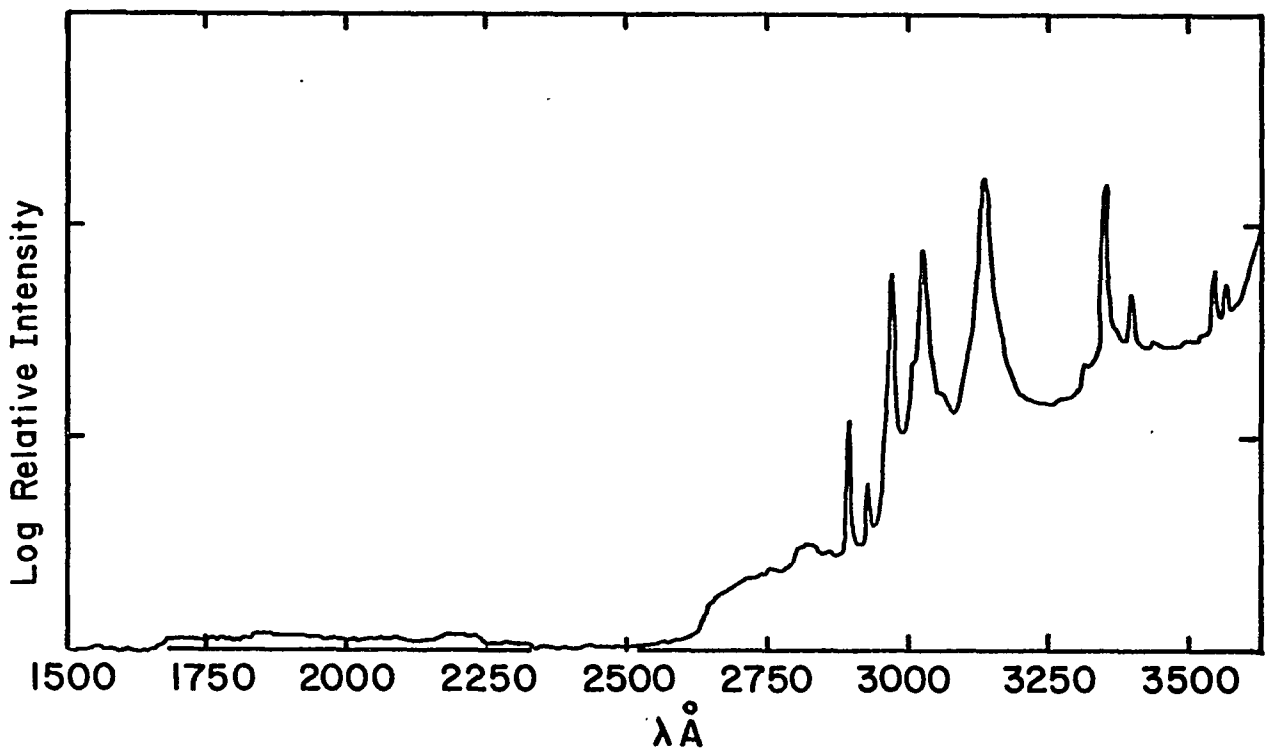

Figure 32. Relative spectrum of the HPXeHg-(0-53) UV source.

Low-Pressure Hg Source. The low-pressure Hg lamps used here were of the pencil variety and are characterized by two primary intense lines in the $\lambda_i \leq 3000$ Å region, one line at 1850 Å and another at 2537 Å. The unfiltered spectrum of this source (measured with the monochromator purged and a sodium silicate coated photomultiplier to provide essentially linear response for $\lambda_i \leq 3000$ Å) is shown in Figure 33. Unfiltered, this source will be designed as LPHg-(UF). The intensity of the 1850 Å line, which will subsequently be seen to be very effective for aerosol formation in environmental air, was calibrated by measuring the O_3 concentration produced in dry air. (See Appendix C.) This source was used in conjunction with three transmission filters to allow successively shorter wavelengths to enter the photoreactors. The filtered spectra are shown in Figures 34 and 35. Specifically, LPHg-(O-53) has little radiation less than 2850 Å, both the 1850 and 2537 Å lines having been filtered. For LPHg-(9-54), the 1850 Å line has been filtered, while the 2537 Å line is unattenuated. For the source designated LPHg-(9-58), the 1850 Å Hg line has attenuated by a factor of 2.2. A summary of the sources discussed here is given in Table 1.

Discussion of Contaminants

Particle Formation Due to Trace Gases in the Air. In order to establish that the photochemical aerosol formation was due to the presence of trace gases in the air and not to contaminants present in the system, a number of experiments were carried out. A small glass

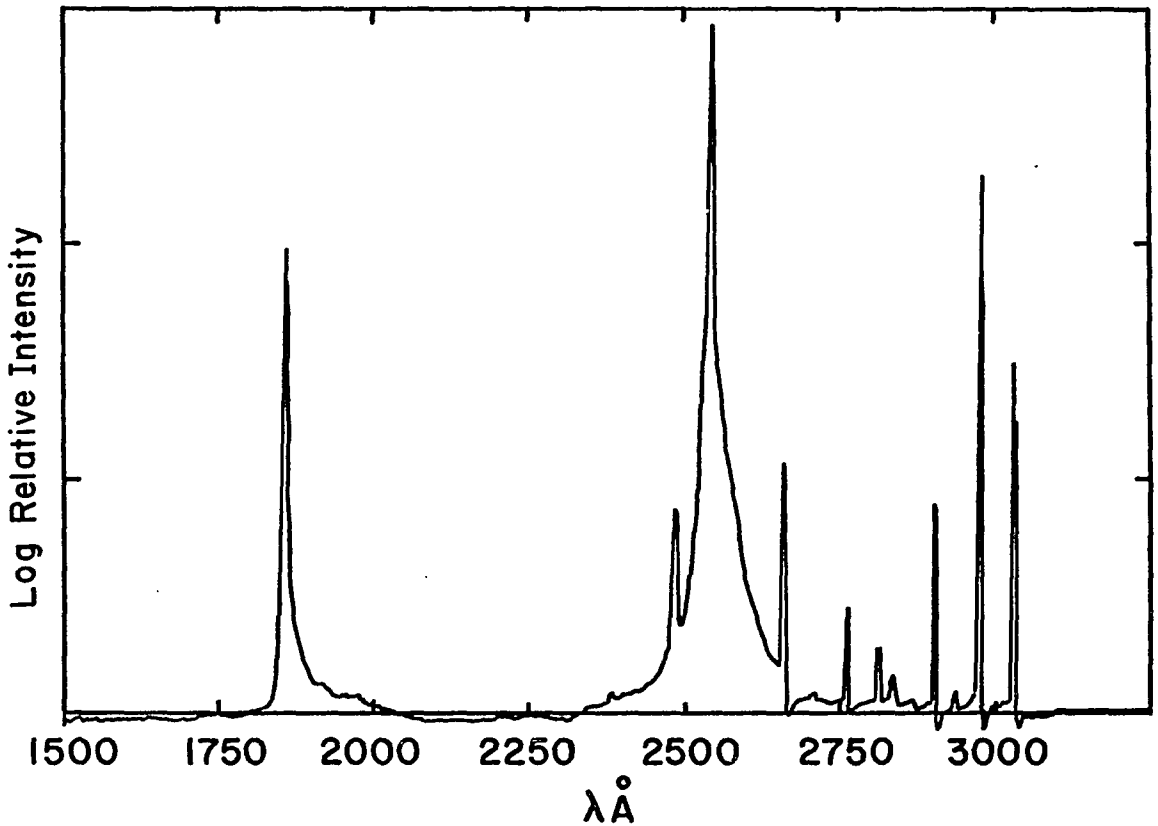

Figure 33. Relative spectrum of the LPHg-(UF) UV source.

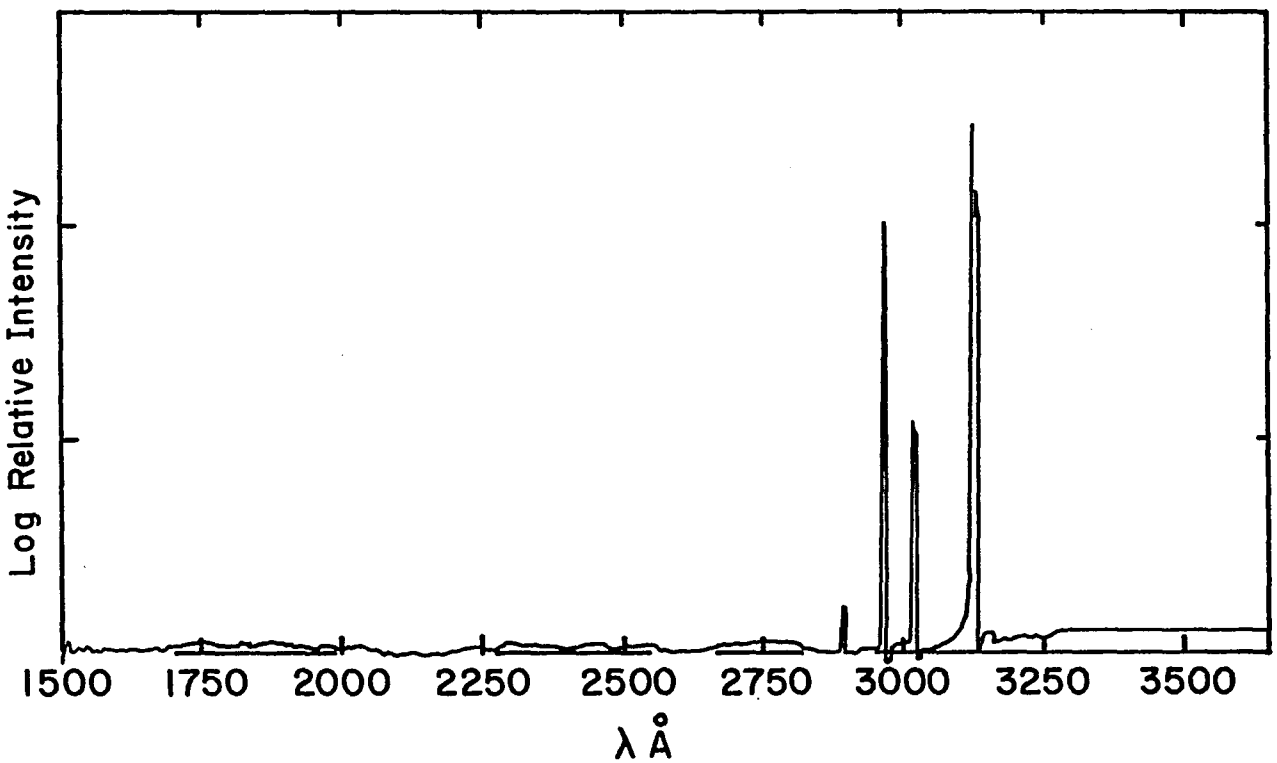

Figure 34. Relative spectrum of the LPHg-(0-53) UV source.

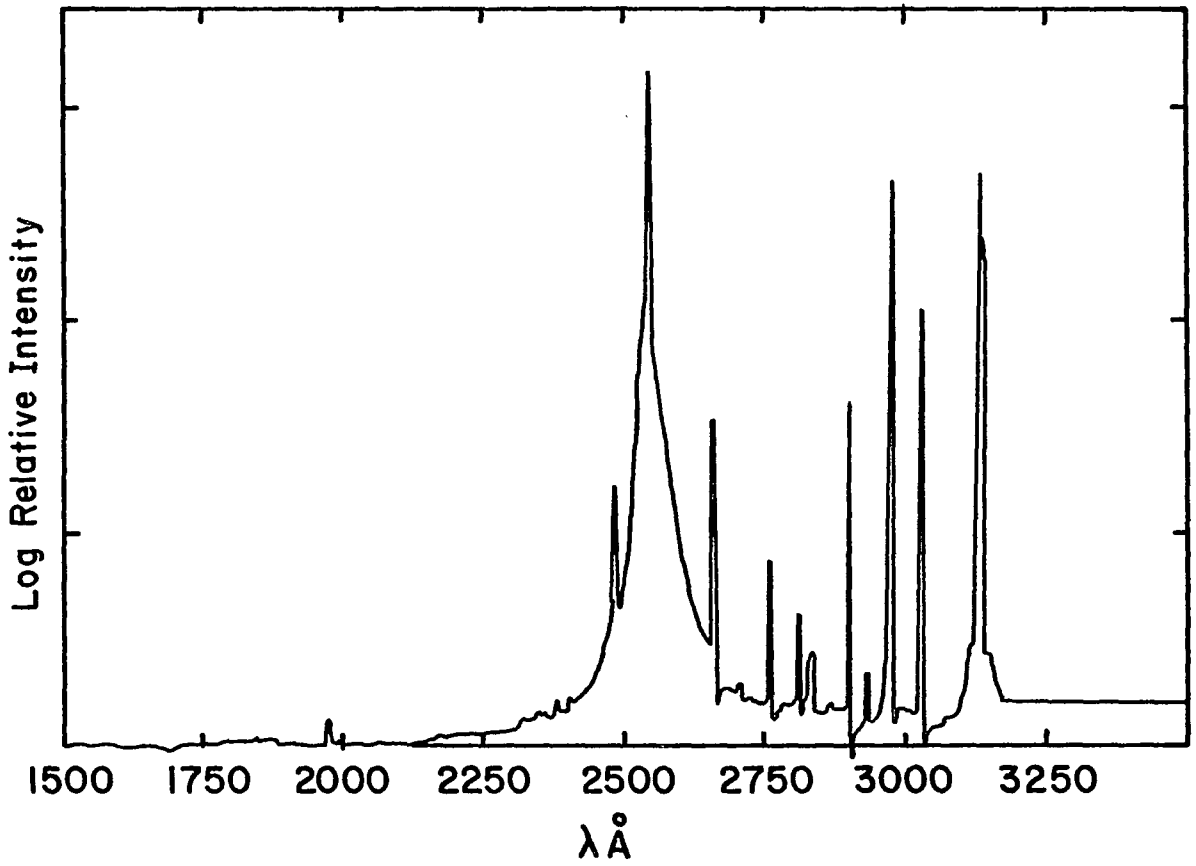

Figure 35. Relative spectrum of the LPHg-(0-54) UV source.

Table 1. Summary of the Various Sources Used and the Wavelengths Present in the Photoreactor

Source	λ Present	$\Phi = \int_{\lambda_1}^{\lambda_2} I_\lambda d\lambda \, cm^{-2}s^{-1}$	Comment
Solar	$\lambda \geq 3000$ Å (walls) $\lambda \geq 2863$ Å (windows)		
HPXeHg-(UF)	$\lambda \geq 2100$ Å	$5 \times 10^{13} cm^{-2}s^{-1}$ 2100 Å $\leq \lambda \leq$ 2450 Å	
HPXeHg-(0-53)	$\lambda \geq 2500$ Å		2100-2450 Å radiation removed
LPHg-(UF)	$\lambda \geq 1850$ Å	$4 \times 10^{14} cm^{-2}s^{-1}$ in 1850 Å line	1850 and 2537 Å lines present
LPHg-(0-53)	$\lambda \geq 2850$ Å		1850 and 2537 Å lines absent
LPHg-(9-54)	$\lambda \geq 2100$ Å		1850 Å line absent
LPHg-(9-58)	$\lambda \geq 1850$ Å		1850 Å line reduced by a factor of 2

reactor with quartz windows and a ground-glass side attachment was used to introduce various materials upstream of the radiation zone and to allow them to be directly irradiated. Table 2 summarizes these results. All samples were irradiated using the LPHg-(UF) source (1850 Å line present), as it was found that this constituted the most sensitive test for the various materials. The majority of the tests were carried out at high RH (50%), as the rate of nucleus formation increased rapidly with increasing humidity. Only stainless steel, Teflon and thoroughly cleaned glass were used in constructing the photochemical system. The glass manifolds and the 24-liter glass photoreactor were cleaned with chromic acid, thoroughly rinsed with distilled water, and then baked under a dry gas stream (N_2).

Molecular sieves and freshly activated charcoal were used to remove trace impurities from the air samples, in order to establish that aerosol formation was taking place due to trace impurities present in the air. The results of these experiments are shown in Figure 36. Since the charcoal and the molecular sieves dry the air samples, the air was rehumidified before irradiation.

A Particular Anomalous Effect. During the course of these experiments, a number of anomalous effects have been observed which invariably could be traced back to the presence of contamination in the experimental system. When the experiments with solar radiation and the HPXe-Hg sources were first begun (these will be discussed in detail later), large amounts of aerosol were occasionally produced, particularly at high RH. With a thorough cleaning of both the reactor

Table 2. Summary of Study of the Effects of Various Materials in Causing Spurious Nucleus Formation.

Material	Upstream	In Radiation Zone	RH(%)	Aerosol
Quartz	*		50	None
Glass, not previously cleaned	*		50	Nuclei
		*	50	Copious nuclei
Glass (Pyrex) thoroughly cleaned	*		50	No nuclei
		*	50	No nuclei
Teflon tubing	*		50	No nuclei
		*	50	No nuclei
Stainless steel tubing	*		50	No nuclei
		*	50	No nuclei
Tygon tubing	*		50	No nuclei
		*	50	Few nuclei
Plexiglass	*		10	Copious nuclei
		*	10	Copious nuclei
PVC tubing	*		50	No nuclei
		*	50	Few nuclei
Silicone rubber	*		10	Copious nuclei
		*	10	Copious nuclei
Aluminized mylar (only Al side exposed)	*		50	No nuclei
		*	50	Few nuclei

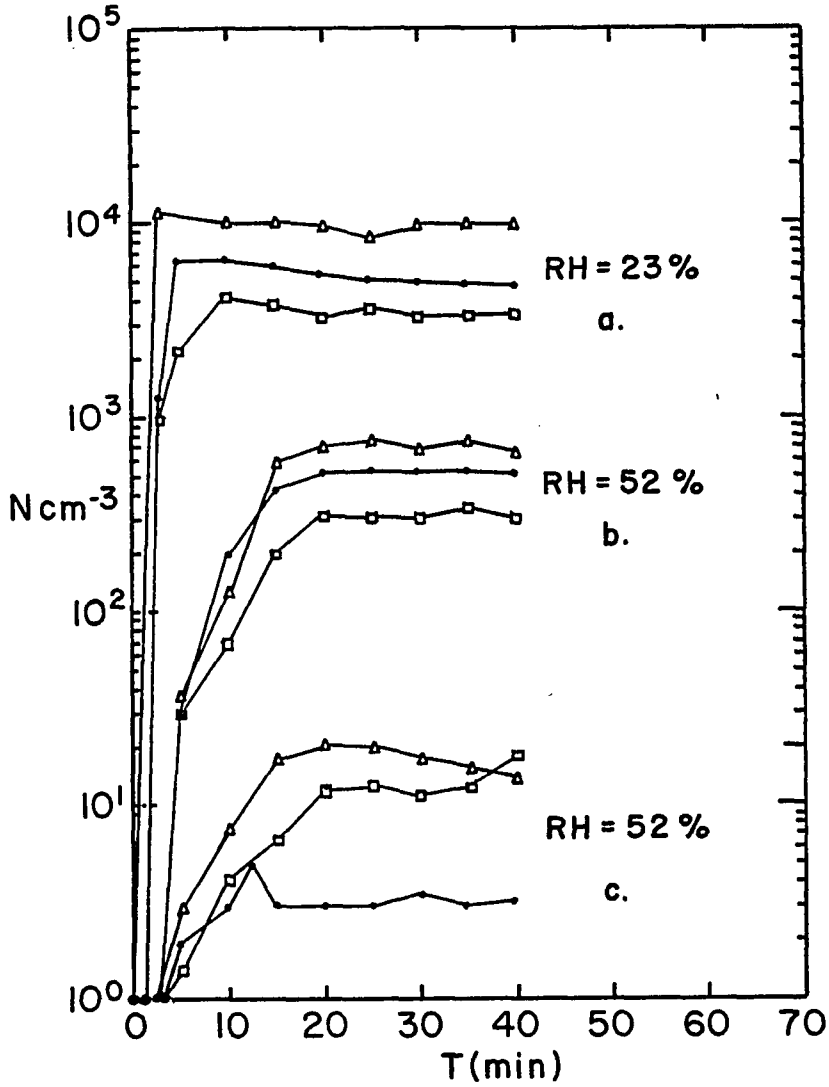

Figure 36. Results of experiment to determine whether or not aerosol formation was due to atmospheric trace gases.

The sets of curves are labeled as follows: a unscrubbed atmospheric air sampels, b the air samples were passed through 500 cm^{-3} of 13x molecular sieve, c the air samples were also passed through 750 cm^{-3} of freshly activated charcoal.

walls and the system manifolds, these effects disappeared. When the LPHg-(UF) source had been used for a long time (1850 Å radiation) to photooxidize either SO_2-air-H_2O mixtures or ambient air samples in the 24-liter reactor, spontaneous aerosol formation would frequently occur without requiring a source of radiation, i.e., aerosol would form in the 24-liter reactor or the 200-liter mylar storage bag without having been irradiated. On several occasions, this effect was somewhat astounding, as the aerosol continued to grow and maintain a constant concentration for some 24 hours. Figure 37 shows the particle concentration and particle size[2] as a function of time in the mylar storage bag. This effect, interesting though it is, was not pursued in detail. Once the photoreactors were again carefully cleaned, the effect abruptly disappeared. More on the matter of aerosol formation in the dark will be discussed in a later section.

Great care must be taken in constructing the filters used to remove the ambient aerosol particles. The filter used was constructed entirely of stainless steel and thoroughly baked at high temperatures under an N_2 gas flow. The original filtering element used was sterile cotton, but it was soon found that cotton tended to absorb and then rerelease traces of photochemically active gases. Glass wool has proved superior in this regard and was used as the filtering element.

It has been found that pure N_2 humidified to an RH of $\geq$ 50% and irradiated with 1850 Å radiation constitutes an extremely sensitive test for wall contaminants, particularly on glass surfaces where this

---

[2]The particle size, r_m, shown in Figure 44 and subsequent figures is the modal radius and was estimated using the Nuclepore filters.

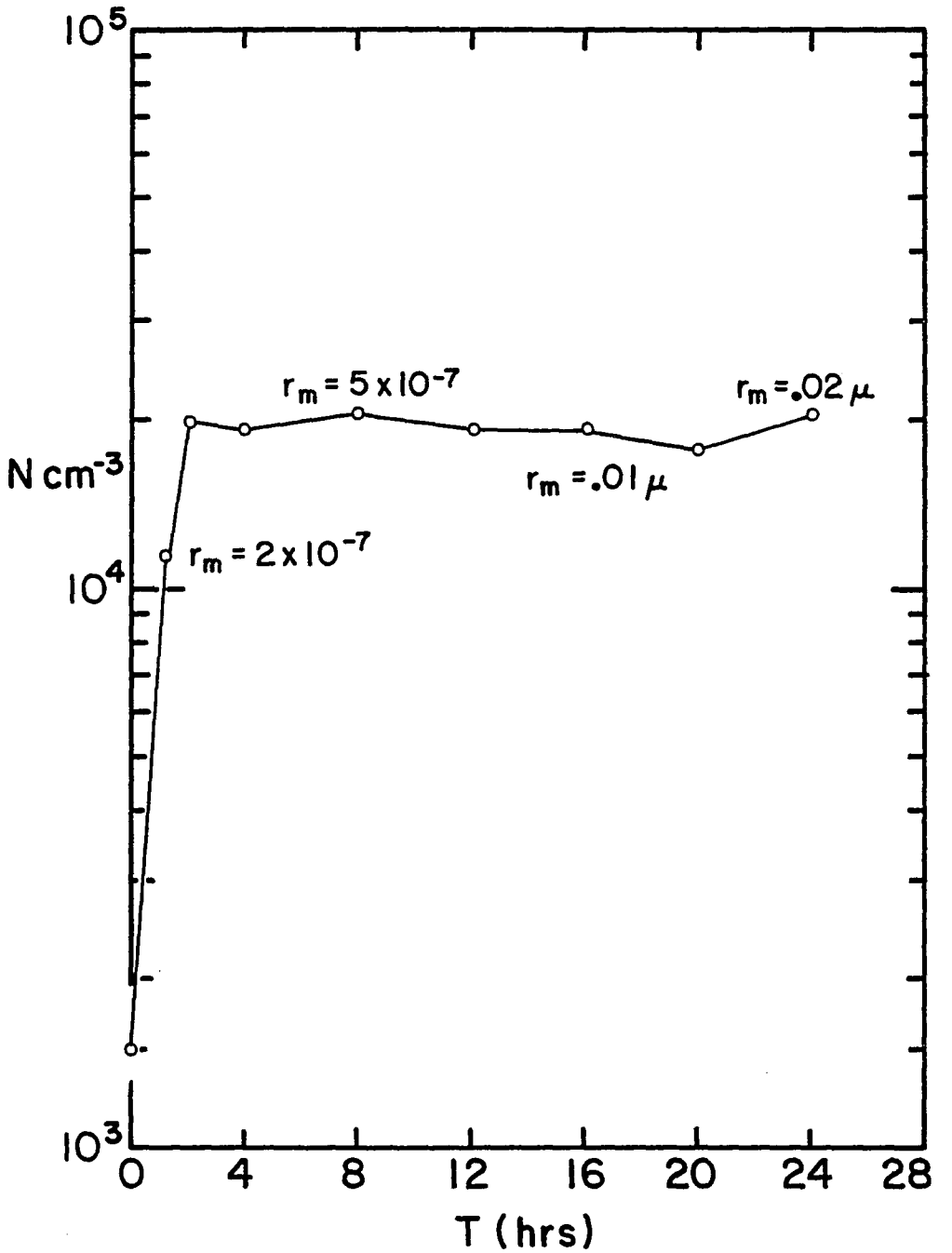

Figure 37. Spontaneous (dark phase) aerosol formation in the mylar bag.

short UV is strongly absorbed. In this regard, it was found that quartz was far superior as a reactor material. Although it is not always possible, it is highly advantageous to prevent the short UV (1850 Å) radiation from directly illuminating a highly absorbing (glass) surface.

Photochemical Production of Nuclei

Tucson Environmental Air

Continuous Irradiation in the 24 ℓ Pyrex Reactor.

1. Solar irradiation: The particle concentrations which were produced by solar irradiation are shown as a function of time in Figures 29, 38, and 39 for varying amounts of added SO_2. When .5 ppm of SO_2 was added to the air samples, nucleus formation began after 10-20 minutes of irradiation. The nuclei formed were initially very small (r_m = .002 - .004 μ) and grew to .01 μ after 2 hours of irradiation. When the experiment was repeated at lower SO_2 levels, several effects became apparent: the peak nucleus concentration was markedly reduced, the nuclei grew more slowly, and the time for the onset of nucleus formation (homogeneous nucleation) greatly increased. This last effect is of particular importance and was a pronounced one: only 10-20 minutes were required with .5 ppm (i.e. 500 ppb) of added SO_2 whereas 2-3 hours were needed when 10-20 ppb of SO_2 were added. As shown in Figure 39, particle formation was not observed without added SO_2 even at RHs up to 70%. If homogeneous nucleation takes place at all in the atmosphere at the trace gas levels present in the Tucson

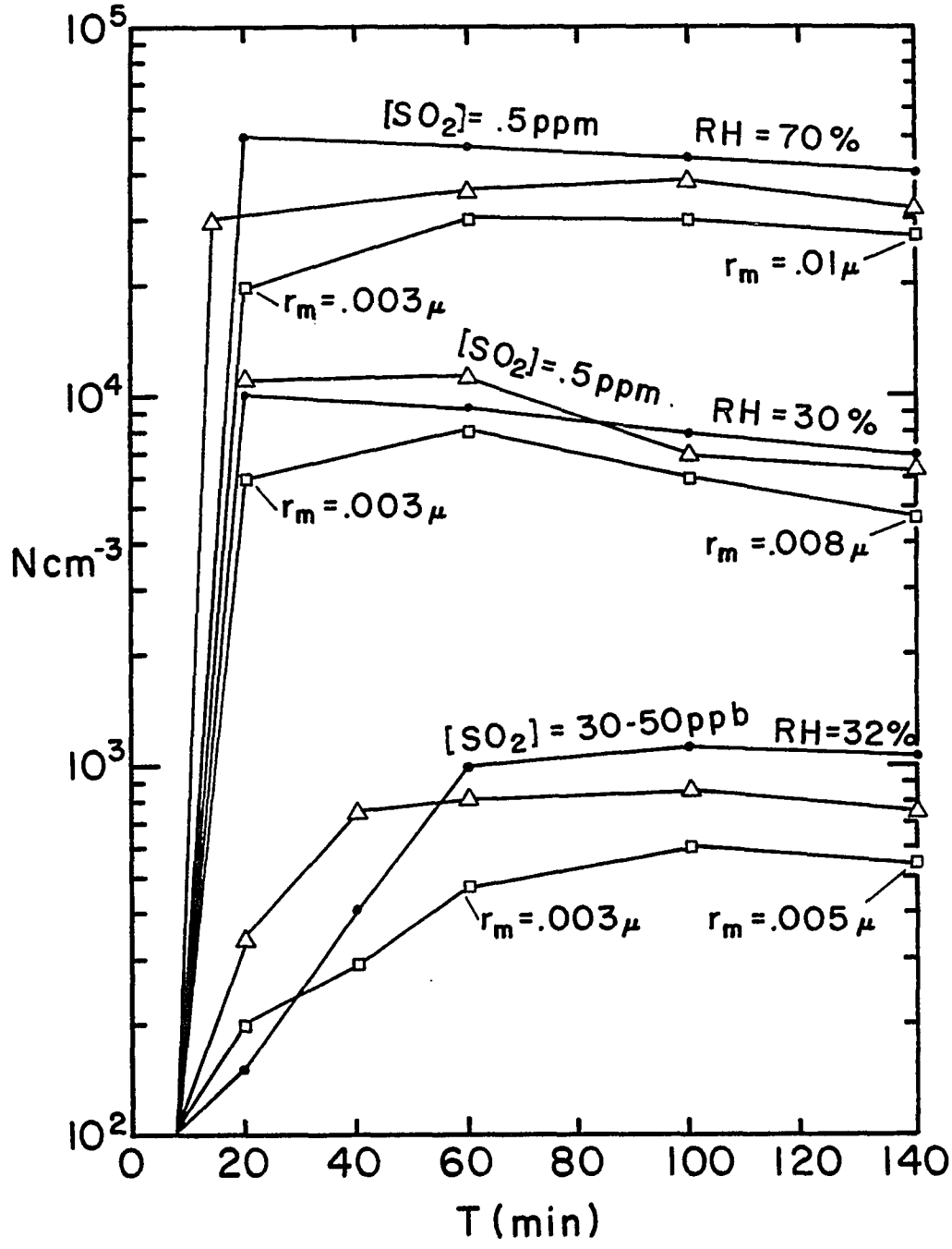

Figure 38. Solar photooxidation of ambient air with added SO_2.

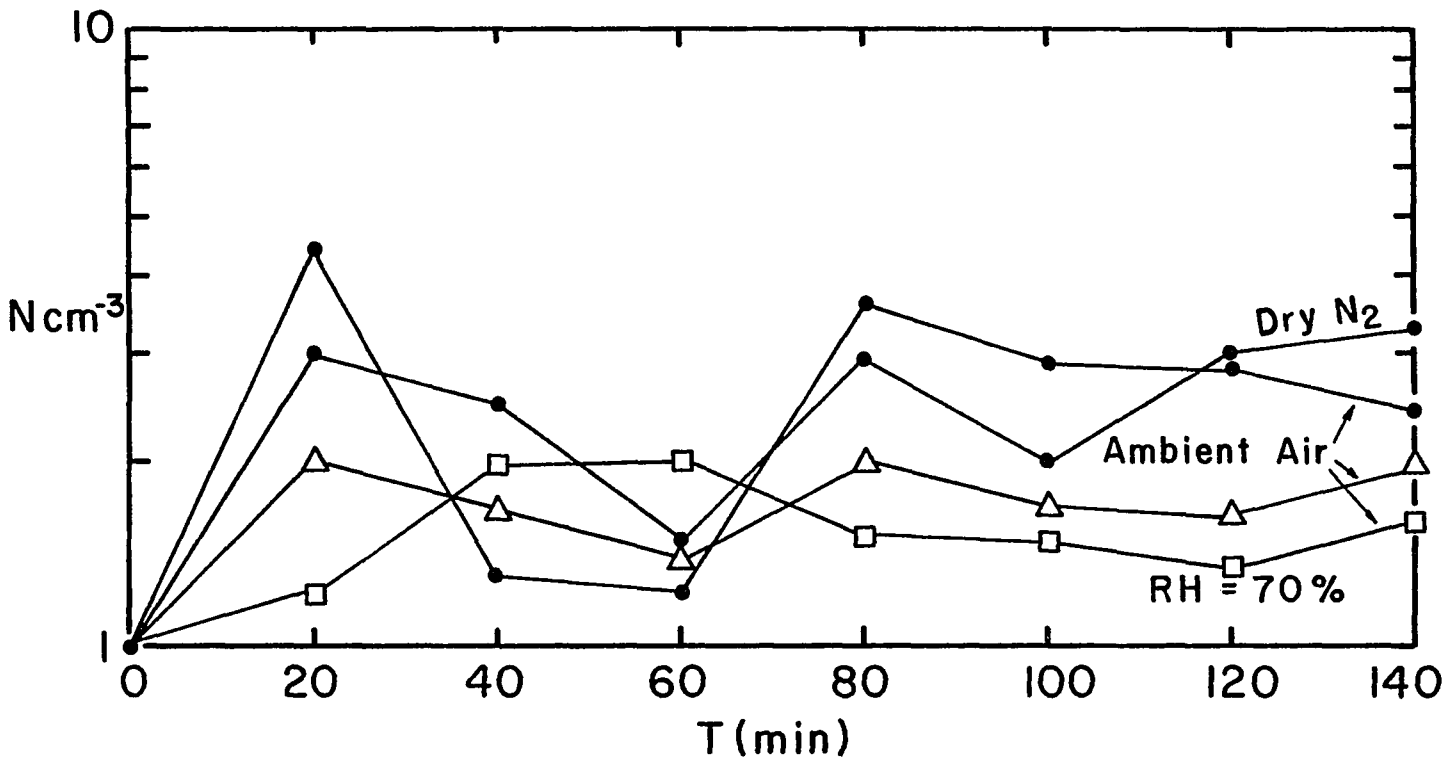

Figure 39. Solar photooxidation of atmospheric air without added SO_2 at 70% RH.

area, the time required is considerably longer than the 2-3 hours required with 10-20 ppb of added SO_2.

The shapes of the curves in Figure 38 suggest the following physical model: when initially particle free air is irradiated, the concentration of nucleogen increases until a large number of small nuclei are formed by homogeneous nucleation. Thereafter new nucleus formation is suppressed--presumably there then exists sufficient aerosol surface to accommodate the newly formed nucleogen and new aerosol formation stops. With .5 ppm of added SO_2 the curves reach a peak concentration of some 4×10^4 cm^{-3}--presumably a particle concentration sufficient to inhibit further homogeneous nucleation. This photochemical aerosol has a modal radius of .004 μ and, therefore, a surface area of about 8×10^{-8} cm^2. The existing atmospheric aerosol has an approximate surface area (as determined from measured size distributions) of 5×10^{-7} cm^{-2} which, barring appreciable differences in accommodation, should suffice to suppress effectively new particle formation. This may be made more quantitative using the average molecular survival times calculated in Appendix B for the measured size distributions, i.e., a newly formed nucleogen molecule on average survives only several minutes before it encounteres the surface of an existing particle. If times on the order of hours or longer are required to reach the homogeneous nucleation level, new particle formation is unlikely to take place.

It is important to note that the size distributions presented earlier (for the Tucson samples) indicate that there is only a small amount of particulate material present in the $r \leq .005$ μ size range.

The nuclei formed with the SO_2-enriched air samples are about .003 μ in radius and require (at the 30-50 ppb level of added SO_2) some 2 hours to reach .005 μ. It seems likely that if large numbers of such small nuclei were forming in ambient atmospheric air, one should on occasion find large amounts of aerosol in the $r_i \leq .005$ μ region of the size distribution. In some two years of size distribution measurements this has never been observed.

2. High pressure Xe-Hg sources, HPXeHg-(UF), HPXeHg-(0-53): Despite the presence of significant amounts of radiation in the 2100 Å $\leq \lambda_i \leq$ 2450 Å region in the HPXeHg-(UF) UV source, nucleus formation has never been observed. Continuous irradiation with both of these sources for 12 hours at RHs up to 85% has failed to result in any aerosol formation whatsoever.

3. Low pressure Hg sources, LPHg-(UF), -9(58), -9(54):

a. Wavelengths responsible for aerosol formation: Figure 40 shows the results of irradiating filtered atmospheric air for 50 minutes using the LPHg-9(54) source (2537 Å line present, 1850 Å line filtered). After 50 minutes the filter was removed allowing the 1850 Å radiation to enter the reactor and, as can be seen in Figure 40, nucleus formation began within less than a minute. Figure 41 shows the nuclei formed vs. time of irradiation with the various low pressure Hg sources at comparable humidities. Nucleus formation did not take place unless the 1850 Å radiation was present in the photoreactor. The intense 2537 Å Hg line could not have been responsible for aerosol formation.

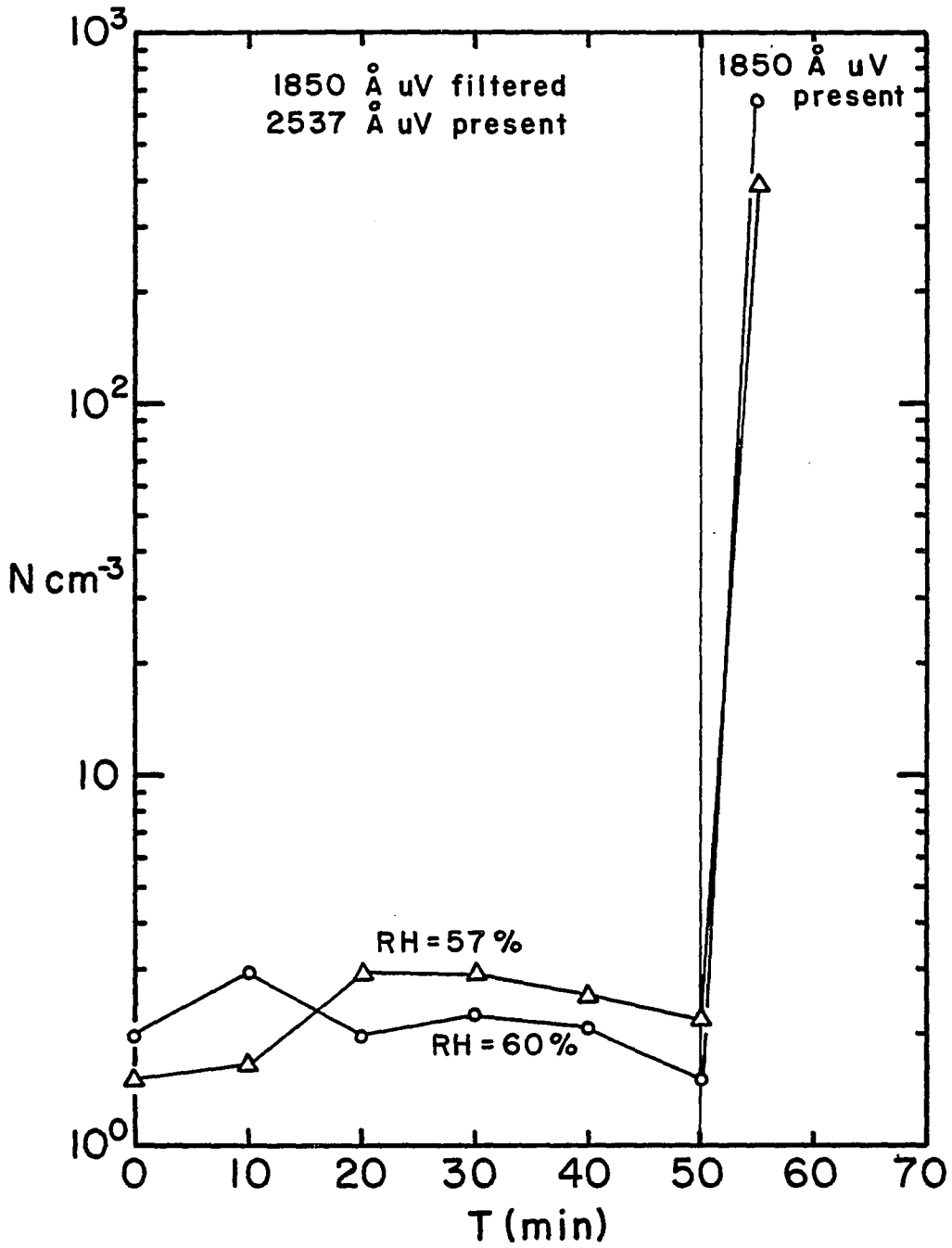

Figure 40. Rate of nucleus formation with and without the 1850 Å line present in the photoreactor.

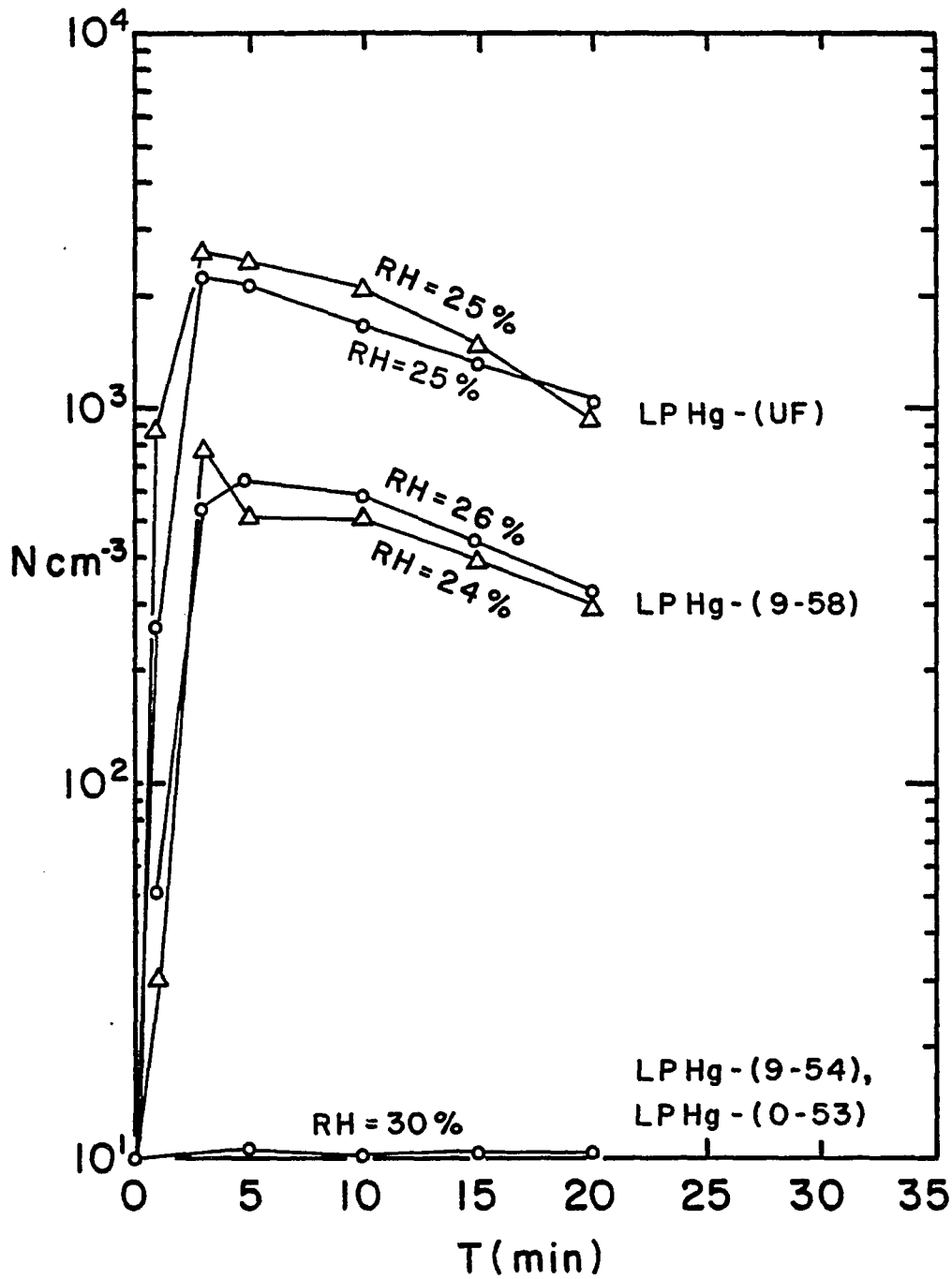

Figure 41. Photochemical nucleus formation with the various LPHg radiation sources.

See Table 1 for a summary of the wavelengths present in the photoreactor.

b. Dependence on relative humidity: As shown in Figure 42 the number of nuclei formed increased rapidly with the RH of the air sample. A change in RH by a factor of 2 resulted in an increase of one or more orders of magnitude in the number of nuclei formed. The marked similarity in shape of these curves to those of Figures 29 and 38 is to be noted. In each instance a large number of nuclei initially formed which then effectively suppressed further particle formation. The curves illustrate the fact that the time required for the onset of nucleus formation did not depend sensitively on the humidity of the air sample (at least for RH's $\geq$ 23%). In addition the increase of nucleation rate with RH indicates that at least a binary molecular system was involved.

c. Effect of added SO_2: the effect of adding SO_2 is shown in Figure 43. The peak nucleus concentration increased by about an order of magnitude with a 60% increase in the added SO_2. Note that in contrast to the results with solar irradiation, the time required for nuclei to first appear was <u>not</u> markedly sensitive to the SO_2 concentration. These results suggest that although SO_2 may well have been involved in nucleus formation, other trace constituents were also playing an important role.

d. Role played by SO_2: The result of passing filtered atmospheric air samples through 500 cm^3 of 13x molecular sieve and 750 cm^3 of activated charcoal and then adding SO_2 and H_2O vapor before irradiation is shown in Figure 44. Several effects are clearly discernible. Simply restoring SO_2 to the 10-30 ppb level did not restore particle formation back to the rates originally observed in the

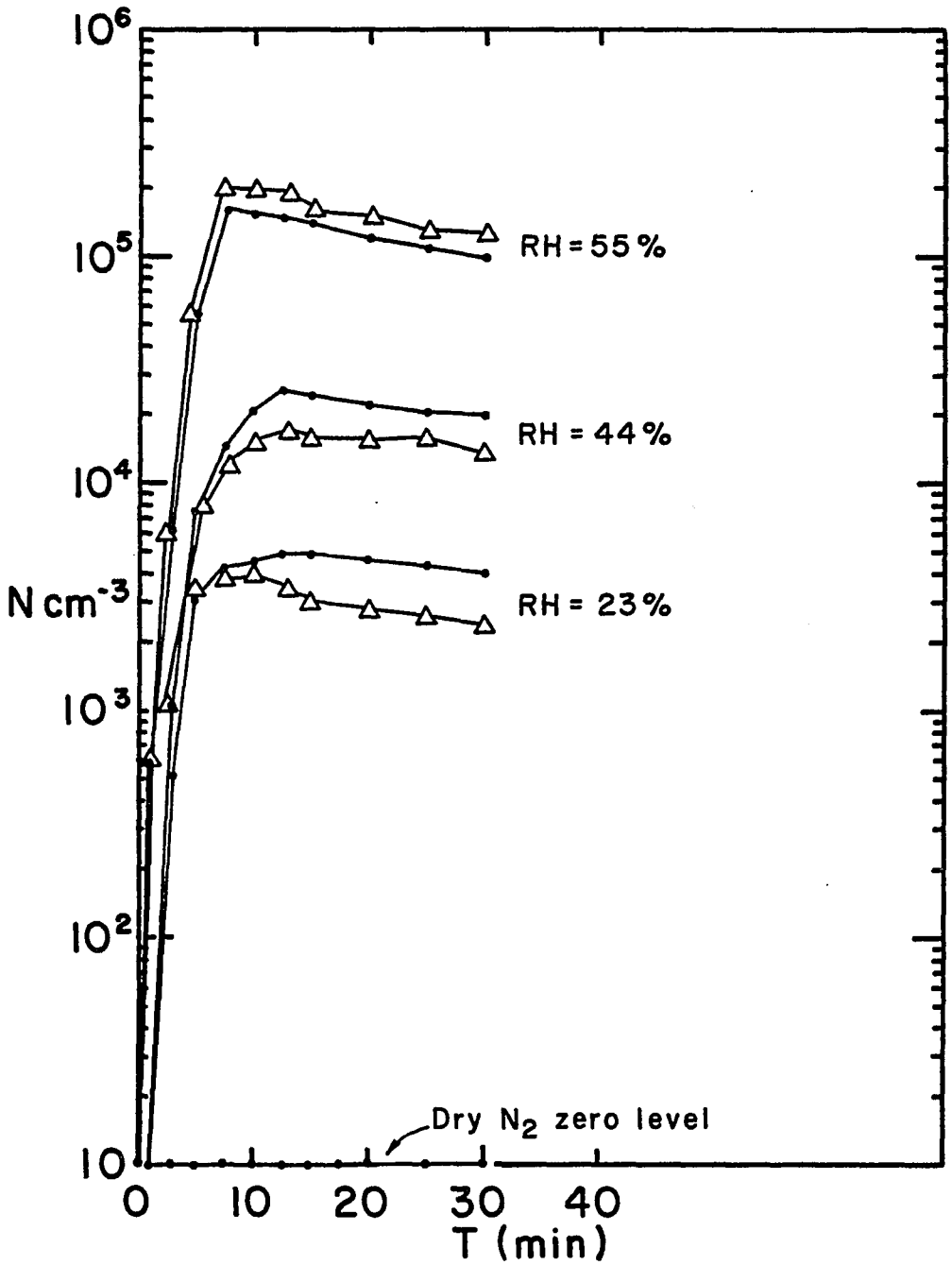

Figure 42. Nucleus formation at various relative humidities with the LPHg-(UF) UV source (1850 Å).

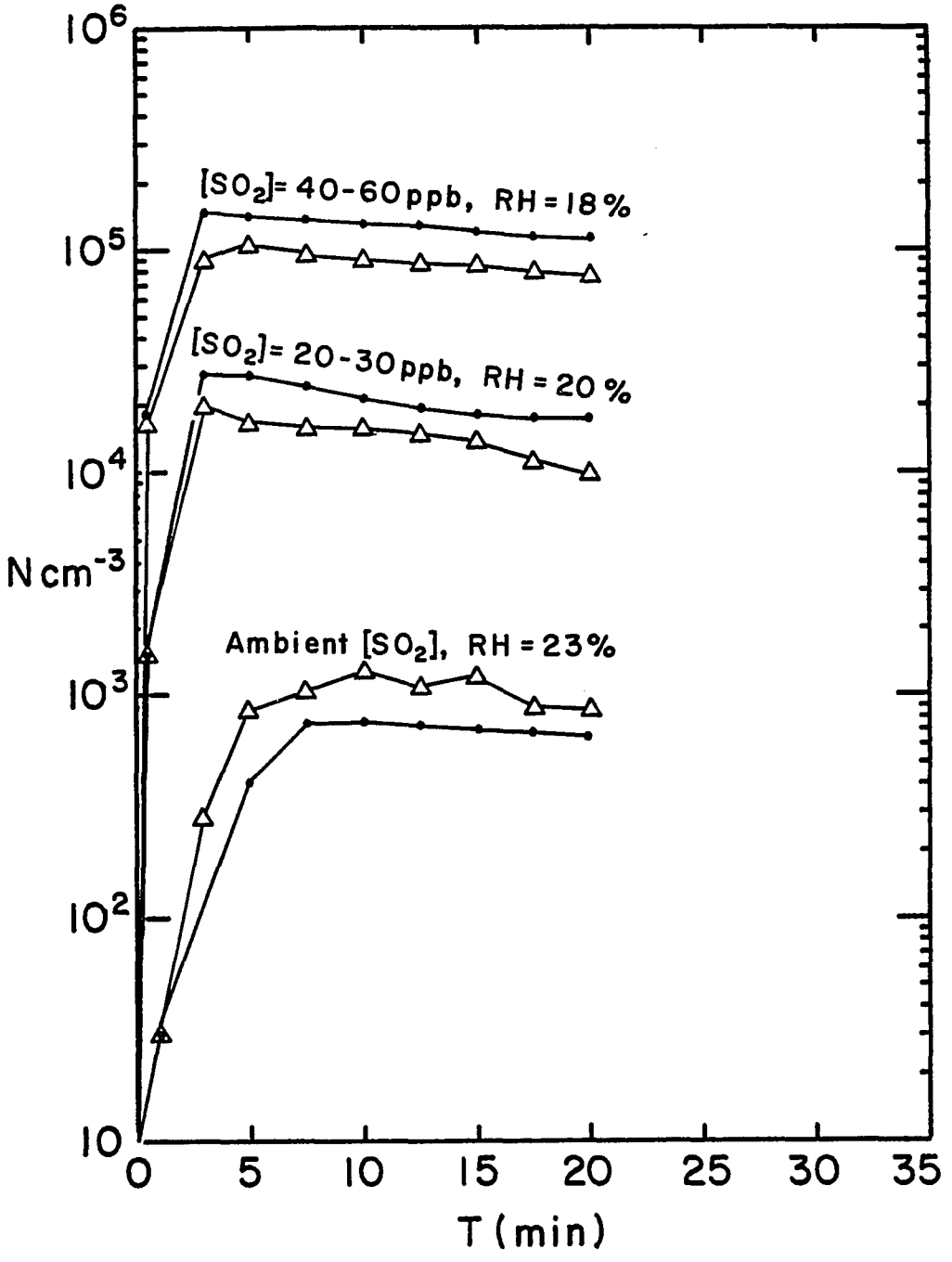

Figure 43. Nucleus formation in atmospheric air enriched in SO_2 using 1850 Å UV radiation.

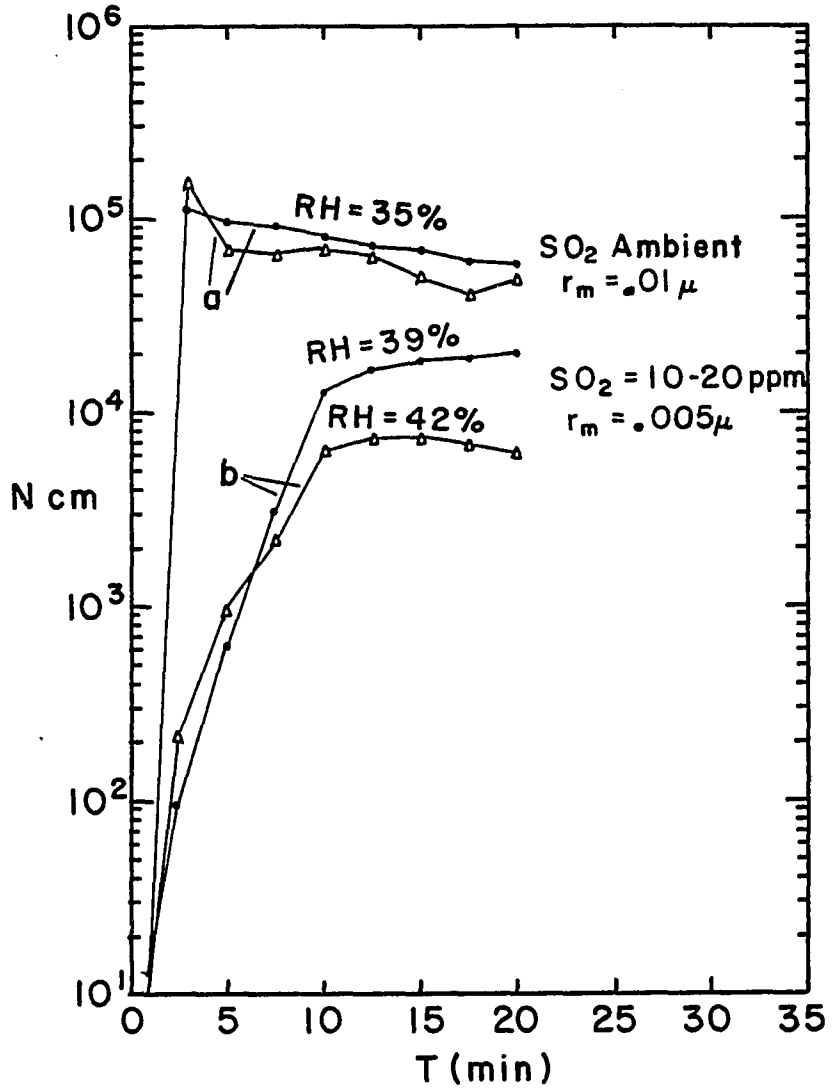

Figure 44. Role of SO_2 in accounting for nucleus formation.

The sets of curves are labeled as follows: a corresponds to humidified atmospheric air, b to air samples which were passed through 1000 cm^3 of 13x molecular sieve and 750 cm^3 of freshly activated charcoal and then humidified and enriched in SO_2.

unscrubbed atmospheric air. Furthermore the size of the nuclei was markedly smaller in the restored air samples, i.e., in the original unscrubbed air the nuclei grew to .01 μ in 20 minutes while in the restored air samples the modal radius was only .004 - .005 μ. These results suggest that gases (other than SO_2) affected both the number of nuclei formed and their rate of growth.

e. Rate of growth of the nuclei: The growth rate of the nuclei was measured by passing the reactor samples through various Nuclepore filters. The fraction transmitted through a given Nuclepore filter can be written $T_N = \int_{r_c}^{r_m} K_n(x)\ f(x)\ dx/N_T$; that quantity is shown as a function of time in Figure 45. Here r_c, r_m are respectively the lower and upper cutoff radii for the nth Nuclepore filter (see Figure 3), $K_n(x)$ is the nth filter transmission kernel, N_T is the total number of particles, and f(x) is the aerosol size distribution. T_N is an indicator of particle size in the following sense: only those particles with radius greater than r_c are transmitted by the filter, that is, the appearance of nuclei through a given filter implies that the leading edge of the size distribution f(x) has begun to exceed the cutoff radius of that filter. The physical meaning of the T_N may be further clarified by considering two particular idealized cases. In the first case let the $K_n(x)$ have, hypothetically, the following form

$$K_n(x) = \begin{cases} 1 & r_c \leq r \leq r_m \\ 0 & \text{otherwise} \end{cases}$$

If all of the particles have radii less than r_m, T_N would just be the fraction of the particles whose radii were greater than r_c, i.e., T_n would numerically be equal to the normalized cumulative distribution. In the second case let the $K_n(x)$ be real but consider a size distribution of the form $f(x) = N_T\delta(x-x_o)$. We then have $T_N = \int_{r_c}^{r_m} K_n(x)\ \delta(x-x_o)\,dx$ which would be just $K_n(x_o)$. Therefore for this case T_n would numerically be the value of the nth kernel evaluated at x_o.

Figure 45 shows that the nuclei rapidly grew past .001 μ but that 20-30 minutes were required to reach a radius of .01 μ. The number of cloud nuclei active at a .75% supersaturation is also shown in Figure 45. Note that the appearance of the cloud nuclei coincided with the appearance of nuclei through the fourth nuclepore filter, i.e., the nuclei had to reach .01 μ before functioning as CCN at a .75% supersaturation. According to nucleation theory that requires particles which exceed a minimum size which varies weakly with composition but is $\sim$ 0.015 μ for common inorganic salts.

f. Relationship between the number of nuclei with radii $\geq$ .01 μ, the total number of nuclei, and the number of CCN active at .75%. Figure 46 illustrates some of the salient points relating to the nature of the nuclei and their rate of growth. Observe that after some 35 minutes of continuous irradiation very few of the nuclei were $\geq$ .01 μ (this being the cutoff radius of the Nuclepore filter) and that of these 30-50% were cloud condensation nuclei.

4. Static irradiation with the ambient nuclei present: In this series of experiments unfiltered atmospheric air was continuously

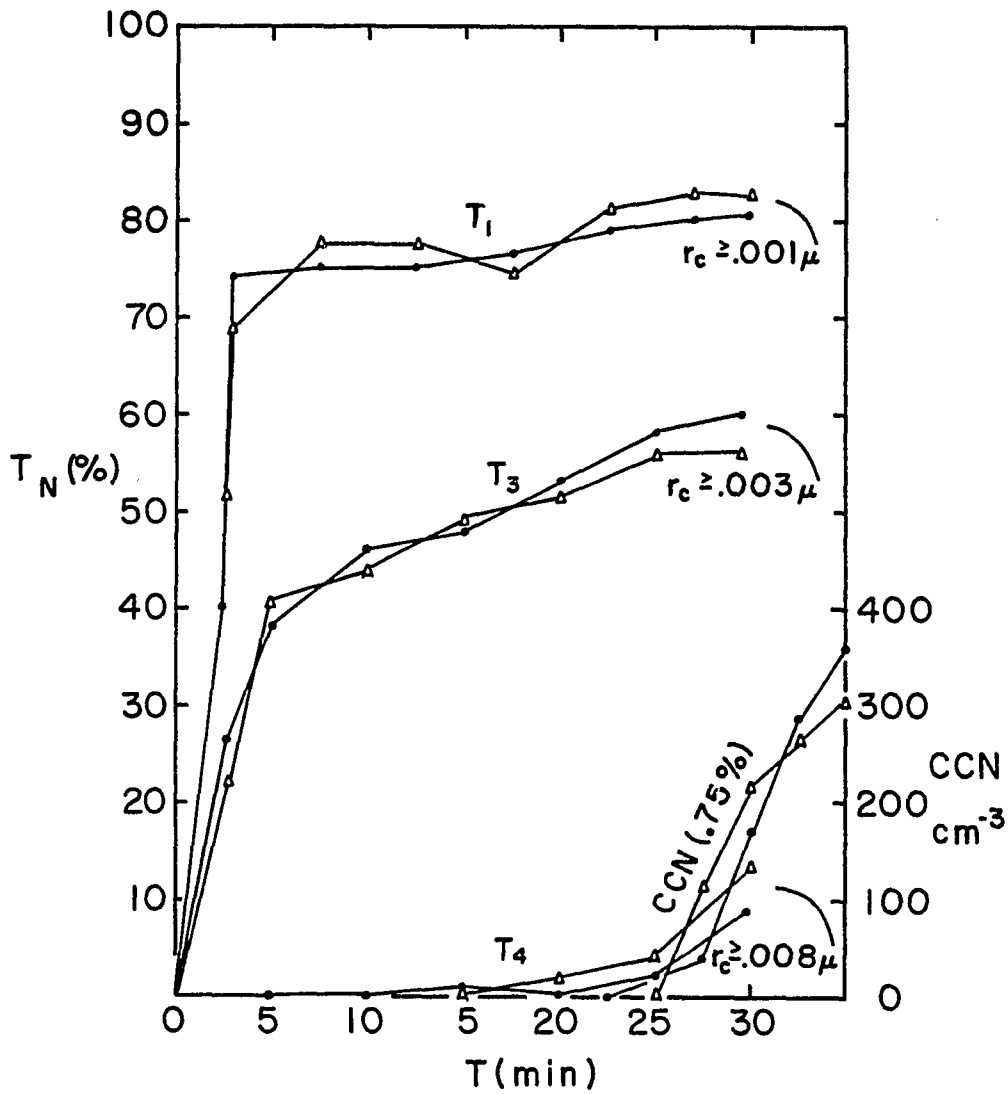

Figure 45. Condensational growth of the nuclei produced in atmospheric air samples with 1850 Å UV radiation.

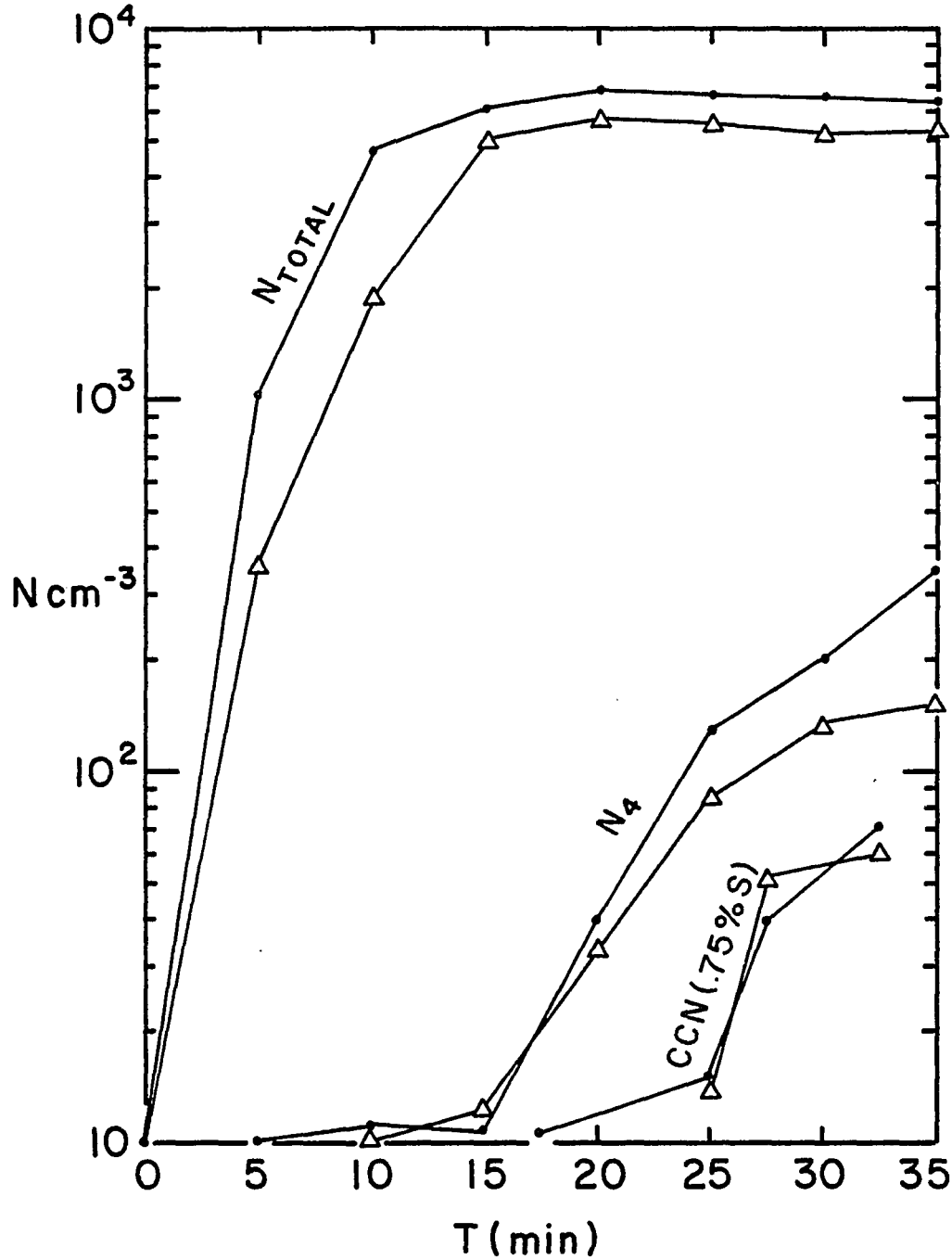

Figure 46. Relationship between the total number of nuclei, the number transmitted through the number 4 Nuclepore filter and the number of CCN.

irradiated with the various UV sources. As discussed earlier the particle filter tended to remove trace gases and as such the possibility existed that some trace gases involved in aerosol formation (particularly with solar irradiation) might have been partially removed. In addition it is well known that trace gases such as O_3 are rapidly destroyed when passed through stainless steel tubing and particle filters. It is also possible that the surfaces provided by the existing aerosol might catalyze the formation of new aerosol. In order to prevent the possible destruction of various trace gases and to allow the existing particles to be present in the reactor the sampling was done using only 6 feet of Teflon tubing and a high sampling rate. The use of Teflon prevents the destruction of O_3. As shown in Figure 47 it was only with the LPHg-(UF) radiation source (i.e., 1850 Å radiation) that new nucleus formation was observed. With all of the other sources there was no detectable difference in the rate of decay of the nucleus concentration from the unradiated case. It thus appears that the existing particles did not promote new particle formation.

Experiments With the .3 Liter Quartz Flow Reactor. In this set of experiments the air samples were pulled through the particle filter and flow reactor into a 200 ℓ aluminized mylar bag. This arrangement allowed the air samples to be irradiated for a well defined time. The quartz reactor allows for a simple flow and irradiation geometry. The 200 ℓ bag served as a large volume reaction chamber and was prefilled with various aerosol-gas mixtures. The bag was of sufficient size that the complete aerosol size distribution of the nuclei could be obtained.

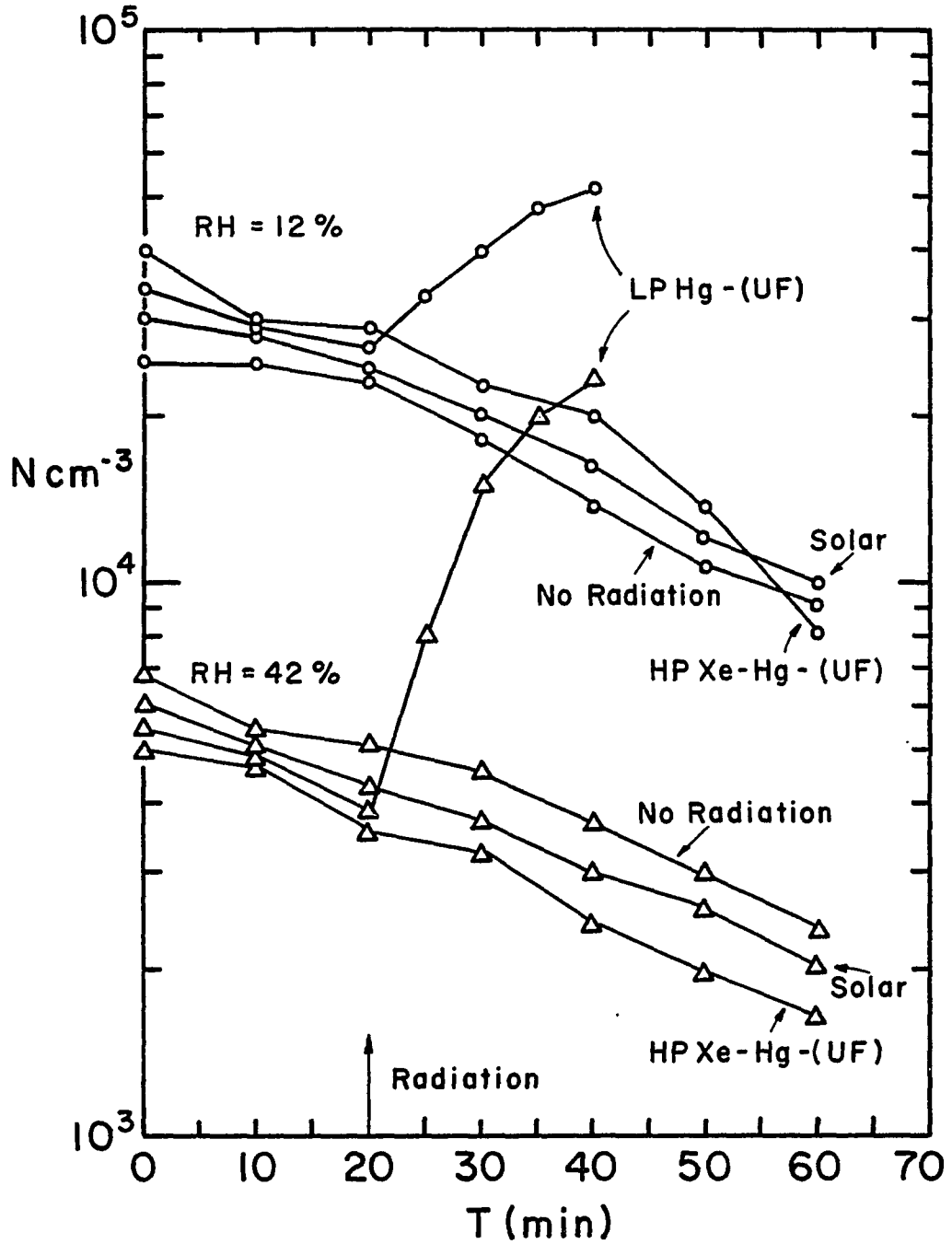

Figure 47. Nuclei formed during the irradiation of unfiltered atmospheric air.

1. Storage of irradiated atmospheric air: Using the LPHg-(UF) source (1850 Å UV present) air samples were pulled through the reactor and stored in the mylar bag. Figure 48 shows the behavior of the nuclei when a 10 minute filling time was used with a reactor residence time of 3 sec. The bag was prefilled with 125 ℓ of dry, clean, bottled air. The total sample volume was 65 liters for each of the curves shown. The curves labeled a, b, c, and d are repetitious of the experiment using filtered atmospheric air. The behavior of the nuclei concentration as a function of time was always the same, i.e., new nuclei were not formed during storage of the irradiated air. After some 10-15 minutes the nuclei had a modal radius of .01 μ. For purposes of comparison a 10-20 ppb SO_2 - H_2O - clean air mixture was irradiated and stored under identical conditions. This result, labeled e, is also shown in Figure 48. Note that new nuclei formed during storage and that after 10-15 minutes the modal radius was only .004 μ. The size distribution of the nuclei corresponding to curves a and e of Figure 48 are shown in Figure 49.

2. Effect of passing the irradiated air and gas samples through the fourth Nuclepore filter before storage: The previous result suggested that in irradiated SO_2 - H_2O - Air mixtures nucleus formation was taking place from the gas phase during storage, i.e., new nuclei continued to form during storage. Note the resemblance of curve e, Figure 48 with those of previous figures when static irradiation was used. This behavior of atmospheric air samples suggests that the bulk of the gaseous nucleogen was converted into the aerosol phase in the

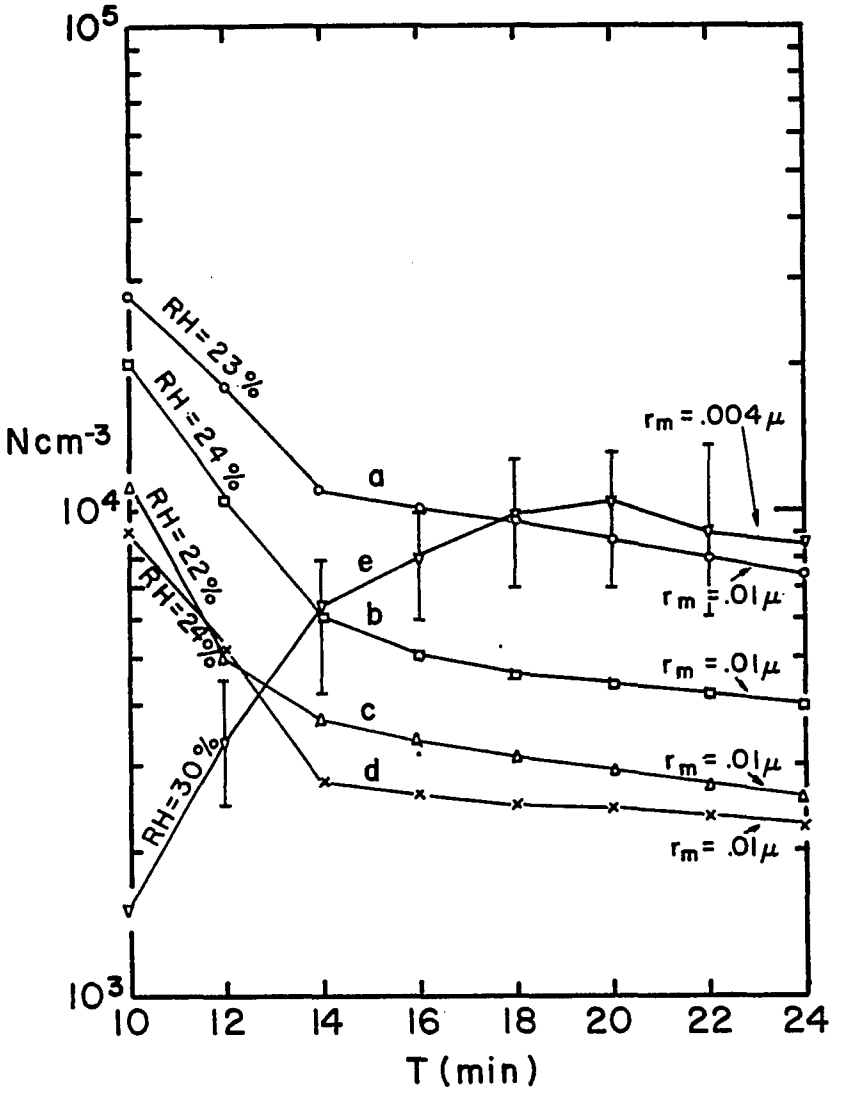

Figure 48. Formation of nuclei during storage using the quartz reactor and 1850 Å UV radiation.

The curves labeled a, b, c, d, show the nuclei formed in atmospheric air with a 10 min. filling time, the curve labeled e shows the results of irradiating 10-20 ppb SO_2-Air-H_2O mixtures under identical conditions.

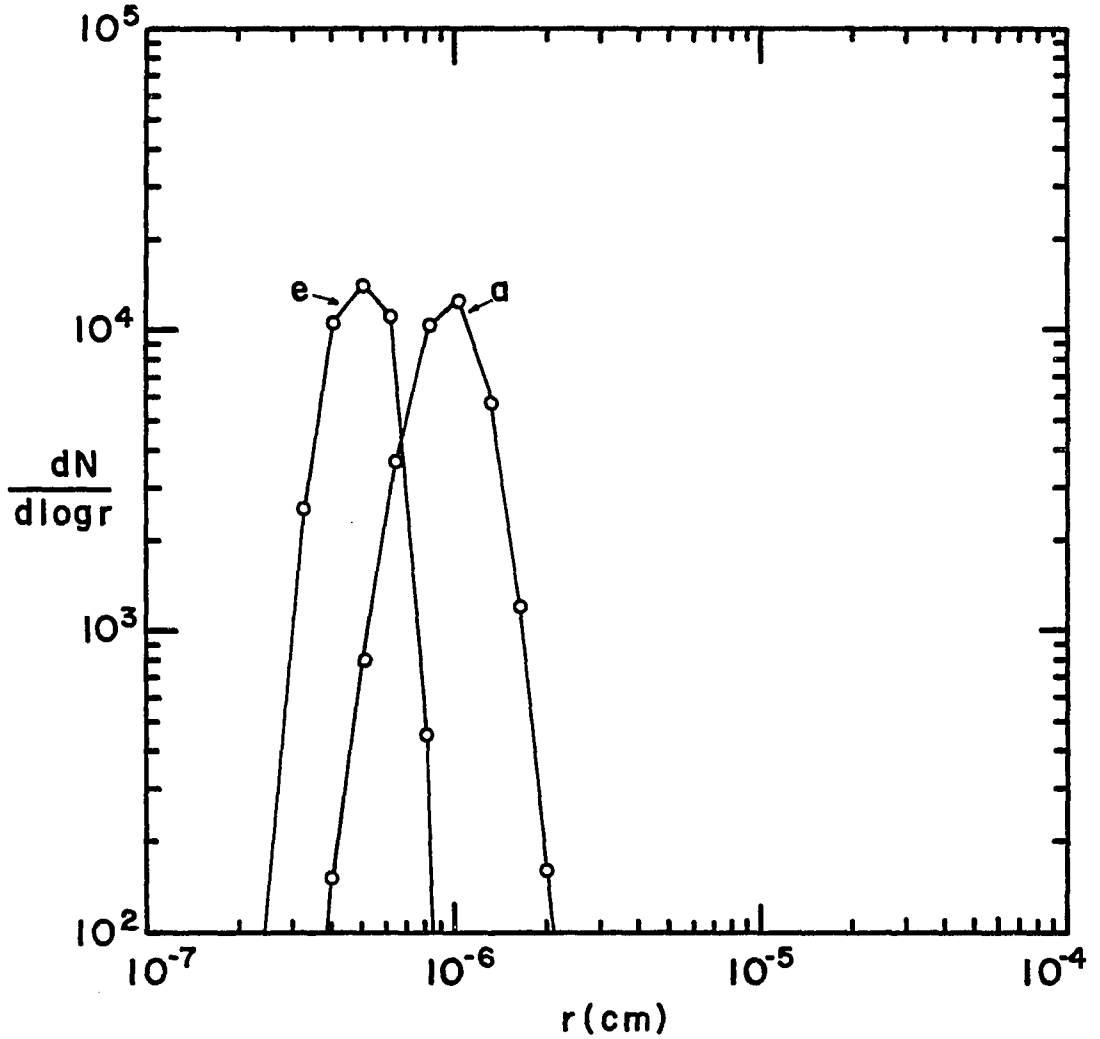

Figure 49. Size distributions of the nuclei corresponding to curves a and e in Figure 48.

photoreactor. If this was the case then passing the irradiated mixture through a particle filter should markedly effect the results using atmospheric air but would have much less effect on the gas phase reactions associated with the SO_2 - H_2O - Air mixtures. The results of an experiment carried out to test this expectation are shown in Figure 50. As this figure illustrates, the Nuclepore filter had no discernible effect on the SO_2 - Air - H_2O mixtures but it completely suppressed nucleus formation in atmospheric air.

3. Behavior of irradiated atmospheric air samples using a 1-minute filling time: With a 1-min filling time new nuclei were observed to form on storage as shown in Figure 51. Note that the shape of these curves, the total nucleus concentration, and the size of the nuclei bear a marked resemblance to curve e in Figure 48. These last three experiments all strongly suggested that other trace gases than SO_2 were necessary to explain the behavior of the irradiated atmospheric air samples. The size distributions corresponding to the curves in Figure 51 are shown in Figure 52. Note two important features of these distributions: the virtual absence of particles larger than .01 μ and their highly monodisperse character.

4. Effect of storing irradiated samples in bottled gas mixtures vs storage in atmospheric air: The previous results suggested that trace gases other than SO_2 play an important role in nucleus formation. An important question is whether or not these gases were involved in the photochemistry itself or whether they were playing a chemical role. To clarify this, consider the following possible reactions:

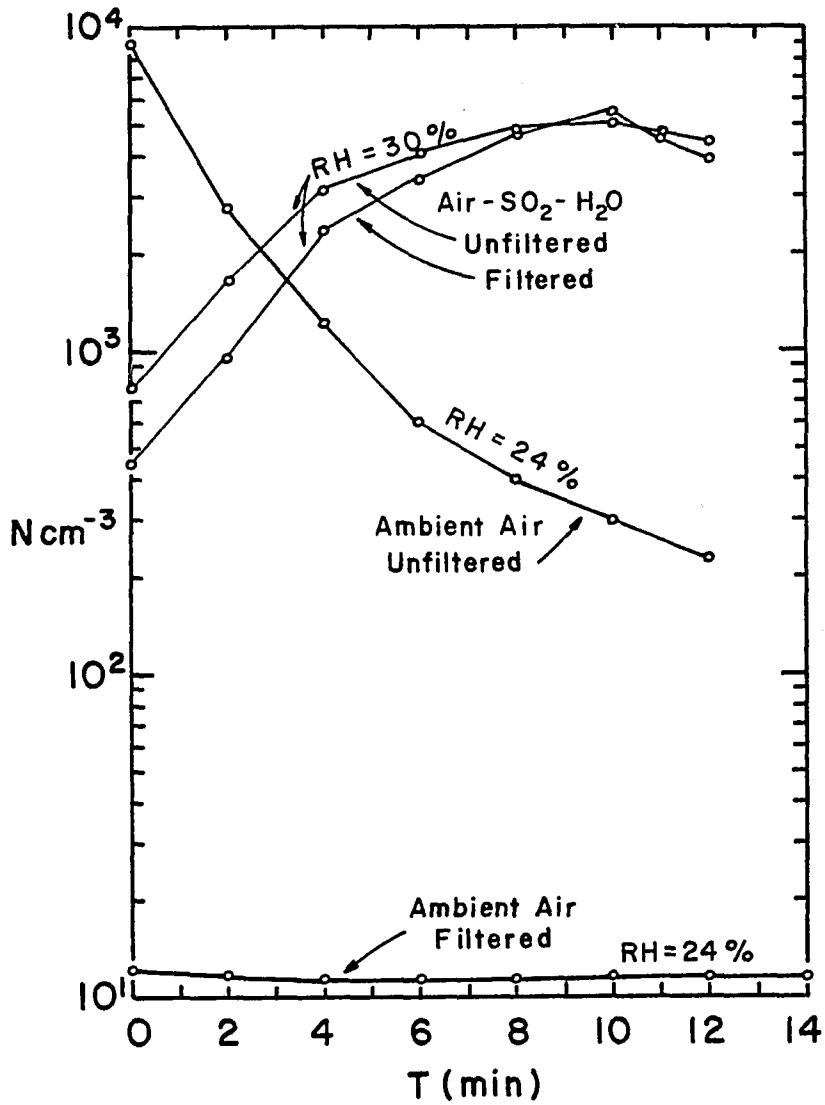

Figure 50. Effect on nucleus formation of passing the irradiated gas samples through a Nuclepore filter before storing in the mylar bag.

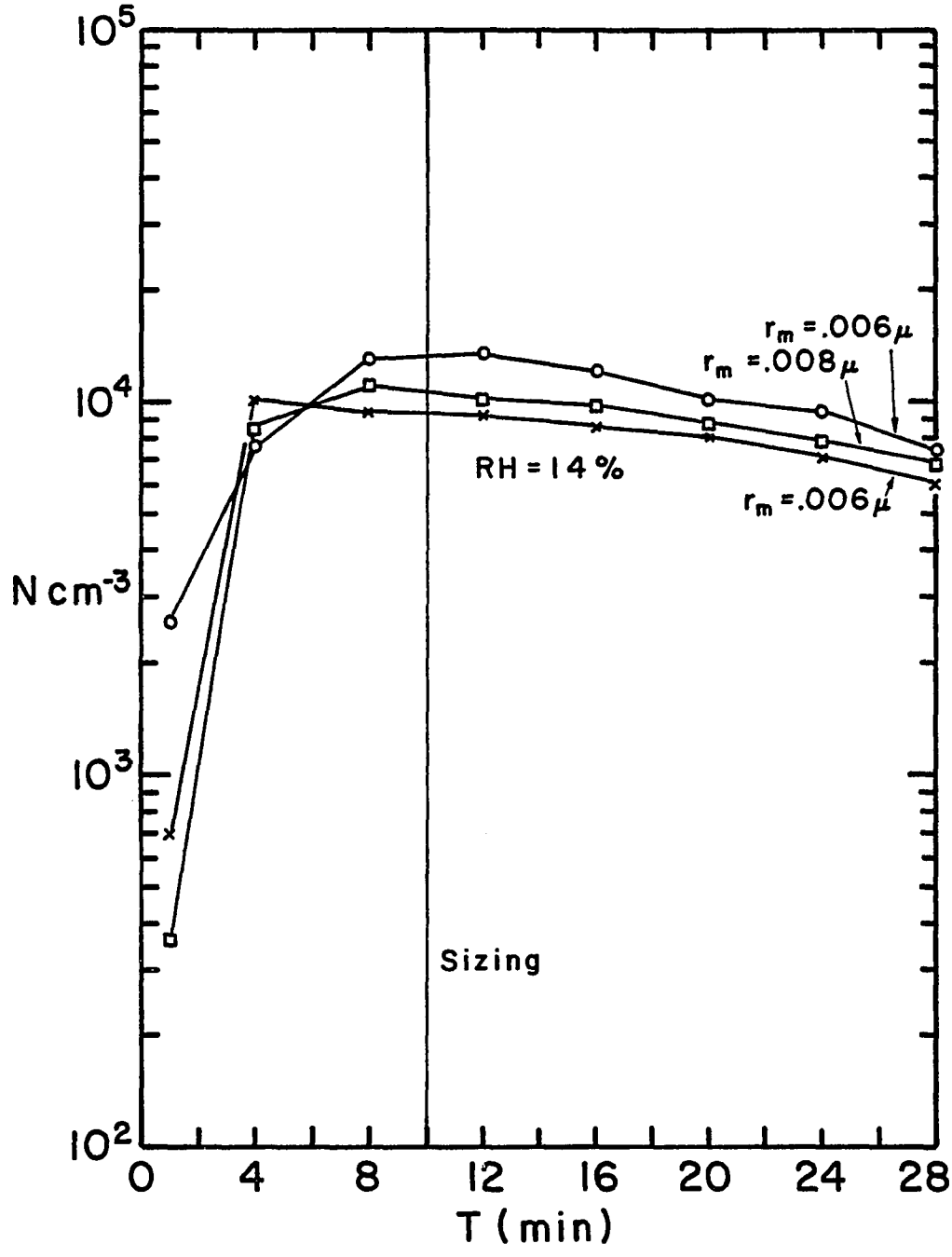

Figure 51. Nuclei formed during storage with a 1 minute filling time.

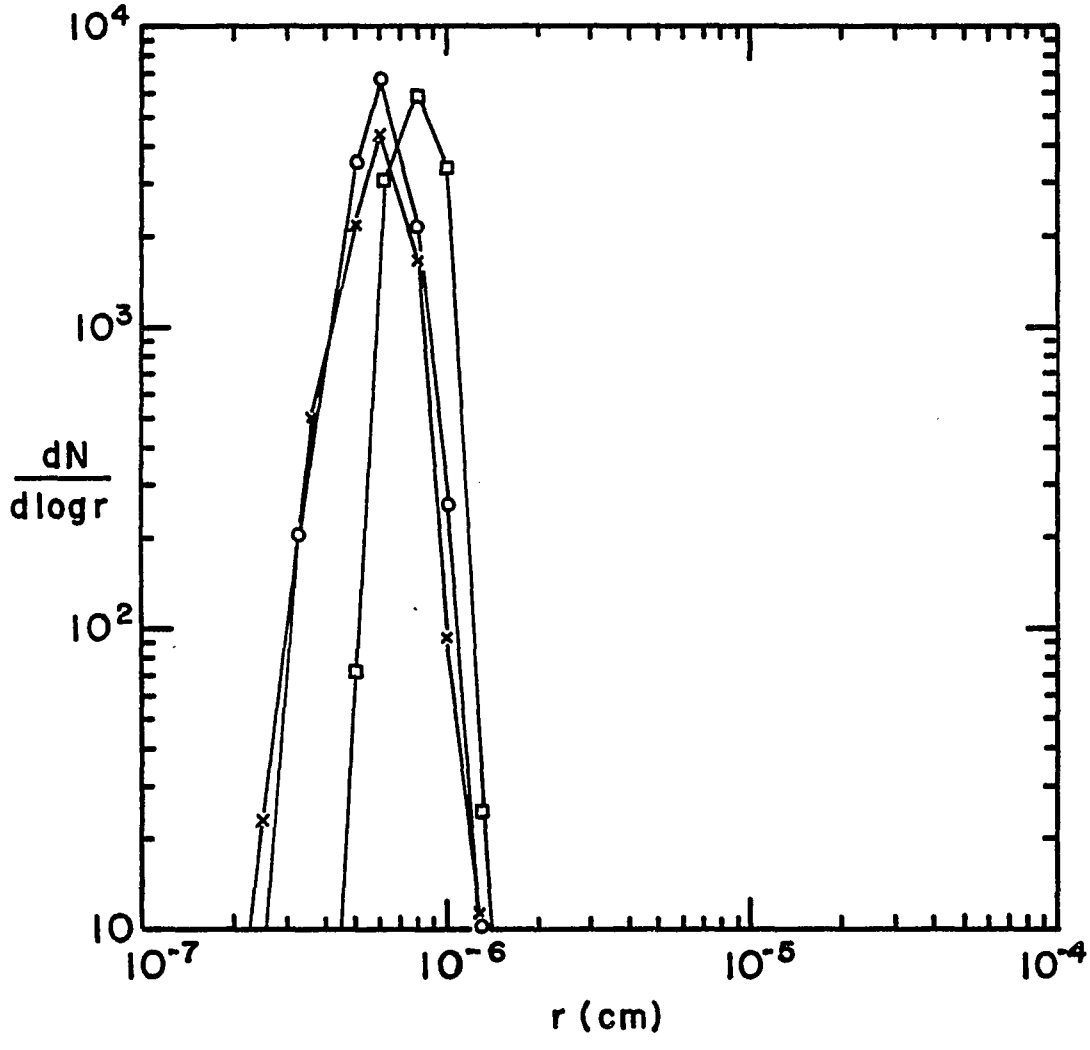

Figure 52. Size distributions of the nuclei corresponding to the curves in Figure 51.

$$A \xrightarrow{UV} x$$

$$B \xrightarrow{UV} y$$

$$x+y \longrightarrow Zm$$

where A, B are two trace molecules which are photochemically converted into x and y and form Zm a supersaturated nucleogen. In this case both gases A and B are involved in the photochemistry, i.e., both are photochemically converted into other molecular species. On the other hand, suppose the B plays only a chemical role that is:

$$A \xrightarrow{UV} x$$

$$x+B \longrightarrow Zm$$

If the first case is true, then species B would need to be present in the photoreactor while in the latter case B would not need to be irradiated, but could be introduced into the gas mixture after irradiation. In the present experiment irradiated atmospheric air and SO_2 - H_2O - Air mixtures were stored in the mylar bag which was prefilled with either scrubbed bottled air or with filtered atmospheric air. The effect on nucleus formation is shown in Figures 53 and 54. In Figure 53 a 10-20 ppb SO_2 - H_2O - Air mixture was stored in clean bottled air and in filtered atmospheric air. Note the substantial increase in both the number of nuclei formed (by a factor of 20) and in the size of the nuclei when the bag contained atmospheric air. The

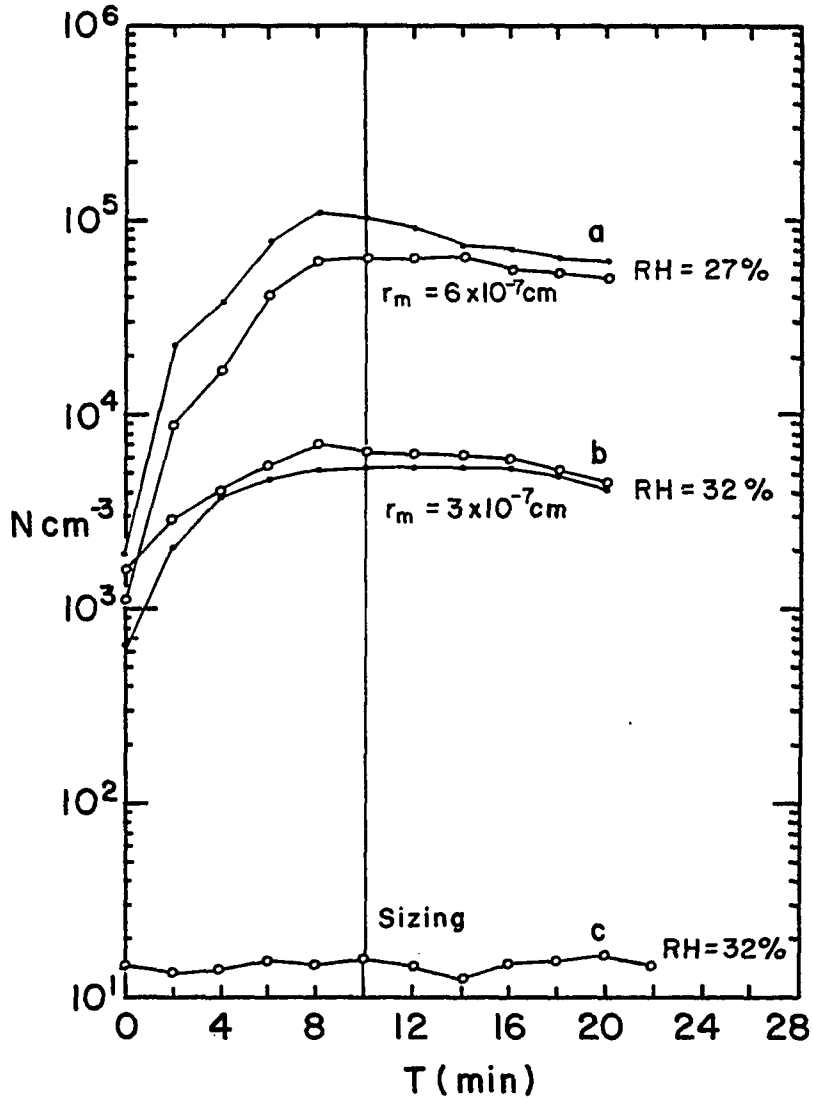

Figure 53. Effect of storing irradiated SO_2-Air-H_2O mixtures in atmospheric and in scrubbed bottled air.

The curves are labeled as follows: a. Irradiated SO_2-Air-H_2O mixtures stored in filtered atmospheric air, b. irradiated SO_2-Air-H_2O stored in scrubbed bottled air, c. irradiated Air-H_2O mixture stored in atmospheric air enriched with 10-20 ppb of SO_2.

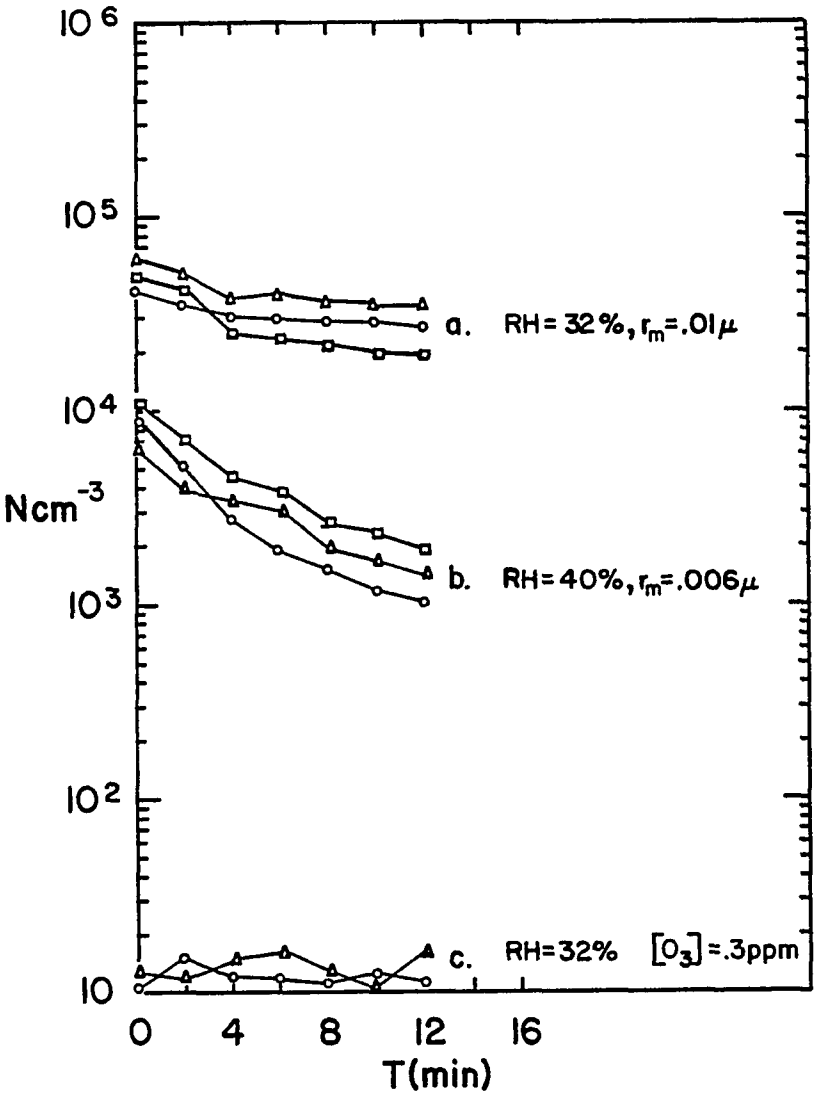

Figure 54. Effect of storing irradiated atmospheric air in filtered atmospheric and scrubbed bottled air.

The curves are labeled as follows: a. irradiated atmospheric air stored in filtered atmospheric air, b. irradiated atmopsheric air stored in scrubbed bottled air, c. irradiated bottled air stored in atmospheric air.

same effect was observed when irradiated atmospheric air was stored in atmospheric air. These results are clearly consistent with the second reaction scheme. Although short UV (1850 Å) radiation was used in this experiment, if there are trace gases present in the atmosphere which play a similar role, it would be of significant importance in explaining nucleus formation at the longer solar wavelengths. To the author's knowledge this effect has not been reported before in the literature and it would seem to be of sufficient importance to justify further experimental work.

The bottom curves in Figures 53 and 54 show the result of storing irradiated clean Air - H_2O mixtures in filtered atmospheric air to determine the effect of the high levels of O_3 produced with the 1850 Å UV. O_3 itself did not form nuclei when injected into atmospheric air stored in the mylar bag. Nucleus formation also did not take place if the bag was filled with atmospheric air enriched with 10-20 ppb of SO_2 and then enriched in O_3 to the .3 ppm level.

5. Effect of storing irradiated atmospheric air samples in air containing preexisting nuclei: In this series of experiments the bag was filled with air containing various concentrations of ambient natural nuclei or previously formed photochemical nuclei. Irradiated air samples were then injected into the bag and the nucleus concentrations monitored as a function of time. Figure 55 shows the variation of the nucleus concentration with time for various initial ambient nucleus concentrations. With preexisting nuclei concentrations greater than about 2-3 x 10^4 cm^{-3} new aerosol formation was not observed. There are

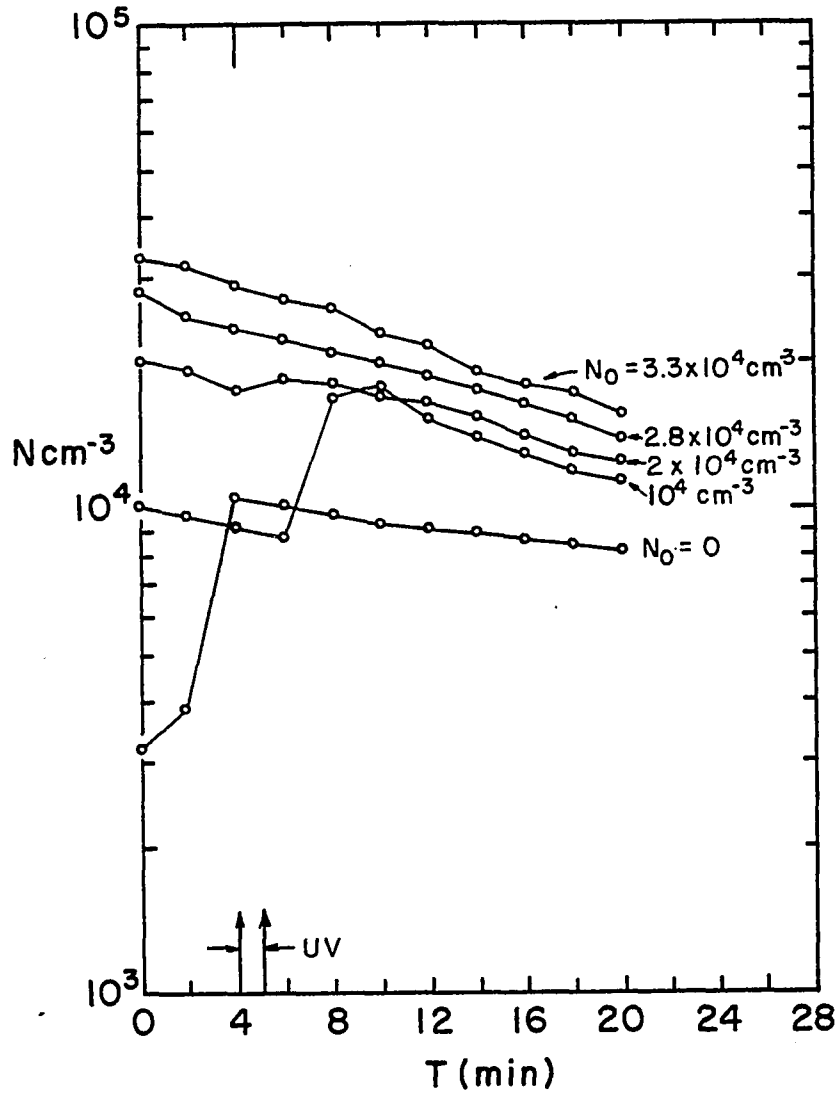

Figure 55. Effect of storing irradiated atmospheric air in unfiltered atmospheric air.

The curves are labeled according to the number of nuclei (N_0) initially present.

a number of explanations but it seems that a reasonable one is that the existing nuclei readily accommodated the photochemical nucleogen and/or coagulated with the newly formed aerosol particles. The particle survival lifetimes calculated earlier (see Figure 16) may be used to estimate the importance of coagulative removal. The average survival lifetime of the newly formed photochemical aerosol (r_m = .005 μ) in the presence of the particles already present in the mylar bag was about 10^2 seconds. This implies a removal rate of about 10^{-2} particles/cm^3 - 5. With an initial concentration of 10^4 cm^{-3} (the $I_0^- = 0$ curve) it follows that some 10 days would have been required to remove the particles by purely coagulative means. It thus appears that the primary effect of the existing aerosol was accommodation of the gaseous nucleogen. Figure 56 shows the same experiment using aged photochemical nuclei rather than ambient nuclei. With preexisting nucleus concentrations on the order of 10^4 cm^{-3} new aerosol formation did not take place. There are two important points which demand attention. First of all, note that only slightly higher (by a factor of 2) nucleus concentrations were necessary to stop new aerosol formation when the ambient nuclei rather than previously aged photochemical nuclei were initially present. This result is perhaps somewhat surprising as one would naturally expect the photochemical nuclei (being of the same composition) to be substantially more effective in accommodating the newly formed nucleogen. This did not, however, appear to be the case. Secondly, even though the irradiated air samples already contained sufficient nucleogen

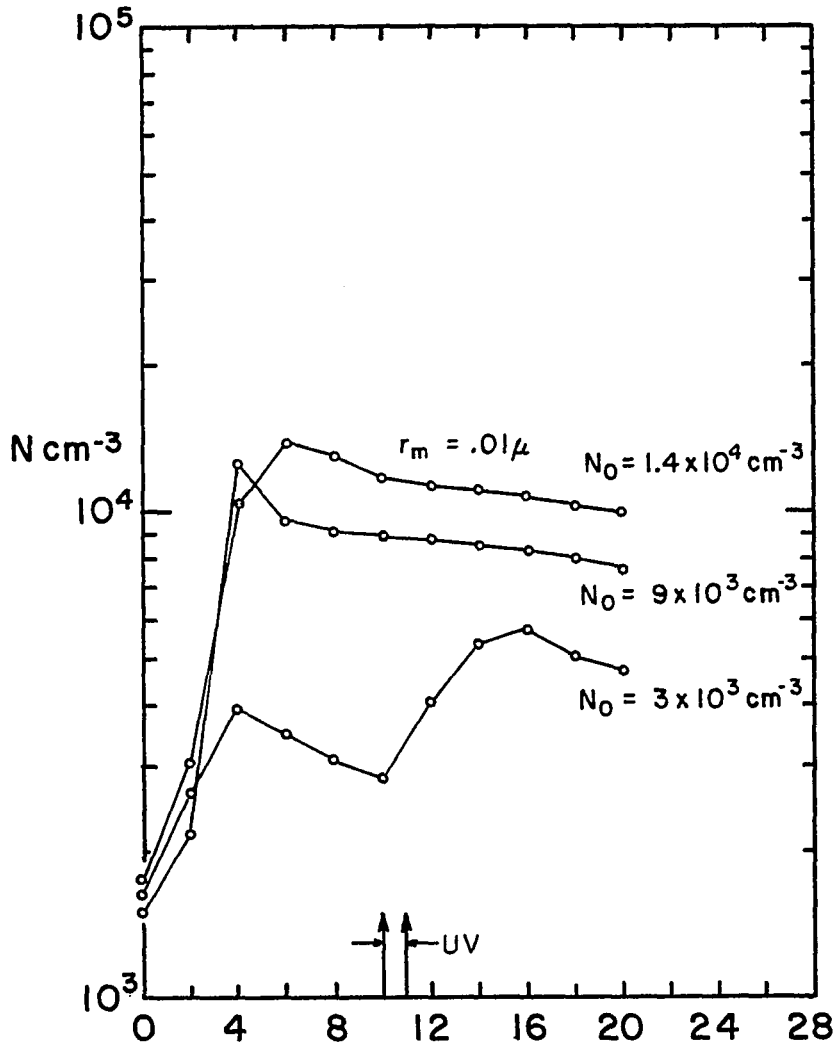

Figure 56. Effect of storing irradiated atmospheric air in air containing previously formed photochemical nuclei.

concentrations to homogeneously nucleate (the $N_0 = 0$ curves in Figures 55 and 56), when there were particles already present in the bag, the homogeneous nucleation process was stopped.

Since the photoxidation rate at 1850 Å is orders of magnitude higher than at solar wavelengths (recall that nucleus formation using solar radiation was not observed) it increasingly seems likely that the major fate of newly formed solar photochemical nucleogen is attachment to the existing aerosol surfaces rather than homogeneous nucleation.

Nucleus Formation in Remote Air Samples in the Short UV

In order to determine to what extent the nuclei formed in the short UV (1850 Å) were due to modification of the air samples by the urban (Tucson) environment, air samples were collected in the rural countryside some 30 miles outside of town. The samples were collected with the apparatus shown in Figure 57. The air samples were pushed through the quartz reactor by compressing the mylar bag with high purity N_2. Samples were also taken at almost the same times on the University of Arizona campus (from the roof of the Physics-Atmospheric Sciences Building), and the rate of nucleus formation compared with the remote samples. These results are presented in Figure 58. Both samples were passed through the flow reactor at the same flow rates and under identical irradiation conditions. The different curves refer to samples collected on different days. The nucleogens responsible for aerosol formation do not appear to be significantly higher in the

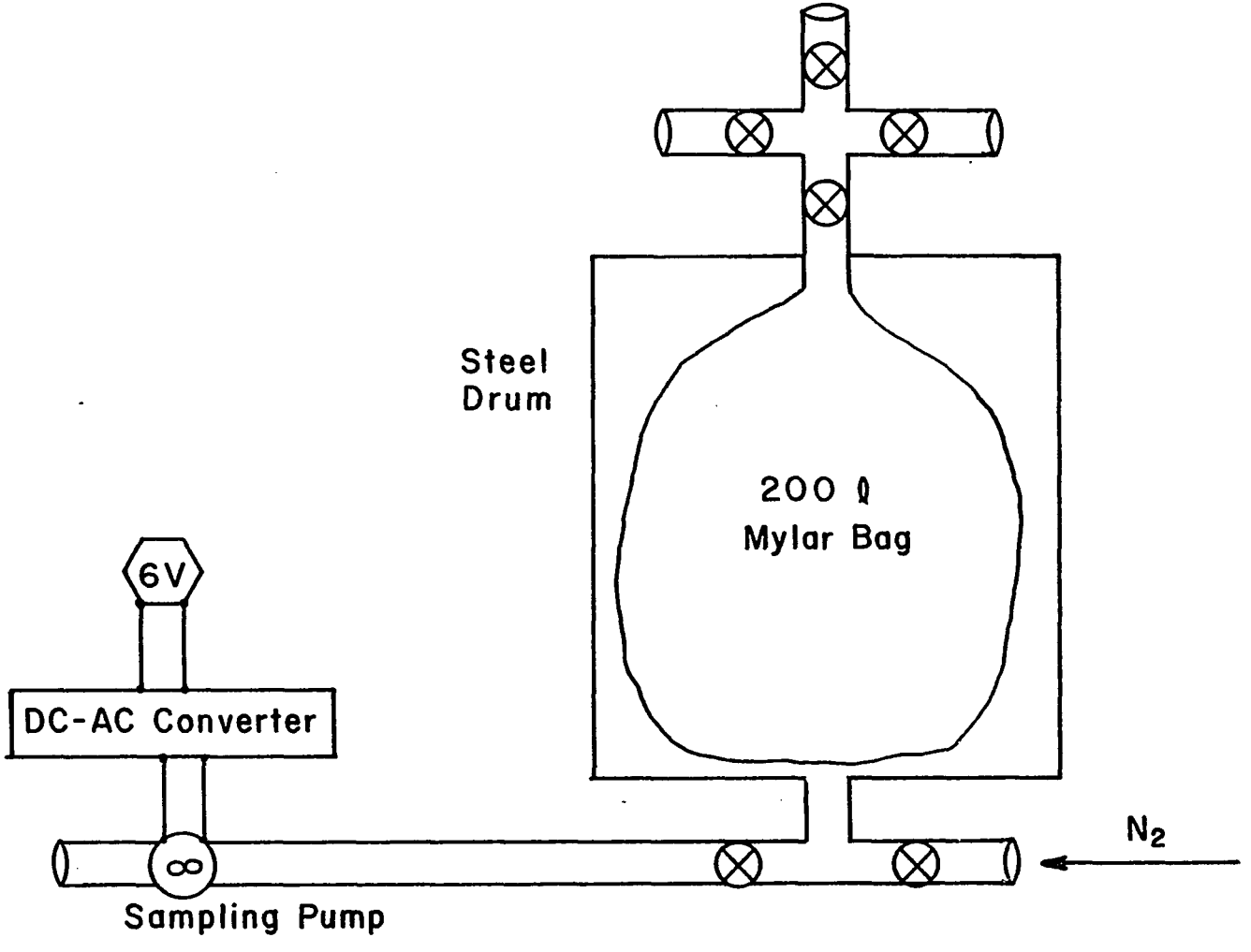

Figure 57. The remote air sampler.

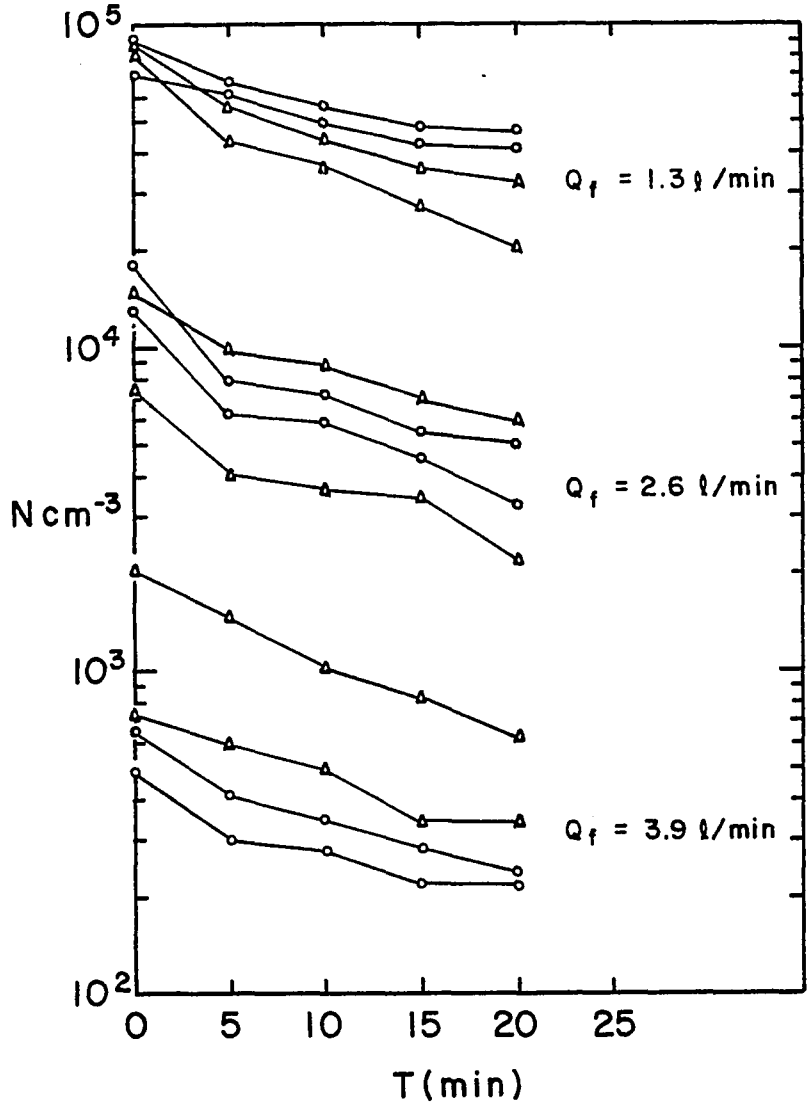

Figure 58. Comparison of photochemical nucleus formation between Tucson and rural air samples.

The different sets of curves are labeled according to the volumetric flow rates through the quartz reactor. The curves drawn with circles refer to rural samples while those drawn with triangles refer to Tucson samples.

Tucson environment than in the rural countryside, i.e., they appear to be generally present in the continental desert air. Bottled air passed through 500 cm^3 of 13X molecular sieve and 750 cm^3 of activated charcoal failed to produce nuclei at the slowest flow rate used and an RH of 25%.

Miscellaneous Experiments

A number of workers have reported spontaneous nucleus formation in the dark, as well as ion-induced nucleus formation. A set of experiments was carried out to examine these mechanisms in the air samples under study here.

Aerosol Formation in the Dark

Outside air was filtered to remove the existing aerosol and stored in the 200-liter mylar bag for periods up to 24 hours without observing aerosol formation. The RH of the air samples was increased up to 75% without being able to detect aerosol formation. If the incoming air samples were passed through the 24-liter photoreactor before storage, aerosol formation was occasionally observed after several hours of storage in the mylar bag. It was subsequently found that this effect took place only after substantial quantities of SO_2 or outside air had been photooxidized in the reactor. When the reactor was then thoroughly cleaned, this effect abruptly disappeared. When the reactor had been extensively contaminated by previous nucleogen, ambient air stored in the reactor itself gave rise to aerosol formation after some 12-15 hours. The number of nuclei formed increased with

both the [SO_2] and RH. Again, however, after a thorough cleaning, this effect abruptly ceased.

When outside air was enriched with .5 ppm of SO_2 and .3 ppm of O_3 at an RH = 50%, spontaneous, in the dark, aerosol formation was occasionally observed. This result is shown in Figure 59. The nuclei so formed are very small, $r_m = 2 \times 10^{-7}$ cm. Although there are many potential mechanisms for aerosol formation, the most likely one is a direct reaction between O_3, SO_2 and traces of olefines to produce H_2SO_4 acid nuclei. It was necessary for all three components to be present for aerosol formation to take place, that is, the outside air had to be humidified and enriched in both SO_2 and O_3. It should be emphasized, however, that ambient air enriched in O_3 alone (to the .3 ppm level) and humidified to an RH of 50% has consistently failed to produce nuclei.

Ion-Induced Aerosol Formation

Filtered outside air was passed through an ionization chamber containing a 200 μCi polonium 210 source. The total ion pair concentration at the exit of the ionizer was estimated as some 2×10^{10} cm^{-3} ion pairs. The ionized air sample was then stored in the 24-liter glass reactor and also in the 200-liter mylar bag. No aerosol formation was observable with RH up to some 70%. In subsequent experiments, the Po^{210} source was placed directly in the photoreactor and humidified air samples continuously exposed to the ion source. No aerosol formation was observed. An additional 50 ppb of SO_2 was added without resulting

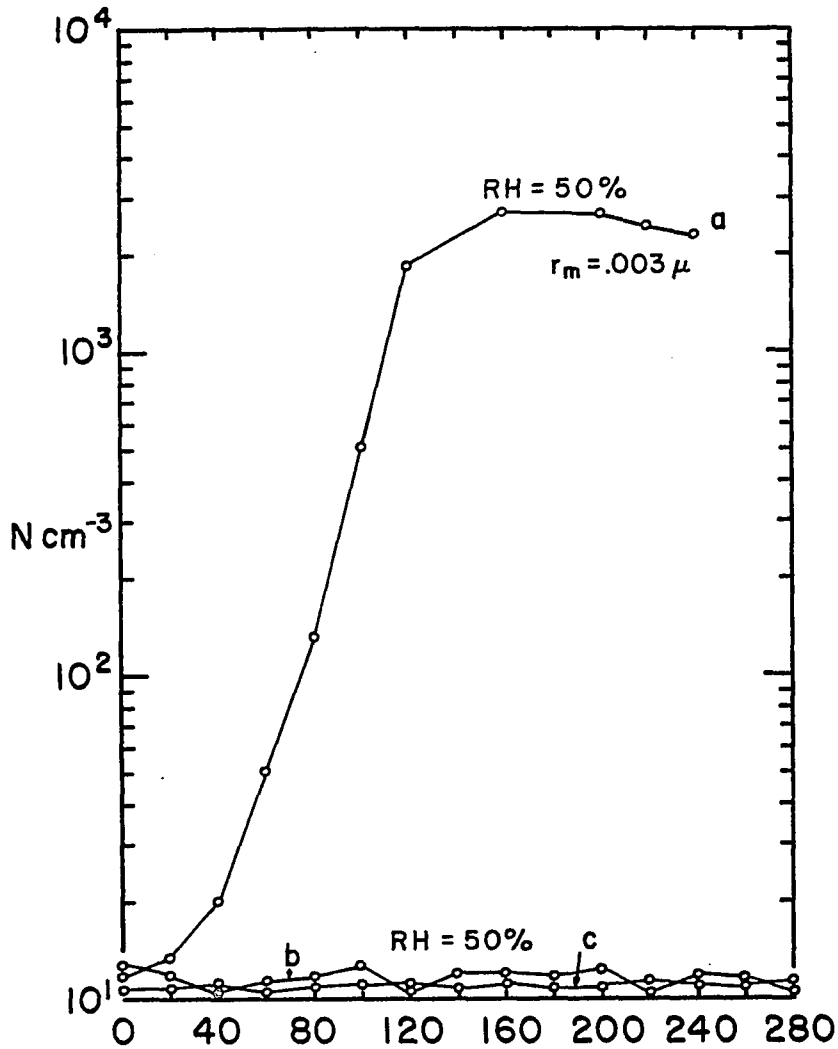

Figure 59. Aerosol formation in the dark.

The curves are labeled as follows: a. $[SO_2]$ = .5 ppm, $[O_3]$ = .3 ppm, b. $[SO_2]$ = .5 ppm, ambient $[O_3]$, c. ambient $[SO_2]$, $[O_3]$ = .3 ppm.

in aerosol formation. Similar experiments with a 3.4 μCi source of γ radiation also failed to produce aerosol.

Evaporation of Photochemical Nuclei

On a number of occasions when filtered atmospheric air samples were irradiated in the quartz reactor with the LPHg-(UF) source and then stored in the mylar bag, an apparent evaporation of the nuclei occurred. As shown in Figure 60 the nucleus concentration decreased by a factor of 3-5 in less than one minute. For small particles (r_m estimated at .003 μ using the nuclepore filters) at concentrations of 10^4 cm^{-3} coagulation cannot account for such losses. For particles of this size losses to the walls of the bag (see Appendix B, Figure B.2) also cannot account for such rapid rates of loss. Though other mechanisms are possible, it seems most likely that the newly formed nuclei (produced in the flow reactor) found themselves in a subsaturated environment when transferred to the storage bag. As can be seen in Figure 60 a second peak in the particle concentration reappeared after some 5 minutes. This aerosol phase was stable and decayed at the previously observed rates which suggests a different composition from the more transient particles found during the first minute of observation.

Summary and Conclusions

Solar-Induced Nucleus Formation

Time Scale for Onset of Homogeneous Nucleation. The time scale for the onset of solar-induced homogeneous nucleation, if it occurs at

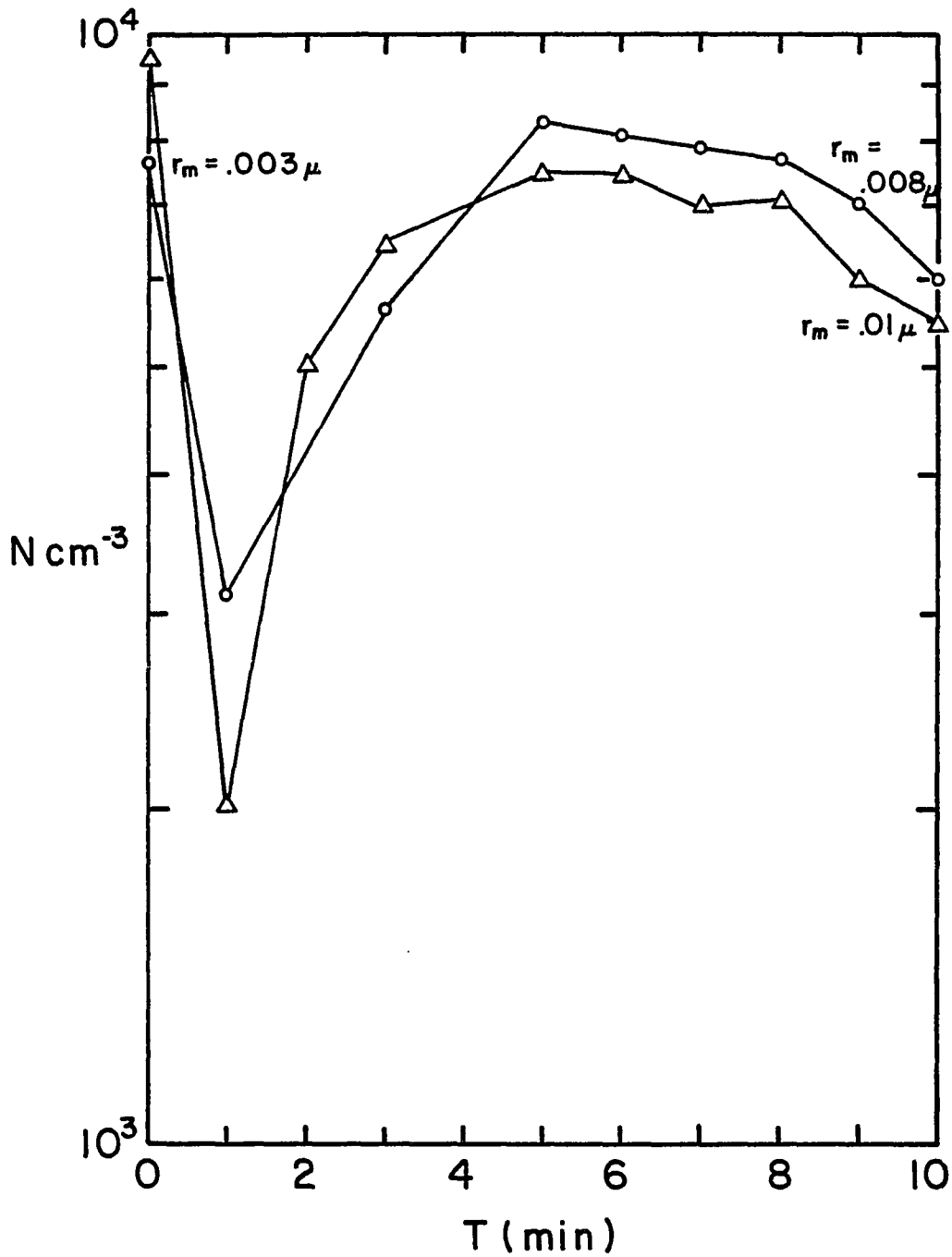

Figure 60. The apparent evaporation of photochemical nuclei.

all, is at least 2-3 hours in Tucson environmental air, even at a RH of some 70%. Only when SO_2 has been added at the 10-20 ppb level has it been possible to observe solar induced aerosol formation.

Time Scale for Loss of Newly Formed Nucleogen to the Existing Aerosol Surfaces. The characteristic time scale for loss of newly formed nucleogen to the existing aerosol surfaces is on the order of several minutes (assuming efficient accommodation). It must be borne in mind, however, that the calculation must only be regarded as an approximate one until such time as information is available concerning the details of the interactions between gaseous nucleogens and particle surfaces, and possible physical or chemical changes in particulate material following condensation.

Primary Fate of Newly Formed Nucleogen. To the extent that the air samples examined are representative of a moderately polluted continental environment, it is concluded that, under these conditions, the primary fate of newly formed nucleogen is attachment to the existing aerosol surfaces rather than new nucleus formation. The measured size distributions consistently indicate the absence of large amounts of aerosol in the $r \leq .005\ \mu$ region, a result which is in accord with inability of solar radiation to produce large amounts of very small new aerosol.

In laboratory experiments losses of newly formed nucleogen and small aerosol to the photoreactor walls constitute a problem which one cannot assess in detail. The calculations presented in Appendix B suggest, however, that losses to the reactor walls are not significantly

greater than losses to the existing aerosol particles. In addition, using the assumption of a completely mixed interior, wall losses are only diminished via the surface to volume ratio so that a reactor volume of some 24,000 ℓ would be needed to gain an order of magnitude decrease in wall losses. The author's experience suggests that it would be virtually impossible to thoroughly clean such a reactor to the level where one could be confident that the wall contaminants were not the major source of nuclei. Regarding the importance of reactor size, an experiment carried out by Husar, Whitby and Liu (1972) in conjunction with the Pasadena Smog Project is illuminating. Husar et al. were able to observe the onset of homogeneous nucleation in filtered atmospheric air on time scales of tens of minutes without added water or SO_2 in a 15 ℓ pyrex photoreactor with no quartz window using Pasadena air samples.

The relative humidity of the air samples is important for several reasons. First of all, the rate of both new particle formation and/or condensational growth is a rapidly increasing function of RH; secondly, the newly formed nucleogen is much more readily converted into the aerosol phase at higher humidities so that losses of molecular nucleogen are markedly reduced. Despite this fact, atmospheric air samples have consistently failed to produce aerosol with solar irradiation at a RH up to 70% once adequate precautions were taken to thoroughly clean the reactor walls.

Maintenance of the Ambient Size Distribution. The calculated aerosol mass transports indicate that, on average, an aerosol mass of some 3×10^{-18} g-cm^{-3}-s^{-1} must be replaced in the $r \leq .01$ μ region if

the size distribution is to be maintained. Since, as has been discussed in Chapter 1, the measurement of the size distributions indicates that the distributions are maintained on time scales of at least days, a new particle source (with an average particle radius of .005 μ) of some 10 particles per cm^{-3} per sec or 600 cm^{-3} min^{-1} is needed. A nucleation rate of that extent is easily observed with the present experimental arrangement, but has never been obtained with solar radiation.

Comparison With the Results of Other Workers

The rates of solar-induced aerosol formation reported by other workers, notably Bricard et al. (1969), Vohra et al. (1970) and Verzar and Evans (1961) have not been reproduced in this study. The sources of the discrepancies are many but system contaminants and air quality are believed to be of primary importance. As has been discussed previously, substantial pains have been taken to eliminate contaminants but it is not always clear that other workers have taken similar steps to insure that nucleus formation was really due to trace gases in the air. Although the air samples used invariably contain higher concentrations of NO_x, hydrocarbons, and other trace gases than one would find in remote rural areas, these trace gases are not present in sufficient concentrations to produce detectable levels of nucleus formation in the present experimental arrangement. By the same token Twomey and Thorndike (1971) have also failed to produce nuclei with solar irradiation.

Nucleus Formation With the HPXeHg Sources

The source HPXeHg-(0-53) has consistently failed to produce nuclei in atmospheric air even with .5 ppm of added SO_2 and a RH of 70%. The HPXeHg-(UF) UV source has consistently failed to produce nuclei in atmospheric air at RHS approaching saturation. With atmospheric air enriched with..5 ppm of SO_2 and a RH of 70% this source has produced modest numbers of small nuclei under static irradiation in the 24 ℓ reactor. (The peak nucleus concentration has never exceeded 3×10^3 cm^{-3} and $r_m \leq .004$ μ.)

Nucleus Formation With the LPHg-(UF) UV Source

The 1850 Å Line. The nuclei formed with the low pressure Hg source were due to the presence of the 1850 Å line, the 2537 Å radiation playing no detectable role in nucleus formation.

Ozone and Aerosol Formation. The high levels of O_3 produced by the 1850 Å radiation were not solely responsible for aerosol formation. Nuclei have never formed in atmospheric air samples enriched in O_3 to the .3 ppm level with a RH of up to 50%.

SO_2 and Aerosol Formation. Although SO_2 is strongly photo-oxidized at 1850 Å (see Appendix D), added SO_2 alone, on the 10-20 ppb level, could not account for either the nucleation rate or the rate of growth of the nuclei in atmospheric air samples. Irradiated SO_2 - Air - H_2O mixtures result in aerosol formation which readily took place from the gas phase and such aerosol formation was not strongly suppressed by the presence of a Nuclepore filter in the flow

stream. By marked contrast, however, the presence of the filter stopped aerosol formation in irradiated atmospheric air. This behavior is not fully understood at the present time. It, tentatively, appears that most of the nucleogen produced in atmospheric air was so readily converted into the aerosol phase (in the photoreactor itself) that there was an insufficient concentration remaining for new nucleus formation to take place upon storage in the mylar bag.

Suppression of Aerosol Formation by the Preexisting Aerosol. New aerosol particles did not form if irradiated air samples were injected into air which already contained a nucleus concentration greater than 2×10^4 cm^{-3}.

The Effect of Storing Irradiated Gas Samples in Atmospheric Air. The rate of nucleation of SO_2 - Air - H_2O mixtures and of photooxidized ambient air was markedly enhanced (by a factor of 10-50) when irradiated gas samples were stored in atmospheric rather than clean (scrubbed) bottled air. Regarding the atmospheric air samples this result strongly suggests that there are trace gases present which play a non-photochemical role in enhancing nucleus formation. These gases do not themselves need to be irradiated but may well react with the photochemical nucleogen to produce a more highly supersaturated molecular species. It is interesting to note in this regard that both Hoppel (1975) and Friend et al. (1973) have found that nucleation in the H_2SO_4 - H_2O system is markedly enhanced by the presence of NH_3.

Cloud Condensation Nuclei Produced. The CCN formed with the short UV (1850 Å) radiation were associated with the aerosol fraction for $r \geq .01$ μ.

Comparison of Tucson and Remote Samples. The trace gases responsible for aerosol formation do not appear to be associated solely with the Tucson environment as nucleus formation in the rural samples took place at a rate comparable to that in the urban samples. In this regard both Twomey (1977) and Hoppel and Dinger (1973) have observed nucleus formation with similar low pressure Hg sources in air samples collected in quite different environments. Twomey's samples were taken in rural S.E. Australia and Hoppel's in a series of aircraft measurements over southern Arizona.

Relevance to the Atmosphere. Although the 1850 Å UV is of too short a wavelength to be of importance for particle formation in the troposphere,[3] the very high gas to particle conversion efficiency at this wavelength may make it of some importance in the stratosphere.

Miscellaneous Experiments

Aerosol Formation in the Dark and Spontaneous Aerosol Formation. Aerosol formation in the dark has not been observed with atmospheric air at a RH up to 50% and O_3 concentrations of some .5 ppm. Dark phase aerosol formation was occasionally observed (in 3 out of 10 repetitions of the experiment) when atmospheric air was also enriched in .5 ppm of SO_2. When dark phase (spontaneous) aerosol formation (using atmospheric

[3]The estimated optical depth of the atmosphere at 1850 Å is on the order of 10^4.

air and no added trace gases) has occurred, it has been found to be due to the presence of nucleogen and/or aerosol deposited on the reactor walls during the previous photooxidation of the air samples in the short UV. The observation of dark phase aerosol formation by Bricard et al. (1969) has not been reproduced in the present study.

Ion-Induced Mechanisms. Ion-induced mechanisms (if any) were too slow to be directly observed in the present experimental arrangement at a RH of 50% and with up to 50 ppb of added SO_2.

APPENDIX A

COAGULATION COEFFICIENTS $K(r_1, r_2)$

The coagulation coefficient for two particles of radii r_1 and r_2 is

$$K(r_1, r_2) = 4\pi \frac{\bar{r}}{\frac{r_1+r_2}{2}} \frac{\bar{D}}{\frac{D_1+D_2}{2}} \beta$$

The diffusion coefficients were calculated using the Millikan, Knudsen, Weber formula

$$D = \frac{kT}{6\pi\eta r} \left[1 + A \frac{\lambda}{r} + \frac{Q\lambda}{T} e^{\frac{-br}{\lambda}} \right]$$

with $A = 1.246$, $b = .870$, $Q = .420$ and $\lambda = .653 \times 10^{-5}$ cm. The kinetic correction factor β was calculated from formulae taken from Fuchs (1964) as follows:

$$\beta = \left[\frac{\bar{r}}{\bar{r} + \frac{\delta r}{2}} + \frac{4\bar{D}}{G_r \bar{r}} \right]^{-1}$$

where δ, the effective collision radius for a particle of radius r is

$$\delta = \frac{1}{6r\ell_B} \left[(2r + \ell_B)^3 - 4(r^2 + \ell_B^2)^{3/2} \right] - 2r .$$

Here ℓ_B, the "aerosol particle mean free path" is calculated as follows:

$$\ell_B = \frac{\overline{G}}{T} \qquad \overline{G} = \left(\frac{8kT}{m\pi}\right)^{1/2} \qquad T = \frac{mD}{kT} \quad .$$

For two colliding particles with radii r_1 and r_2:

$$\delta_r = \sqrt{\delta_1^2 + \delta_2^2} \qquad\qquad G_r = \sqrt{G_1^2 + G_2^2} \, .$$

These coagulation coefficients are twice as large as those given by Fuchs (1964). The factor of 1/2 necessary to insure that only collision pairs are counted was included in the equation for the mass transport and as such was not included in the coagulation coefficients.

APPENDIX B

SURVIVAL TIMES

We wish to estimate the distribution of lifetimes for a group of newly formed aerosol particles or nucleogen molecules in the presence of the photoreactor walls and in the presence of the existing atmospneric aerosol.

Let $n_x(t)$ be the number of molecules of type x or the number of aerosol particles of size x (per unit volume) present at time t and $n_x(0)$ the number initially present. Let $\xi_x(t)$ be the lifetime distribution function. Then we have for the general case:

$$\int_t^\infty \xi_x(t')\, dt' = \frac{n_x(t)}{n_x(0)}$$

or

$$\xi_x(t) = -\frac{dn_x(t)}{dt}\ \frac{1}{n_x(0)}$$

and the average survival lifetime is just

$$\langle t_s \rangle = \int_0^\infty t'\, \xi_x(t')\, dt'$$

Survival Times in the Presence of the Existing Atmospheric Aerosol

Newly Formed Aerosol Particles of Radius x

In this case, neglecting coagulation of the newly formed particles among themselves and condensational growth, we have simply:

$$\frac{dn_x(t)}{dt} = - n_x(t) \int_0^\infty n_a(y)\ K(y,x)\ dy\ ,$$

where $n_a(y)$ is the aerosol size distribution of the existing aerosol and $K(y,x)$ is the usual coagulation coefficient. Assuming small changes in $n_a(y)$ with time, then

$$n_x(t) = n_x(0)\ e^{-K_x t}\ ,$$

where $K_x = \int_0^\infty n_a(y)\ K(y,x)\ dy$, or

$$\langle t_s \rangle = K_x \int_0^\infty t' e^{-K_x t'}\ dt'$$

$$= \frac{1}{K_x}\ .$$

Survival Times for Molecules

The analysis for molecules is the same, except that K_x is replaced by K_g, where

$$K_g = \int_0^\infty n_a(y)\ \frac{4\pi y \overline{D}}{\frac{y}{y+\Delta} + \frac{\overline{D}}{\alpha v y}}\ dy$$

where Δ = molecular mean free path

$\overline{D} = D_a + D_g \simeq D_g$ (diffusivity of the gas molecules)

$v = \sqrt{\frac{kT}{2m}}$

and α = the molecular accommodation coefficient.

Survival Times in the Presence of Photoreactor Walls

Static Diffusion Model

This model is based on the formal solution to the three dimensional diffusion equation in the interior of a sphere (Crank 1956). With the initial and boundary conditions

$n(0,t)$ finite as $r \to 0$

$n(a,t) = 0 \ \forall_t$ (perfect wall accommodation)

$n(r,0) = n_o$ (initially uniformly mixed),

the formal solution is just

$$n(r,t) = \frac{2n_0 a}{\pi r} \sum_{n=1}^{\infty} \frac{(-1)^{n+1}}{n} \sin \frac{n\pi r}{a} e^{-\frac{n^2\pi^2}{a^2} Dt}.$$

The total flux at $r = a$ is

$$F_T(0,t) = 8\pi n_0 Da \sum_{n=1}^{\infty} e^{-\frac{n^2\pi^2}{a^2} Dt} \text{ (particles/sec)}.$$

The fraction of particles (or molecules) remaining after a time t is:

$$\frac{N(t)}{N(0)} = \frac{6}{\pi^2} \sum_{n=1}^{\infty} \frac{1}{n^2} e^{-\frac{n^2\pi^2}{a^2} Dt}$$

or $$\xi(t) = \frac{6D}{a^2} \sum_{n=1}^{\infty} e^{-\frac{n^2\pi^2}{a^2} Dt} .$$

Hence $$\langle t_s \rangle = \int_0^{\infty} t\xi(t)\, dt = \frac{6D}{a^2} \cdot \frac{a^2}{D^2\pi^4} \sum_{n=1}^{\infty} \frac{1}{n^4} .$$

Using $\sum_{n=1}^{\infty} \frac{1}{n^4} = \frac{\pi^4}{90}$,

$$\langle t_s \rangle = \frac{a^2}{15D}$$

This result represents a lower limit on the rate of loss and goes like a^2, that is $V^{2/3}$.

Mixed Interior Diffusion Through a Boundary Layer

For this case, we have

$$F = -D \frac{\partial n}{\partial r} = - D \frac{n}{r_b}$$

where r_b is the thickness of the boundary layer, and

$$\frac{dN}{dt} = - \frac{4\pi a^2 D}{r_b} n$$

$$\frac{dn}{dt} = - \frac{4\pi a^2 D}{V r_b} n$$

$$n(t) = n_0 e^{-\xi Dt}$$

where

$$\xi = \frac{4\pi a^2}{V_{rb}} = \frac{3}{ar_b}$$

or

$$r_b = \left(\frac{\xi V}{4\pi a^2}\right)^{-1} = \frac{3}{a\xi} .$$

In this case, the rate of decay goes like 1/a, i.e., the surface-to-volume ratio, and

$$\langle t_s \rangle = \frac{1}{\xi D}$$

The value of ξ, in effect the thickness of the boundary layer, must be determined experimentally. A platinum hot-wire aerosol and an H_2SO_4 aerosol were used to examine the rate of decay for several different particle sizes. Figure B.1 shows several typical measured rates of decay in the 24-liter reactor for a hot-wire aerosol size distribution of 0.01 μ modal radius and monodisperse to within the resolving power of the sizing technique (one-half width of .23 decade). Fitting of these curves yielded an average value of ξ of 3.5 cm^{-2}, corresponding to a boundary layer thickness of some .5 mm. Figure B.2 shows the measured vs. calculated rates of decay for several aerosol sizes. The measured curves for r_m = 0.015 μ were obtained using a hot-wire aerosol and an H_2SO_4 - H_2O aerosol for the r_m = 0.003 μ curve. For r_m = 0.015 μ, the curves agree well, since ξ was calculated from the measured decay of this aerosol, but they appreciably overestimate the rate of decay for smaller particles; hence, the value of ξ used

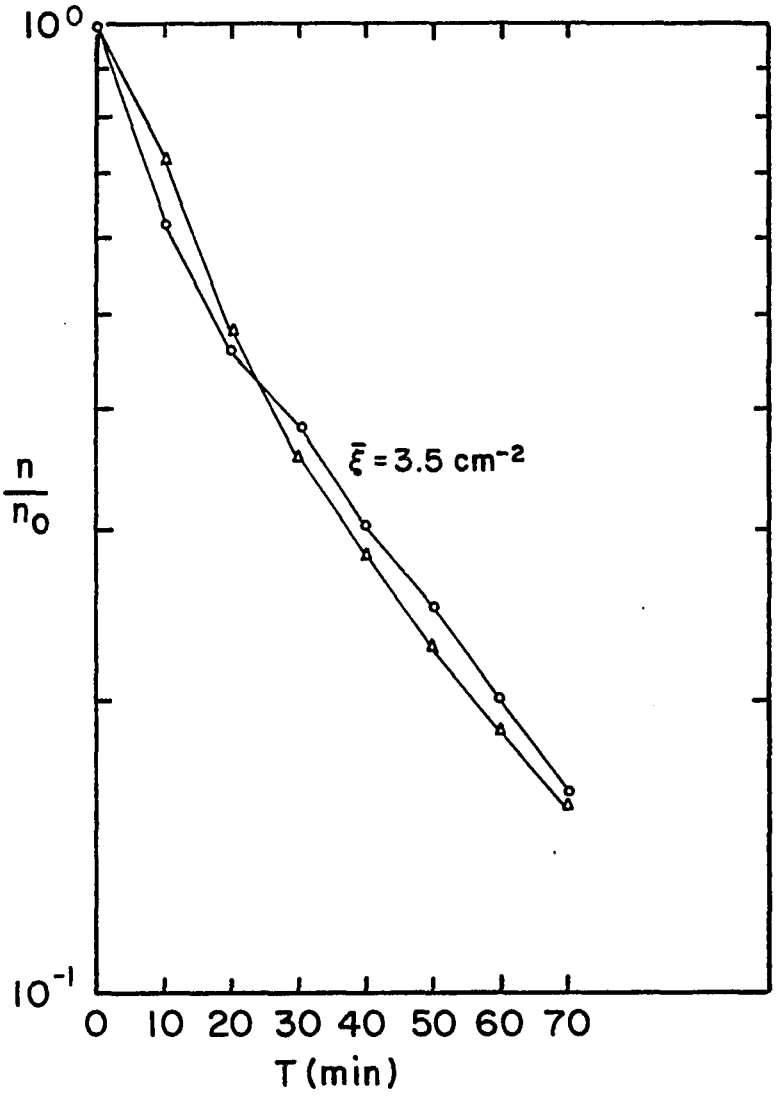

Figure B.1. Characteristic decay curves for the 24 ℓ reactor used to estimate ξ.

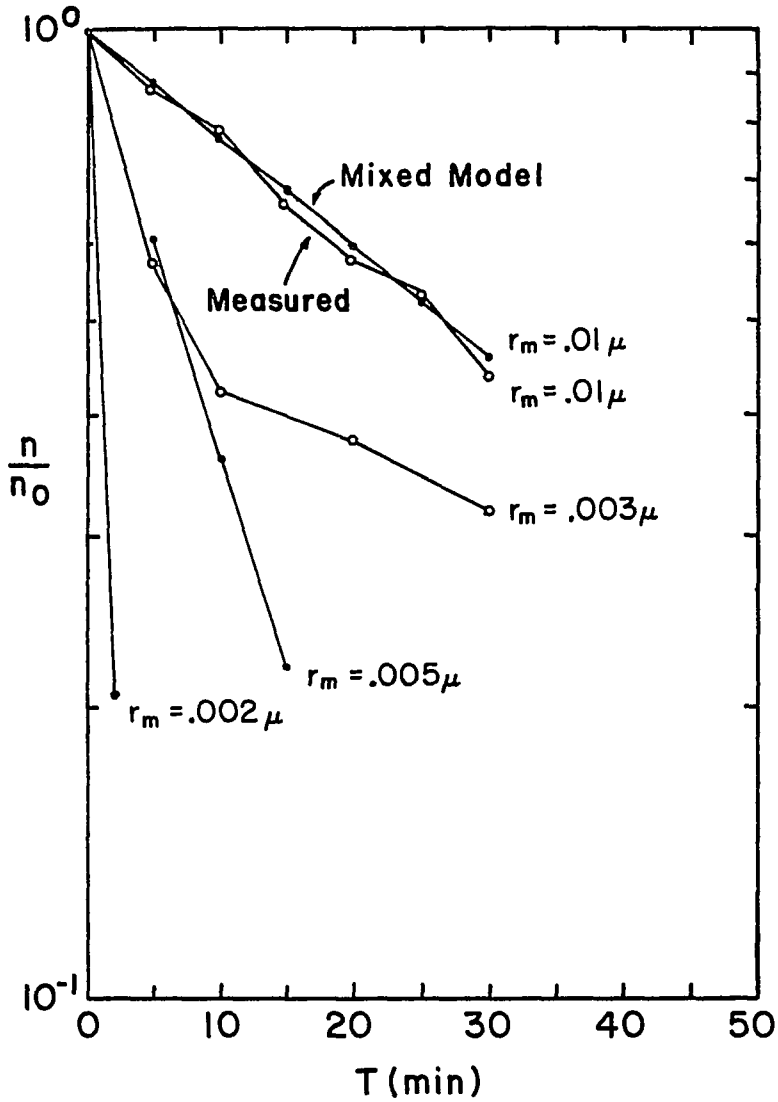

Figure B.2. Calculated and measured decay curves for different size particles.

The curves labeled Mixed Model were calculated using the mixed interior model with a ξ value of 3.5 cm^{-2}.

here represents an upper bound on the rates of decay. It should be emphasized that the thoroughly mixed interior model represents a gross simplification of the particle loss process and is to be interpreted only as an estimate of wall losses. Figure B.3 shows the average survival times for newly formed aerosol for both the best (static) and worst (mixed) cases in the reactor and in the presence of the ambient aerosol. For molecules (for perfect accommodation by both the reactor walls and the existing particles), the worst case estimate is $\langle t_s \rangle_m \sim 3$ s and 2×10^2 s for the best case in the photoreactor, and some 10^2 s in the presence of the existing aerosol. From these estimates, it seems reasonable to assume that loss of newly formed aerosol and nucleogen would not be expected to be significantly greater than that to the existing aerosol surface. It should, furthermore, be observed that, to the extent that the completely mixed model holds, one gains only in average loss time via the surface-to-volume ratio, so that, for example, a total reactor volume of some 24,000 liters would be necessary to achieve an order of magnitude increase in survival time. Experience in the present study suggests that cleaning such a reactor would be virtually impossible.

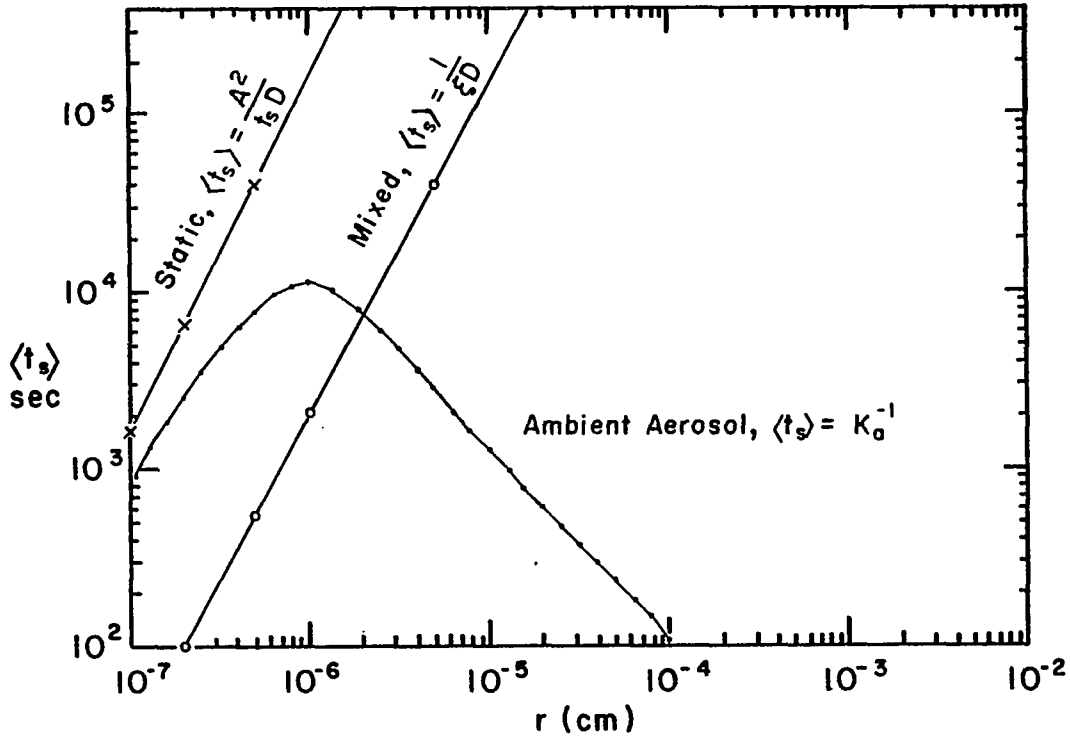

Figure B.3. Comparison of the average survival times of newly formed aerosol in the photoreactor with that in the presence of the existing aerosol

APPENDIX C

ESTIMATING THE SPECTRAL IRRADIANCE OF THE 1850 Å LINE

The spectral irradiance of the 1850 Å line in the low-pressure Hg sources was estimated by measuring the amount of O_3 produced in a continuously flowing stream of dry air passing through the small quartz reactor. An arrangement of optical stops and shields served to produce a well-defined radiated volume. The $[O_3]$ was measured with a Dasibi 1003-AH O_3 monitor at the reactor exit after the gas had flowed through 20 cm of Teflon tubing. The $[O_3]$ produced with LPHg-(UF), LPHg-(9-58), and LPHg-(9-54) is shown in Figure C.1. O_3 formation is associated almost entirely with 1850 Å radiation. With the time scales ($\sim$ 1 sec) involved here, the following reactions are the only ones of importance:

$$\frac{d[O]}{dt} = 2[O_2]\int_{\lambda} I_\lambda \sigma^{O_2}_\lambda \phi_\lambda \, d\lambda - k[O][O_2][M] = 0$$

$$\frac{d[O_3]}{dt} = k[O][O_2][M]$$

where I_λ is the spectral irradiance, $\sigma_\lambda^{O_2}$ the absorbtion cross section of O_2 and ϕ_λ is the quantum efficiency for the conversion of O_2 into O_3 at 1850 Å. To a good approximation:

$$\int_{\lambda} I_\lambda \sigma^{O_2}_\lambda \phi_\lambda d\lambda = I_{1850} \sigma^{O_2}_{1850} \phi_{1850} \Delta\lambda$$

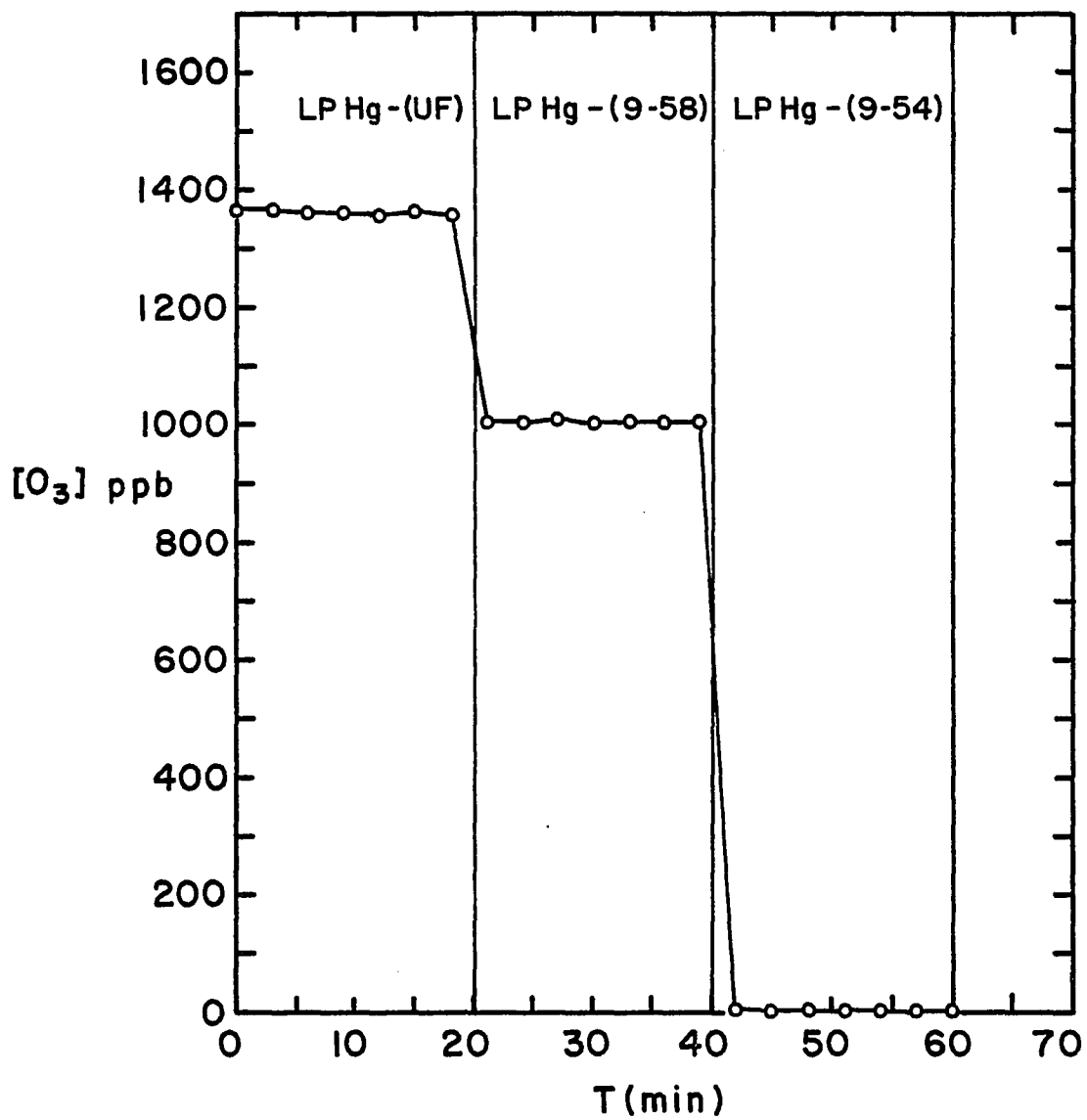

Figure C.1. $[O_3]$ produced in continuous flow using the various LPHg sources of UV.

hence

$$\frac{d[O_3]}{dt} = 2\, I_{1850}\sigma^{O_2}_{1850}\phi_{1850}\Delta\lambda\, [O_2]$$

and

$$[O_3]_{exit} = \frac{2\, I_{1850}\sigma^{O_2}_{1850}\phi_{1850}\Delta\lambda\, V_r\, [O_2]}{Q_V}$$

where V_r is the radiated volume and Q_V is the volumetric flow rate. Using the values V_r = 38.5 cm^3, Q = 33.3 cm^3/s, ϕ_{1850} = 1, $[O_2]$ = 5 x 10^{18} cm^{-3}, $\sigma^{O_2}_{1850}$ = 1.8 x 10^{-21} cm^2 and a measured $[O_3]$ of 3.4 x 10^{13} cm^{-3} yields:

$$I_{1850}\Delta\lambda = 8 \times 10^{14} \frac{\text{photons}}{cm^2 - s} .$$

The combined uncertainties are such that $I_{1850}\Delta\lambda$ is reasonably known to within a factor of 2.

APPENDIX D

H_2SO_4 AEROSOL FORMATION IN SO_2-AIR-H_2O MIXTURES AT 1850 Å

Since SO_2 is very rapidly photooxidized at 1850 Å (Cox 1973, Driscoll and Warnek, 1968) and since this wavelength was responsible for aerosol formation in ambient air samples, a study of H_2SO_4 aerosol formation at 1850 Å was carried out for purposes of comparison with the ambient samples. Cox (1973) studied the H_2SO_4 aerosol produced in SO_2-N_2-H_2O mixtures, but, to the author's knowledge, the H_2SO_4 aerosol produced in SO_2-Air-H_2O mixtures has not been explicitly studied. Driscoll and Warnek (1968) found the quantum efficiency for the reaction $SO_2 \xrightarrow{1850\ Å} SO_3$ to be about one half for mixtures of 8% SO_2 in O_2. One cannot, however, extrapolate this quantum efficiency down to the ppb level with any certainty.

The experimental arrangement for this study is shown in Figure D.1. SO_2 was metered into the system using an SO_2 permeation membrane held in an ice-water mixture. The SO_2 membrane was supplied and calibrated by the manufacturer. The lower SO_2 concentrations were obtained using the ice-H_2O bath and a dynamic dilution system and are known to within 50%. Figure D.2 shows the aerosol concentration at the exit of the reactor (corrected for diffusion loss in the connecting lines to the Pollak counter) as a function of SO_2 concentration and RH.

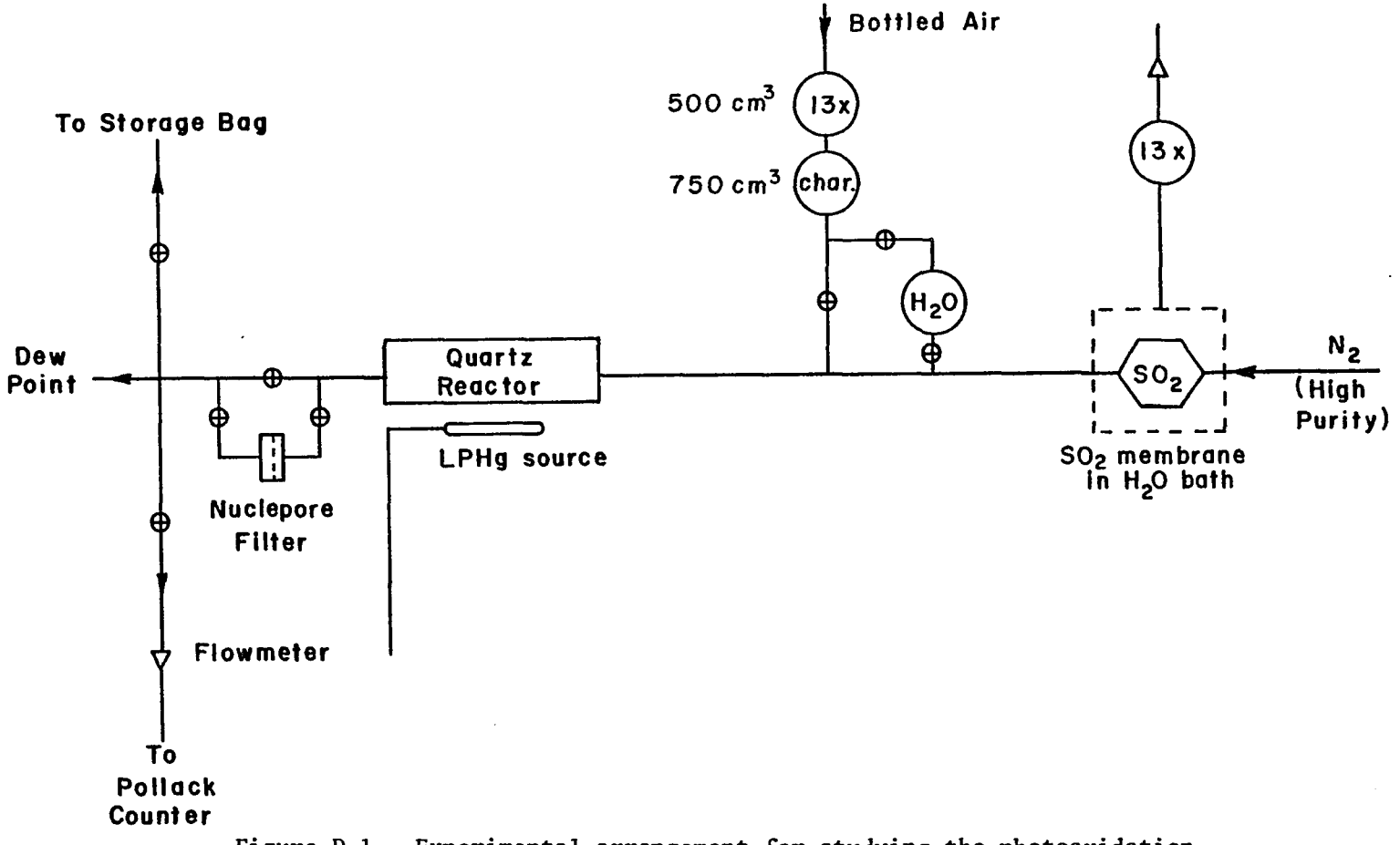

Figure D.1. Experimental arrangement for studying the photooxidation of SO_2-Air-H_2O mixtures at 1850 Å.

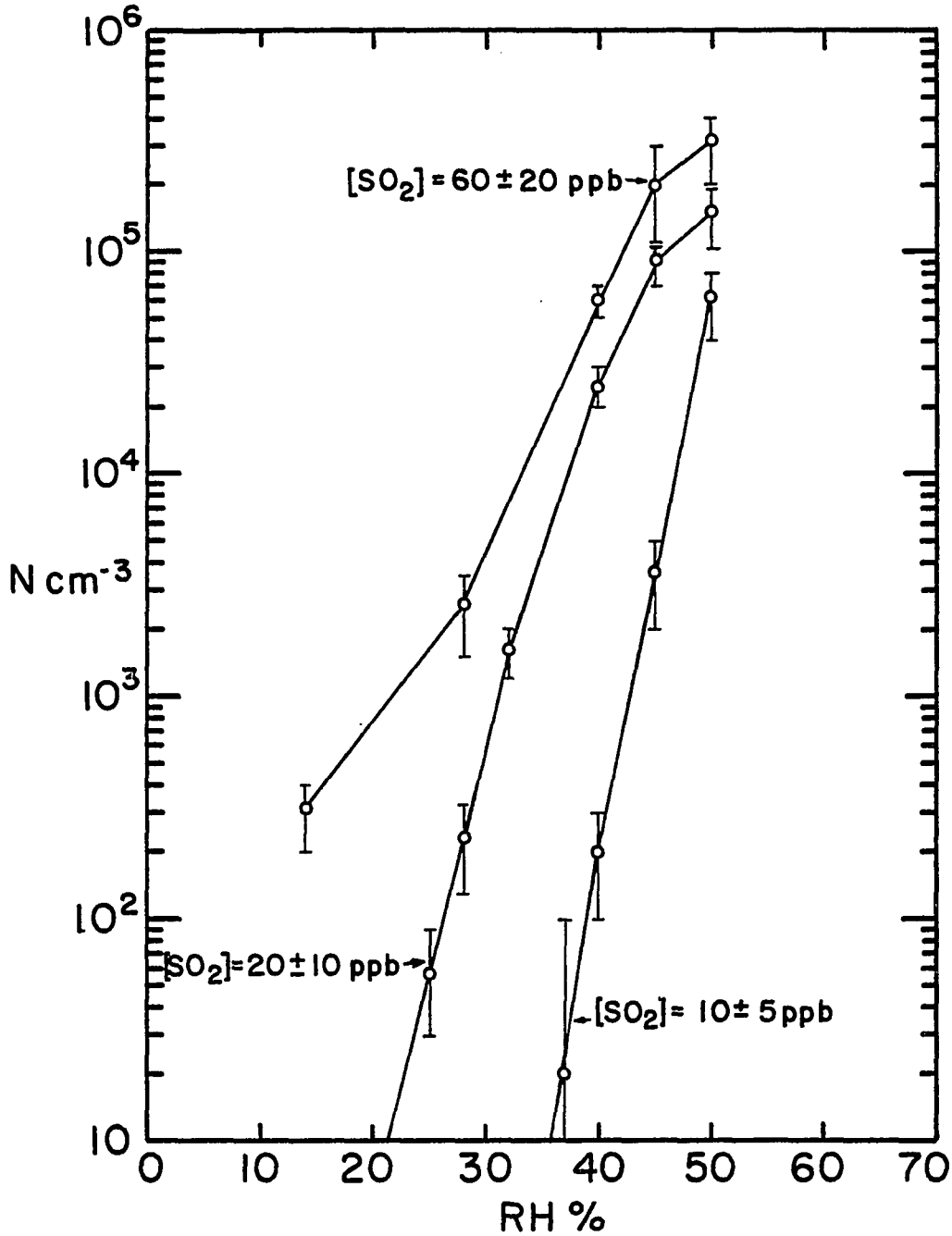

Figure D.2. Nuclei formed when SO_2-Air-H_2O mixtures were irradiated with the LPHg-(UF) UV source (1850 Å).

These nucleation rates imply (see Kiang, Stauffer, Mohnen, Bricard and Viglas 1973) that the $[H_2SO_4]$ of about 0.01 ppb is achieved with the low-pressure Hg source. [At 40% RH and 0.01 ppb H_2SO_4, the calculated nucleation rate (see Kiang et al. 1973) is about 10^2 cm^{-3} s^{-1}.) This allows an estimate of the quantum efficiency to be made

$$[H_2SO_4] = \phi_{1850} F_{1850} \sigma_{1850} [SO_2] t_r$$

$$\phi_{1850} \sim \frac{[H_2SO_4]}{t_r F \sigma [SO_2]}$$

Here t_r is the reactor residence time, F is the irradiance ($F = I_{1850}\Delta\lambda$), σ_{1850} is the absorption cross section of SO_2 at 1850 Å and ϕ_{1850} is the quantum efficiency for the conversion of SO_2 into SO_3 at 1850 Å. Using t_r = 2.75, $F = 1.4 \times 10^{14}$ cm^{-2} s^{-1}, $\sigma_{1850} = 3.7 \times 10^{-18}$ cm^2 (taken from Golomb, Watanabe and Marmo 1962), $[SO_2]$ = 12 ppb and a $[H_2SO_4]$ of .01 ppb yields

$$\phi_{1850} \sim .3 .$$

This is to be regarded only as an order of magnitude estimate, but these results do suggest that ϕ_{1850} for conversion of SO_2 in air is close to unity. This then implies a fractional conversion rate of

$$\frac{1}{[SO_2]} \frac{d[H_2SO_4]}{dt} \sim \sigma\Phi \sim 10^{-2} \text{ min}^{-1} .$$

This is some 3 orders of magnitude higher than the measured rates of SO_2 photooxidation by solar radiation [2×10^{-5} min^{-1} having been obtained by Gerhard and Johnstone (1955)].

As with the ambient air samples, nucleus formation appears to be uniquely associated with the 1850 Å radiation. As shown in Figure D.3 with the 1850 Å line filtered but the 2537 Å line present, no aerosol formation took place.

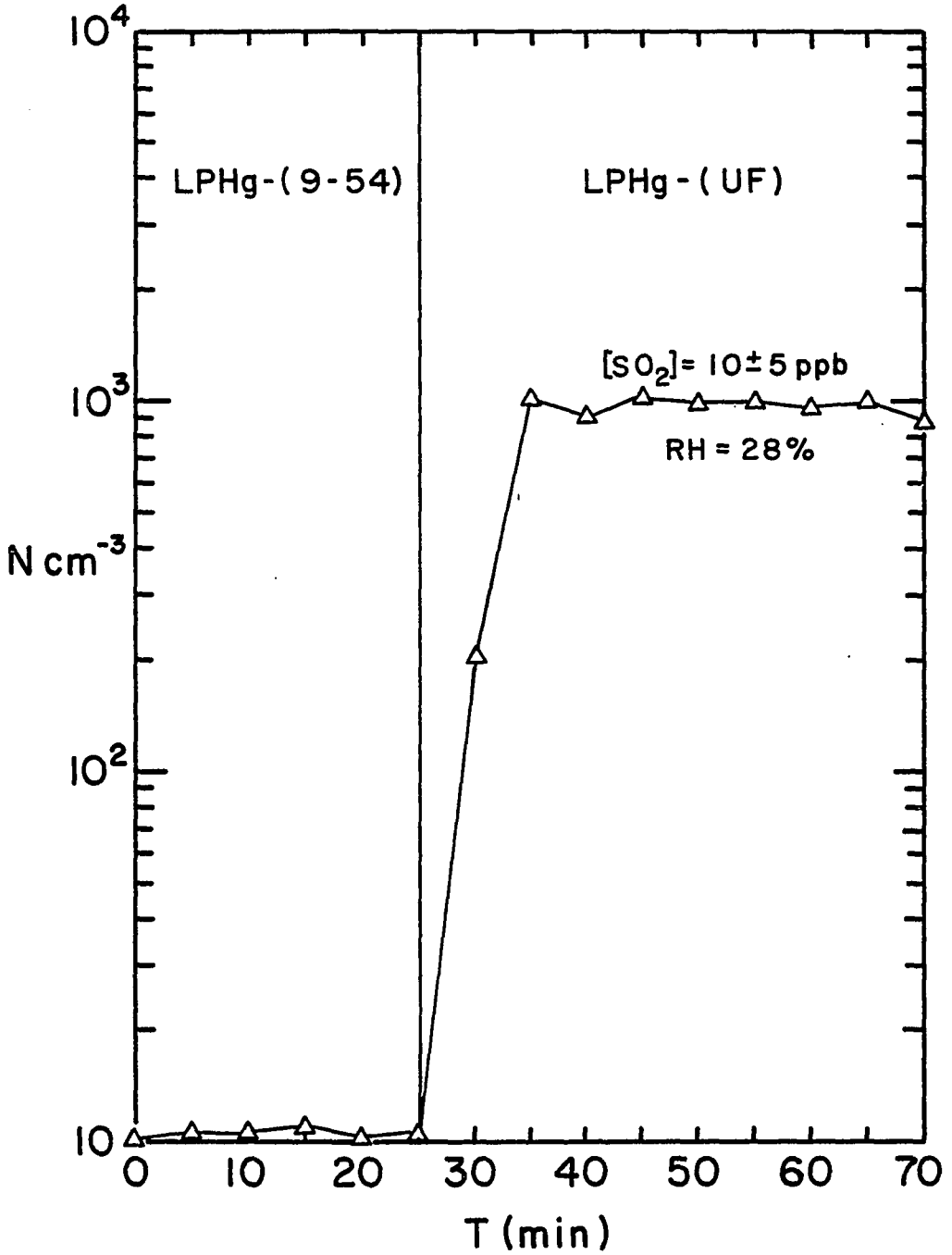

Figure D.3. Nuclei formed when SO_2-Air-H_2O mixtures were irradiated with and without the 1850 Å UV.

LIST OF REFERENCES

Atkinson, J. R., 1955: Uncharged nuclei produced by ultraviolet light. Geofisica Pure Appl., 31, 54-59.

Bricard, J., F. Billard, and G. Madelaine, 1969: Formation and properties of radiolytic and photolytic condensation nuclei in atmospheric dust free air. Planetary Electrodynamics, 1, 233-242, Gordon and Breach, N.Y.

Bricard, J., M. Cabane, G. Madelaine, and D. Vigla, 1972: Formation and properties of neutral ultrafine particles and small ions conditioned by gaseous impurities in the air. Aerosols and Atmospheric Chemistry, 27-43, Academic Press, New York.

Cox, R. A., 1973: Some experimental observations of aerosol formation in the photo-oxidation of sulphur dioxide. Aerosol Science, 4, 473-483.

Crank, J., 1956: The Mathematics of Diffusion. 2nd ed., Oxford University Press, 84-98.

Doyle, G. J., 1961: Self-Nucleation in the Sulfuric Acid-Water System. Journal of Chemical Physics, 35, 795-799.

Driscoll, J. N., and P. Warnek, 1968: Primary processes in the photolysis of SO_2 at 1849 Å. J. of Physical Chemistry, 72, 3736-3740.

Friedlander, S. K., 1960: Similarity considerations for the particle size spectrum of a coagulating, sedimenting aerosol. J. Meteor., 17, 479-483.

Friend, J. P., R. Leifer, and M. Trichon, 1973: On the formation of stratospheric aerosols. J. Atmos. Sci., 30, 465-479.

Fuchs, N. A., 1964: Mechanics of Aerosols, English ed. (Oxford: Pergamon), 294.

Gerhard, E. R., and H. F. Johnstone, 1955: Photochemical oxidation of sulpher dioxide in air. Ind. and Eng. Chem., 47, 972-976.

Golomb, D., K. Watanabe, and F. F. Marmo, 1962: Absorption coefficients of sulfur dioxide in the vacuum ultraviolet. J. of Chem. Physics, 36, 958-960.

Hoppel, W. A., 1975: Growth of condensation nuclei by heteromolecular condensation. J. Rech. Atmos. IX, 167-180.

Hoppel, W. A., and J. E. Dinger, 1973: Production of cloud nuclei by ultraviolet radiation. J. Atmos. Sci., 30, 331-334.

Husar, R. B., K. T. Whitby and B. Y. H. Liu, 1972: Physical mechanisms governing the dynamics of Los Angeles smog aerosol. J. Colloid Interface Sci., 39, 211-224.

Junge, C., and R. Jaenicke, 1969: New results in background aerosols studies from the Atlantic expedition of the R. V. Meteor, Spring 1969. Aerosol Science, 2, 305-314.

Kerker, M., 1972: Some optical and dynamical properties of aerosols. In Aerosols and Atmospheric Chemistry, 3-25, Academic Press, New York.

Kiang, C. S., D. Stauffer, V. A. Mohnen, J. Bricard and D. Viglas, 1973: Heteromolecular nucleation theory applied to gas-to-particle conversion. Atmospheric Environment, 7, 1279-1283.

Martell, E. A., 1977: Radioactive emanations and the formation and composition of aerosols. Proc. Garmisch-Partenkirchen Sympos. on Radiation in the Atmosphere, 44, Science Press, Princeton, New Jersey.

Metnieks, A. L., and L. W. Pollack, 1959: Instruction for use of photoelectric condensation nucleus counters. Geophys. Bull., 16, School of Cosmic Physics, Dublin Institute for Advanced Studies.

Mohnen, V. A., 1971: Discussion of the formation of major positive and negative ions up to the 50 km level. Pure and Appl. Geophys., 84, 141-153.

Nolan, P. J., and C. P. O'Toole, 1959: Geofisica Pura Appl., 42, 117-120.

Peddar, M. A., 1971: The measurement of size and diffusion characteristics of aerosols with particle sizes less than .01 μ using the Pollack condensation nucleus counter. Brit. J. Appl. Phys., 4, 531-538.

SMIC, 1971: Inadvertent Climate Modification: Report of the Study of Man's Impact on Climate (SMIC), 185-211, MIT Press, Cambridge, Mass.

Twomey, S., 1975: Comparison of constrained linear inversion and an iterative nonlinear algorithm applied to the indirect estimation of particle size distributions. J. Comp. Physics, 36, 958-960.

_____, 1976: Aerosol size distributions by multiple filter measurements. J. Atmos. Sci., 33, 1073-1079.

_____, 1977: Production of particles by ultraviolet irradiation of filtered air. J. Rech. Atmos., 11, 1-7.

Twomey, S., and N. S. Thorndike, 1971: On the production of particles in filtered atmospheric air under intense illumination. J. Rech. Atmos., V, 3, 149-152.

Twomey, S., and R. Zalabsky, 1978: Multifilter technique for the examination of the size distribution of the natural aerosol. Unpublished paper, Dept. of Atmos. Sci., University of Arizona.

Verzar, F., and H. D. Evans, 1961: Production of atmospheric condensation nuclei by sunrays. Geofisica Pura Appl., 13, 259-268.

Vohra, K. G., K. N. Vasudevan, and P. V. N. Nair, 1970: Mechanisms of nucleus-forming reactions in the atmosphere. J. Geophys. Res., 75(15), 2951-2960.

Went, F. W., 1960: Blue hazes in the atmosphere. Nature, 187, 641-643.

Whitby, K. T., R. B. Husar, and B. Y. H. Liu, 1972: The aerosol size distribution of the Los Angeles smog. J. Colloid. Interface Sci., 39, 177-204.

Zalabsky, R., and S. Twomey, 1977: Measurements of cloud nuclei and aerosol size spectra in the semi-arid Southwest, Preprint volume, AMS Conf. on Cloud Physics, Tucson, AZ, October, 1974.